An Experimental Investigation of Settling Velocity of Spherical and Industrial Sand Particles in Newtonian and Non Newtonian Fluids using Particle Image Shadowgraph

by

Shivam Shahi

A thesis submitted in partial fulfillment of the requirements for the degree of

Master of Science

in

Petroleum Engineering

Department of Civil and Environmental Engineering, Faculty of Engineering
University of Alberta

Abstract

The particle settling velocity is a fundamental requirement and key variable for modeling sedimentation processes and simulating particle transportations, especially when suspension is a main process. An experimental study has been conducted to measure the settling velocities of spherical particles with variable size and density as well as naturally occurring sands with non-uniform shape in Newtonian fluids and Power law fluids of variable viscosity and density. The experimental technique (laser based image processing) is unique in its kind and it is very efficient in measuring the size, shape, and settling velocity of the particles, simultaneously. Experiments on spherical particles are conducted using different sizes of glass spheres (0.5-2 mm) in four different concentrations of glycerol-water (10-40% by volume) mixtures and four different mixtures of CMC (0.14-0.29 wt%).

In addition, settling velocity of quartz sands particles under four sieve sizes in the range of 0.35mm-1.18mm have also been measured in Newtonian and non-Newtonian fluid medium using PIS technique. Rheological studies of Glycerine, CMC and Carbopol solutions have been carried out and different empirical correlations to predict the drag and settling velocity of spheres in Newtonian and Non-Newtonian fluid have also been developed. Similar correlations have been developed for the natural sands to predict the settling velocity in different fluid mediums using different equivalent diameter. Comparing to the all published models, the new correlations are found to be more accurate in their predictive capabilities with smaller margin of error. The error in prediction of settling velocity by different developed correlations is coming in the range of 4.1%-15%.

Acknowledgement

I would like to express my heartfelt gratitude to my guide, Dr. Ergun Kuru, for his invaluable guidance and constant support throughout this study. His commitment towards research and his students is exceptional and highly appreciated.

I would also like to express my sincerest gratitude to Mr. Todd Kinnee, for helping me out in procuring instruments and other necessary ingredients required for the study.

Very special thanks to my friends Pramod Sripada, Manjeet Chowdhary, Rohan Gaikwad, Abhinandan, Deepesh, and Khushhal Popli, for their support and help.

I would also like to thank the committee members, Dr. Tayfun Babadagli and Dr. Sina Ghaemi, for serving in my MSc final exam committee. Their time and valuable feedbacks are highly appreciated.

At last I would also like to thank all the staff members of the Civil and Environmental Engineering department for all their help.

This research is financially supported through the funds available from Natural Sciences and Engineering Research Council of Canada (NSERC RGPAS 411966 KURU and NSERC RGPIN 238623 KURU).

List of Figures

List of Tables

Nomenclature

D10- Mean linear diameter

D32- Sauter mean diameter

DV10- Maximum particle size below which 10% of sample volume exist

DV50- Maximum particle size below which 50% of sample volume exist

DV90- Maximum particle size below which 90% of sample volume exist

D_c- Equivalent circular diameter

d_s- Mean sieve diameter

C_D-Drag coefficient

g- Acceleration due to gravity

D- Diameter of the particle

ρ_s- Density of the Solid

ρ_o- Density of the fluid

V_s- Settling velocity

Re_p- Particle Reynolds number

A- Archimedes Buoyancy Index number

υ- Kinematic viscosity of fluid

w- Settling velocity of particle

d_*- Dimensionless diameter

D_n- Nominal diameter of the particle

V_D- Dimensionless velocity

ρ_f- Fluid's density

b- Length of largest axis

c- Length of smallest axis

C- Centricity

D*- Archimedes Buoyancy Index/ Dimensionless Diameter

R_s- Reynolds Number

D'- Specific gravity of particle- specific gravity of fluid

R_{ce}- Equivalent circular radius assuming it to be an ellipse

w_s- Settling velocity of equivalent diameter of sphere

w- Settling velocity of sand

T- Temperature in degree celcius

r- Submerged specific gravity

m – Constant

C- Constant

B- Constant

n- Flow index of the fluid

K- Consistency index of the fluid

X'- Coefficient

Y'- Coefficient

d_p- Particle diameter

μ_a- Effective/ Apparent viscosity

A_c- Equivalent circular area of the particle

A_p- Actual surface area of the particle

Y- Modified drag coefficient

R^2- Regression coefficient

MLR- Multiple Linear Regression

Table of Contents

Chapter 1:

Introduction

Designing and commissioning of an experimental setup for measuring the settling velocity of particles using Particle Image Shadowgraph (PIS) is the preliminary aim of the study. The dissertation focusses on the experimental investigation of settling velocity of spherical and Industrial sand in Newtonian and Non-Newtonian fluid using the developed PIS technique.

In the introductory chapter, a brief overview of the progress made in this regard is given while describing the problem statement of the study. The objectives and methodology of the current investigation have also been presented in this chapter. The chapter ends with delineating the overall structure of thesis.

1.1 Overview

The modern civilization is heavily dependent on minerals. Minerals in their raw form are not readily usable and their processing becomes imperative and inevitable. Particles are thus dealt in a large scale to meet the ever increasing demand of chemicals. Most Industrial processes handle particles from a few microns to big rocks spanning hundreds of centimeters on a daily basis. Understanding the bulk behaviour of particles and the impact of the particle properties on the process parameters is important. Particle characterization in several respects is to be made for optimal and safe operation of the equipment.

Settling velocity and particle size characterization play a vital role in understanding the fluid particle system. The two most important reasons for industries to perform particle characterization is to have a better control on product quality and also to have a better understanding of products, ingredients and processes [1]. Fluid particle system plays a vital role in designing and operation of pipeline. Settling velocity of a single particle in stagnant fluid forms the basis for the selection of an appropriate velocity to carry the particles efficiently in pipeline operations. The knowledge of drag force acting on a particle is a critical input parameter in theoretical models for pipelines, dewatering, filtration and other similar processes [2].The settling velocity of particle in non-Newtonian fluid is an important factor in determining the efficiency of different industrial processes, viz., designing of pipeline, separator, tunnel boring machine, hydraulic fracturing, paint and pigment, pharmaceutical, centrifuge, coastal engineering, sedimentology, petroleum among others. It is a well-known fact that solids are difficult to handle as compared to gas or liquid. In addition to reducing cost and energy consumption, the accurate estimation of settling velocity, size and shape of particle in different fluid medium can lead to increased efficiency of various industrial processes. The study of settling velocity of solids is important because cutting transport and/or hole cleaning associated with the oil and gas well drilling operations greatly depends on the knowledge of particle's settling velocity. It is critical information that is required to know in order to design optimum hydraulics program for cuttings transport during oil and gas well drilling operations and pipeline transportation.

1.2 Problem statement

Relevant works to predict settling velocity were mainly made through either analytical solutions of physical formulas or empirical equations of experimental curves. Factors to influence and control the settling of sediment particles through fluids are well known. However, the functional relationships among settling velocities, particles, and factors moving them through the fluids still need to be experimentally simulated and quantitatively defined. The settling velocity is a fundamental requirement and key variable for modeling sedimentation processes and simulating particle transportation, especially as suspension is a main process. These experimental investigations study and compare the settling velocities of sphere and industrial sand particles in both Newtonian and non-Newtonian fluids in order to develop the new generalized model for predicting the setting velocities over a range of flow regimes.

The use of manual methods viz., sieving, sieve hydrometer among other methods is tedious and not efficient as compared to image processing technique. Rogerio [3] had studied the different optical techniques in detail and found that shadowgraph technique has a great advantage over other techniques. The laser diffraction method which has been commonly used in the past for PSD is found to be erroneous when the particle number is increased because of the multiple scattering phenomenon.

The earliest literature to determine the relationship between settling velocity and particle moving through fluid could be traced back to Stokes Law [4], which was derived by equating the effective weight of a spherical particle to the viscous resistance. Since early 20th century, numerous studies have been conducted and several empirical formulae were established to estimate the settling velocity of a particle. Rubey [5] combined Stokes law and impact law into a general equation, which considers not only the viscous resistance but also the fluid impact. Gibbs et al. [6] derived the empirical equation to estimate the relationship between settling velocity and grains of sphere size. Peden and Luo [7] proposed the drag coefficient correlations for spheres within a limited particle Reynolds's number range, which when compared with the experimental results gave an error of ±16%. Mordant and Pinton [8] experimentally investigated the motion, physics and factors governing the setting of solid spheres using acoustic models and signal processing. Later on, Brown and Lawler [9] studied different settling velocity correlations and experiments available in the literature and suggested two different correlations for spheres. In the case of non-spherical particles, there have been several reports in literature that examine the settling velocities through analytical, empirical or phenomenological models ([10] to [14]).

Authors ([15] to [19]) have proposed the applicability of Newtonian drag for non-Newtonian fluid. In 2002, Chhabra [2] had studied in detail the use of the Newtonian drag curve and found that this method gave an average error of 30% with maximum deviation up to 70%. There are other studies ([20] to [28]) conducted by where they have studied the flow past a sphere in non-Newtonian fluid and tried to assess the drag force acting on the spheres. There exist two different opinions amongst the authors regarding the use of Newtonian drag curve for Non-Newtonian fluid. The latest study has been carried out by Shah [25] wherein he proposed that there exists a strong dependency of drag coefficient on flow behavior index ‘n’.

The shape and size of the particle plays an important role in determining the settling behavior. There exist different terminology like centricity, mean Sieve diameter, volume equivalent diameter, Sauter mean diameter, sphericity, roundness among others to define the shape and size of the non-spherical particles. Roux [29] has presented a wide overview of different available literature related to the particle size, shape and settling velocity for spherical and non-spherical particles including natural grains. The two most commonly used diameters i.e. the sieve diameter and the settling diameter are found to have not taken the shape into consideration [29]. The values of the estimated diameter using these two methods can give a large error which will greatly affect the predicted settling velocity value. In yet similar study conducted by the estimated dimensionless velocity with the observed velocity for the equivalent sieve diameter have been compared [30]. The relations between them were found to be complex and they have proposed four different equations to correlate these two values.

As discussed above, the shape of the particles have an important role in their settling behavior. The most rigorous and complex task is to define the shape of the particle accurately. There exists numerous study and parameters which define the particle's shape differently. There does not exist a universal definition for the shape factor as some of them are efficient for a particular shape while the other are meant for defining some other shapes.

The non-spherical particle in non-Newtonian fluid is an important field of study because in the industry as this state of fluid particle system occurs most frequently. There exist a wide range of literature which covers the non-spherical shaped particles like disc, cylinder, prism, rectangle, star among other regular shapes falling in non-Newtonian fluid ([7], [31], and [32]). They have proposed that the highly irregular particles can be approximated to one of these regular shape and the developed correlations can be used.

For the naturally occurring irregular particle different correlations for estimating drag acting on the particle have been proposed in the literature ([10], [11], [33] to [49]). Particle like natural grains, magnetite ore, and proponent have been studied analytically and experimentally and drag correlation developed. But none of them can be effectively used for natural sand particle in power law fluid.

Most of the early theoretical formulae for estimating sediment settling velocity were developed by assuming grains as spheres, which is proven to be untrue. Moreover, the errors in the prediction from these models were found to be very high. The nature of sand is unique in its kind possessing highly irregular particle shapes. Various studies presented in the literature have used mean sieve diameter as the characteristic diameter to predict the settling velocity of sands. After analyzing various sand particles experimentally, it was found that the mean sieve diameter is not a good presentation of sand's shape and size. However, none of the authors have presented a universally accepted analysis on the naturally available sands which can be used to estimate the settling velocity of sands accurately in Newtonian or non-Newtonian fluid. The models in the literature were found to be complex and the best amongst them was predicting the values with an error of 14.5%.

Although the factors influencing the settling velocity are well known, there is always a need for simulating the functional relationships among settling velocities, particles and the influencing parameters more accurately through modern experimental techniques. Spheres which form the basis and provides fundamental to understand the behavior of most of fluid particle system need to be studied in more detail. The applicability and use of the polymer index which has not been studied in detail need to be examined. Natural sands which occur in most of the industrial process like mining, petroleum, geotechnical, pipeline, slurry transports etc. need to be studied in detail. There does not exist an accurate settling velocity model exclusively for sands. The sand's shape and size which can form the integral part of many designing and other application also need to be studied in detail. The accurate measurement of the settling velocity, shape, and size of the particle increases the efficiency of processes involved and can lead to decrease in the cost involved. The settling velocity, particle size, and shape are important parameter in understanding the transport efficiency of vertical well. The critical velocity for an efficient bore hole cleaning and proper drilling operation is generally determined with the knowledge of single particle settling velocity in stagnant fluid [53]. Cuttings' slip velocity, fluidized bed reactor, transportation of oil sand tailing, drilling mud rheology, pump capacity, designing borehole, and pipeline design are amongst the few application of particle size, shape, and velocity in drilling and petroleum industry.

Keeping in mind the aforementioned needs, an extensive study on the concerned subject of fluid particle system has been conducted.

1.3 Objectives and Scope of the Study

The major objectives of this study are

- ✓ Designing and commissioning of shadowgraph setup for measuring settling velocity and geometry of a particle.
- ✓ Investigation of settling velocity of a spherical particle in Newtonian fluid.
- ✓ Investigation of settling velocity of Natural Sands in Water.
- ✓ Study of sand's shape and size using Shadowgraph approach.
- ✓ Investigation of settling velocity of spherical particle in Power Law fluid (CMC).
- ✓ Study of settling velocity of Natural Sands in Power Law fluid (CMC).
- ✓ Study of settling velocity of a particle in Yield fluid (Carbopol).

The first step of this study was to design and commission a shadowgraph setup which can capture the settling of the particle in a fluid medium. Keeping this in mind, an experimental setup has been designed, assembled, and calibrated properly. The calibration of the camera was done using a specially designed pattern of dots with specified distance between them. The plane for the calibration sheet determine the focal plane for the camera and the particles in the fluid medium are dropped with an aim of making them fall in the focal plane. The distance of the camera from the fluid column should be adjusted to have the field of view required to capture the particle efficiently.

The next phase of the study was to conduct the experiments using spherical particle in Newtonian fluid. To have a greater variation in the density and viscosity of the fluid medium different concentration of water glycerine mixtures were prepared. The rheological property of the fluid which governs the settling of the particle has been measured using the latest multifunctional Bohlin rheometer. The readings for each fluid were taken at least thrice so as to reduce the experimental error which might have occurred during the measurements. The spheres were then dropped in the plane of focus and keeping in mind it should not be close to the wall so as to avoid any wall effect. Three or more sets of measurements have been captured using the double frame camera with an illuminated laser background. Next step was to use Davis image processing software for processing the captured images. After processing the data, the output was checked for any noise that might have occurred during the experiments. The results from all the sets of experiments for same particle were averaged and final readings were then noted.

Next step to aforementioned procedure, the sand particles were analysed using PIS software. Apart from the pre experimental requirements, the sands were sieved properly and segregated into different sizes. Once sand particles were segregated, the experiments were conducted in the same manner as mentioned above for the sphere. The processing of images for sands required some alteration in the Davis software viz., the centricity value and size limit. A detailed statistical study of the sand size and shape has also been carried out.

Experiments were conducted on non-Newtonian fluid in yet another procedure. The Carboxy–Methyl-Cellulose (CMC) has been used in the study. Same experimental setup designed for the Newtonian fluid was used here. The mixing procedure of CMC in water requires some specific procedure which has been explained in detail in the experimental section of Chapter 2. Once the solution was prepared, the rheological measurement was conducted using the Bohlin rheometer under both controlled stress and controlled rate condition. In addition, the rheology of the fluid has also been carried out using high pressure and temperature cell under controlled rate and stress condition. The rheology of the fluid was cross examined using Fann 35 A viscometer at regular time interval during the course of experiment.

Four different concentration of CMC water solution has been prepared to have a varied range of fluid properties. Experiments using Spheres and natural sands were conducted and processed using the same procedure as mentioned in the aforementioned paragraphs.

In the last phase of the study, a detailed rheological study on the Carbopol solution was conducted. The mixing procedure of Carbopol in water is significantly different from CMC. Four different concentrations of Carbopol solution were prepared and the change in the rheological properties with the addition of NaOH was noted using rheometer. Due to the experimental constraint and complex fluid properties, study of the settling of particle could not be carried out, the details for which is explained in Chapter 8.

1.4 Methodology

In the current scenario optical techniques have been comprehensively used in the study of particles, gases or liquid in motion. Shadowgraph imaging techniques stand out to be one of the most powerful and inexpensive tool [50]. The Shadowgraph is based on the principle of difference between the refractive index of a body and its surrounding medium [51].With the presence of back illumination facility used in shadowgraph, the light rays does not get reflected from the object and thus produces a bright background while the refracted light ray from the interface gets dispersed and produces a dark spot.

The shadowgraph (backlighting) technique is a point measurement method and uses a non-intrusive optical image way for measuring particle's velocity and size. This technique is independent of the material and shape of the particle being observed [3].The Davis Particle Master shadow software used for the data processing is found to be an efficient image processing tools for estimating particle shape, velocity, size and other related statistical properties [52].

Particle Image Shadowgraph (PIS) experimental program has been designed and developed to measure the settling velocity, size, and shape for a particle in different fluid medium. Experimental investigation of settling velocity and size of four different sizes of glass spheres in water-glycerine, water, and CMC-water mixtures has been carried out using PIS technique. Different geometrical parameters and equivalent diameters for coarse and fine natural sands have been measured using PIS. The statistical analysis is performed on the measured results which gives a better insight into the shape and size distribution of natural sands. For spheres in power law fluid an improvisation in the existing settling velocity model has been done numerically.

The detailed investigation of settling velocity of natural sands particles of four different sieve sizes in water and power law fluid has been done using the developed PIS technique. For water an empirical equation for predicting settling velocity of sand in water has been developed using a new diameter called as equivalent circular diameter. For power law fluid different empirical correlation using numerous equivalent diameters has been proposed for predicting the settling velocity of sand particle. Multiple linear regression analysis is also performed to develop the relationship between the fluid rheological parameter and settling velocity of sand.

1.5 Structure of the Thesis

The experimental study and results obtained on measuring the settling velocity and other shape parameters for different particles in different fluid medium using particle image shadowgraph are presented here.

Chapter 1 gives a brief introduction about the topic and the research study.

Chapter 2 gives details about the experimental setup, its working, and the methodology to conduct the experiments using the given experimental setup i.e. particle image shadowgraph. A detailed discussion on the other equipment used during the study is also mentioned in this chapter.

Chapter 3 discusses in detail of the size and shape of the industrial sand. The size and shape measurement of the sand particle carried using PIS and different size and shape parameters have been reported. Moreover, a statistical analysis of the geometrical parameter has also been provided.

In Chapter 4, the discussion on the settling velocity of spherical particles in water, followed by the observed experimental results is presented. The detailed descriptions of the developed empirical model to predict the settling velocity and different available model present in the literature is also discussed.

Chapter 5 is dedicated to the study of the settling velocity of industrial sand in water. A comprehensive study on the geometrical parameters (shape and size) for different sieve sizes of sand particle is carried out using PIS. The experimental results on settling velocity and its variation with different shape and size parameters have been presented. The different settling velocity models available in the literature for sands are critically reviewed and discussed. In the next sub-section of the chapter the two developed empirical models to predict the settling velocity of sand in water is given and the steps to use the models are also mentioned.

Chapter 6 comprises the study on the settling velocity of spherical particles in Power Law type non-Newtonian fluid medium. The details about mixing procedure and rheology of the mixture of Carboxy-Methyl Cellulose with water are discussed. The other sub section contains the detailed measured experimental values for different glass spheres in power law fluids. An empirical model for predicting the settling velocity in Non-Newtonian fluid is also reported.

Chapter 7 discusses the detailed experimental investigation of settling velocity of natural sand particles in power law type non-Newtonian fluid. Empirical correlations, which use various equivalent diameter definitions, for predicting the settling velocity of sand particles using were developed and presented. Moreover multiple linear regression analysis the fluid rheological data has been performed and enhanced versions of the correlations are also presented. Last section of the chapter contains the error analysis in the predictions using different proposed correlations followed by a conclusion at the end.

Chapter 8 consist of detailed review of the complexities involved with the measurement of particle settling velocity in yield fluid. Rheological measurement for different concentration of Carbopol polymer in water that was carried out has been reported. The effect of NaOH titration on the rheological properties of Carbopol solution has also been studied experimentally and discussed.

Finally, Chapter 9, last chapter in the thesis, includes the major findings of this study and also key recommendation for future work that can be carried out in this field.

1.6 References

1. Pabst, W., Gregorová E., 2007 “Characterization of Particles and Particle systems-1”, ICT Prague.
2. Chhabra, R.P., 2002, “Sedimentation of particles in non-Newtonian media”, Hydrotransport, Vol. 15, pp. 135-148.
3. Pimentel, Gomes Rogerio., 2006, “Measurement and prediction of droplet size distribution in sprays”, PhD, Faculty of science and engineering, Laval University, Quebec.
4. Stokes, G. G., 1851, “On the effect of the internal friction on the notion of pendulums”, Cambridge Philo. Trans., Vol. 9, No. 2, pp. 8-106.
5. Rubey, W., 1933, “Settling velocities of gravel, sand, and silt particles”, American Journal of Science, Vol. 225, pp.117-119.
6. Gibbs, R.J., Matthews, M.D. and Link, D.A., 1971, “The relationship between sphere size and settling velocity”, Journal of Sedimentary Petrology, Vol. 41, No. 1, pp.7-18.
7. Peden, J.M., Luo, Y., 1987, “Settling velocity of variously shaped particles in drilling and fracturing fluids”, SPE Drill. Eng., Vol. 2, pp.337–343.
8. Mordant, N. and Pinton, J. F., 2000, “Velocity measurement of a settling sphere”, European Physical Journal B, Vol. 18, pp.343–352.
9. Brown, P., and Lawler, D., 2003, “Sphere drag and settling velocity revisited”, Journal of Environmental Engineering, Vol. 129, No. 3, pp. 222-231.
10. Hallermeier, R.J., 1981, “Terminal settling velocity of commonly occurring sand grains”, Sedimentology, Vol. 28, No.6, pp.859-865.
11. Cheng, N. S., 1997, “Simplified settling velocity formula for sediment particle”, Journal of Hydraulic Engineering, Vol.123, No. 2, pp.149-152.

12. Dietrich, W.E., 2009, “Settling velocity of natural particles”, Water Resources Research, Vol.18, No. 6, pp.1615–1626.

13. Ahrens, J.P., 2000, “A fall-velocity equation”, Journal of Waterway, Port, Coastal, and Ocean Engineering, Vol.126, pp.99-102.

14. Ahrens, J.P., 2003, “Simple equations to calculate fall velocity and sediment scale parameter”, Journal of Waterway, Port, Coastal and Ocean Engineering, Vol. 129, No.3, pp.146-150.

15. Dallon, D.S., 1967, “A drag coefficient correlation for spheres settling in Ellis fluids”, PhD Thesis, University of Utah, Salt Lake City, UT.

16. Prakash, S., “M. Tech Dissertation”, B.H.U, Varanasi, 1976 taken from Chhabra, R. P., 1993.

17. Reynolds, P. A., and Jones, T. E. R., 1989, “An experimental study of the settling velocities of single particles in non- Newtonian fluids”, International Journal of Mineral Processing, Vol. 2, pp. 47-77.

18. Lali, A. M., Khare, A. S., Joshi, J. B., and Nigam, K. D. P., 1989, “Behavior of solid particles in viscous non- newtonian solutions: settling velocity, wall effects and bed expansion in solid-liquid fluidized beds, Powder Technology, Vol. 5, No. 1, pp 39-50.

19. Chhabra, R.P., 1990, “Motion of spheres in power law (viscoinelastic) fluids at intermediate Reynolds numbers, a unified approach”, Chemical Engineering Process, Vol.28, pp.89–94.

20. Acharya, A., Mashelkar, R. A., and Ulbrecht, J., 1976, “Flow of inelastic and viscoelastic fluids past a sphere”, Rheological Acta, Vol. 15, pp. 454-461.

21. Warg, J B., 1973, “An analysis of methods for calculating constant terminal-settling velocities of spheres in Liquids”, Mathematical Geology, Vol. 5, No. 1, pp. 59-72.

22. Chhabra, R. P., 1993, “Bubbles, drops, and particles in non-Newtonian fluids”, CRC Press, Inc., Boca Raton, FL.

23. Talmon, A M., and Huisman, M., 2005, “Fall velocity of particles in shear flow of drilling fluids”, J. Tunnelling and Underground Space Tech. incorporating Trenchless Tech.Research, Vol. 20, No. 2, pp. 1-12.

24. Koziol, K., and Glowacki, P., 1988, “Determination of the free settling parameters of spherical particles in power law fluids”, Chemical Engineering Process, Vol. 24, pp. 183-188.

25. Shah, N Subhash, Fadili, EI Youness, and Chhabra, R.P., 2007, “New model for single spherical particle settling velocity in power law (visco-inelastic) fluids”, International Journal of multiphase flow, 33, pp. 51-66.

26. Kelessidis, V.C., 2004, “An explicit equation for the terminal velocity of solid spheres falling in pseudoplastic liquids”, Chem. Engineering Science, Vol.59, pp.4437–4447.

27. Kelessidis, V.C., 2004, “Terminal velocity of solid spheres falling in newtonian and non-newtonian liquids”, Tech. Chron. Sci., 24, pp.43–54.

28. Shah, N Subhash, Fadili, EI Youness, and Chhabra, R.P., 2007, “New model for single spherical particle settling velocity in power law (visco-inelastic) fluids”, Int. J. of multiphase flow, 33, pp. 51-66.

29. Roux Le, J P., 2005, “Grains in motion: A review”, Sedimentary Geology, Vol.178, pp. 285–313.

30. Le Roux, J.P., Brodalka, M., 2004, “An Excel-VBA program for the analysis of current velocity profiles”, Computers & Geosciences, Vol.30, pp.867–879.

31. Chhabra, R P., and Madhav, Venu G., 1994, “Settling velocities of non-spherical particles in non-newtonian polymer solutions”, Powder Technology, Vol. 78, pp. 77-83.

32. Chhabra, R P., and Agarwal, Neha., 2007, "Settling velocity of cubes in newtonian and power law liquids", Powder Technology, Vol. 178, pp. 17-21.

33. Harris, K Courtney, 2003, "Sediment transport processes in coastal environments", a part of online class lecture, Virginia Institute of Marine Science.

34. Deosarkar, P., Manik, Sathe., S, Vivek., and Chandra, Ghamta Kartik., 2010, "C_D-N_{Rep} relationship for solid-liquid suspensions", Int. J. of chemical engineering and applications, Vol. 1, No.1, pp.10-14.

35. Ferguson, R I., and Church, M., 2004, "A simple universal equation for grain settling velocity", Journal of Sedimentary Geology, Vol.74, pp. 933-937.

36. Shah, S.N., 1982, "Proppant settling correlations for non-Newtonian fluids under static and dynamic conditions", Trans. AIME 273 (Part 2), pp. 164–170.

37. Shah, S.N., 1986, "Proppant settling correlations for non-Newtonian fluids", SPE Prod. Eng. (Nov), pp. 446–448.

38. Hasani, Samira., Maleki-Jirsarei , Nahid., and Rouhani, Shahin., 2011, " Irregular motion of a falling spherical object through non-Newtonian fluid, Physics Department, Sharif University, Iran, cited from Research gate.

39. Rajitha,P., Chhabra, R P., Sabiri, N E., and Comiti, J., 2006, "Drag on non-spherical particles in power law non-Newtonian media", Int. Journal of Mineral Processing, Vol. 78, pp. 110-121.

40. Shi, Zhong., Zhou, Jun Hua., Eittreim, L Stephen., and Winterwerp, Johan C., 2003, "Settling velocities of fine suspended particles in the Changjiang Estuary, China", Journal of Asian Earth Sciences, Vol. 22, pp. 245–251.

41. Migniot, C., 1977, "Action of currents, waves and wind on the sediments", White coal, Vol.1, pp. 9-47.

42. VanRijn, L.C., 1997, "Sediment transport and budget of the central coastal zone of Holland", Coastal Engineering, Vol. 32, pp. 61-90.

43. Ibad-Zade, Y A., 1992, "Movement of sediment in open channels", translated by S.P. Gosh, Russian Translator series, Vol. 4.

44. Shah, Y.Q., 1956, "Basic principles of sediment transport", J. of Sediment Research, Vol. 1, No. , pp. 1-54.

45. Zhang, R.J., 1989, "Sediments dynamics in rivers", Water Resources press.

46. Sadat-Helbar, S.M., Amiri-Tokaldany, E., Darby, S., and Shafaie, A., 2009, "Fall Velocity of Sediment Particles", IASME/WSEAS International Conference on Water Resources, Hydraulics and Hydrology, pp.39-45.

47. She., K., Trim, L., and Pope, D., 2005, "Fall velocities of natural sediment particles: a simple mathematical presentation of the fall velocity la", J. of Hydraulic Research, Vol. 43, No. 2, pp. 189-195.

48. Jimenez, J. A., and Madsen, O.S., 2003, "A simple formula to estimate the settling velocity of natural sediments", J. of waterway, port, coastal, ocean engineering, ASCE, Vol. 129, No. 2, pp. 70-78.

49. Soulsby, R.L., 1997, "Dynamics of marine sands", Thomas Telford, London.

50. Garcia-Castrejon, R., Pita-Castrejon, J.R., Martin, G.D., and Hutchings, I.M., 2011, "The shadowgraph imaging technique and its modern application to fluid jets and drops", Revista Mexicana De Fi'Sica, Vol. 57 (3), pp. 266-275.

51. Kowalewski,Tomasz A., 2004, "Experimental methods for quantitative analysis of thermally driven flows", Department of Mechanics and Physics of Fluids, IPPT PAN, Polish Academy of Sciences Warsaw, Poland.

52. Fountain, M S., Blanchard, J., Erikson, R L., Kurath, D E., Howe, D T., Adkins, H., and Jenks, J., 2012, "Design of a Particle Shadowgraph Velocimetry and Size

(PSVS) System to Determine Particle Size and Density Distributions in Hanford Nuclear Tank Wastes – 12280", WM2012 Conference, Arizona, USA.

53. http://petrowiki.org/Cuttings_transport, cited on March 3, 2014.

Chapter 2

Particle Image Shadowgraph, Experimental Setup, and Instrumentation

In this chapter experimental facility and instruments used for measurements are described in different subsections. In the first part, the particle image shadowgraph setup designed for the study has been presented with details of the associated components. The next section contains the description about the material used in the study. It is divided into two subsections solids and fluids; in which the detail of the particles and different fluids used in the study has been discussed. Next section discusses the different rheology measurement tools used during the study with the steps require to operate the instruments. Introduction to shadowgraph technique, working principle, and shadowgraph's components are explained in detail. Calibration procedure for the camera and experimental procedure to measure the settling velocity of particles are presented in detail. The last section consists of best recommendations to avoid possible sources of problems, sources of errors, and difficulties associated with the PIS.

2.1 Description of the Experimental setup

Figure 2-1 is a schematic of the Particle Image Shadowgraph setup and its elements. The experimental setup mainly consists of the following parts: Lavision Image Intense camera, 12X navitar lens, Cubical fluid container, Lavision Davis 8.0 software, Diffuser, Lavision illumination high efficiency diffuser, and New Wave Research laser solo III.

The Particle Image Shadowgraph has been used to measure the settling velocity of particle in different fluids. The designed experimental setup is shown in figure 2-2.The experimental setup mainly consists of four segments

An Illumination Source	Fluid Particle Column
An Image Acquisition Facility	A data processing software

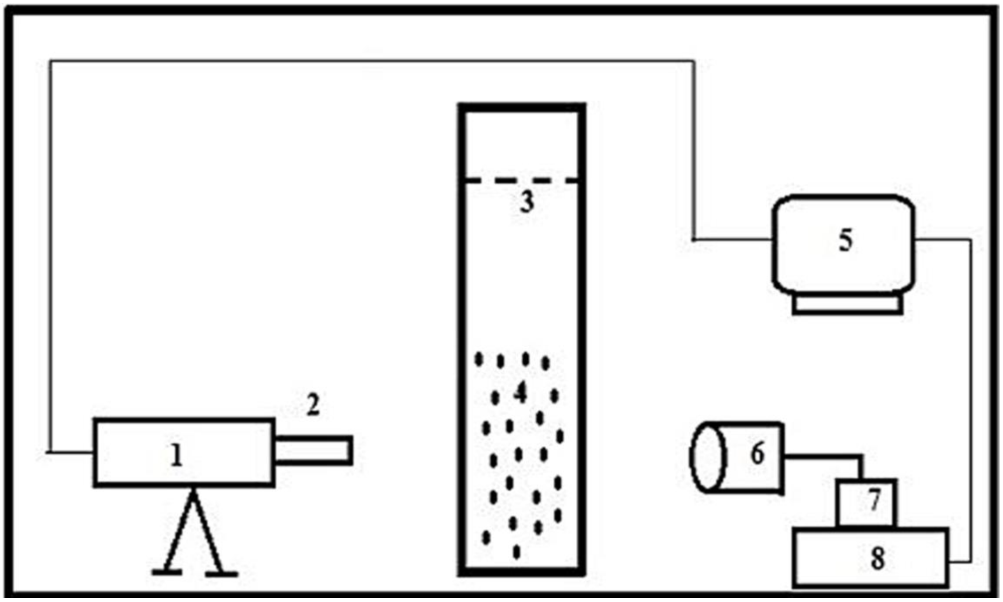

Figure 2-1: Schematic of the experimental setup for measuring settling velocity using PIS [1. Lavision image intense camera 2. 12 X Navitar Lens 3. Fluid medium 4. Particle 5. Lavision Davis 8.0 6. Diffuser 7. Lavision illumination high efficiency diffuser 8. New Wave research laser solo III 15Hz]

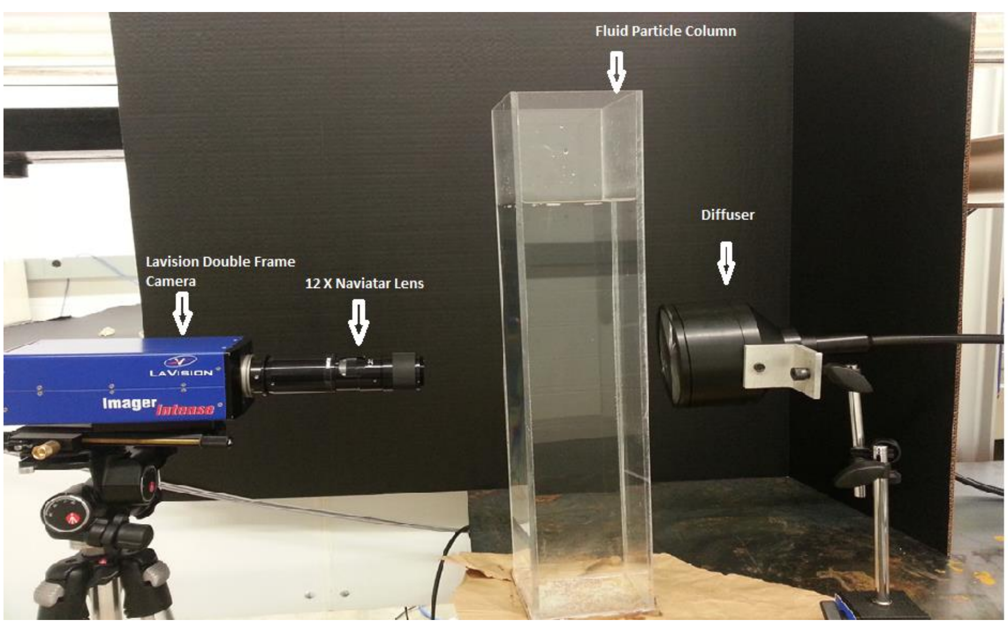

Figure 2-2: Image of the experimental facility

2.1.1 Illumination source

The illumination source is comprised of a double impulse Solo III Class 4 Laser with a frequency of 15 Hz attached to a high efficiency circular diffuser by Lavision. The illumination source is placed at 20 cm above the base and 10 cm away from the fluid particle column.

2.1.2 Fluid particle Column

The fluid particle column is a transparent cuboidal column made of plexi-glass of height 70 cm. Different fluids like water, glycerine-water mixture, CMC-water mixture, and Carbopol-NaOH-Water mixture have been used as fluid medium for different set of experiments. The particle used during the studies includes four different sizes of glass sphere, plastics spheres, and industrial sands.

2.1.3 Image Acquisition Facility

The image acquisition section consists of a double frame camera (Lavision image intense) and a 12X Navitar lens. One can use an adapter along with the lens to increase the zooming capability required when capturing very small particles typically of size less than 500µm. The field of view greatly depends on the type of lens used and the distance between lens front and point of interest. The special feature of the camera is the adjustable recording frequency. One need to fix the frequency as per particle's size and settling velocity so as to allow the camera to capture the particle's image in the field of view during that particular frequency. A double-pulse laser combined with a double frame camera allows investigating size dependent velocities [1].

2.1.4 Image Processing Software

Davis 7.2 software has been used for the image processing. The sizing algorithm consist of two steps first one is to locate the particles in the given field of view and the second step is to analyze it for size, position and shape [1]. The displacement of particles between two consecutive frames is used to calculate the velocity of the particle as shown in Figure 2-2. Recognition is based on the difference between the image intensity. The user interface for the Davis software with brief detail of the different options is shown in figure2-3.

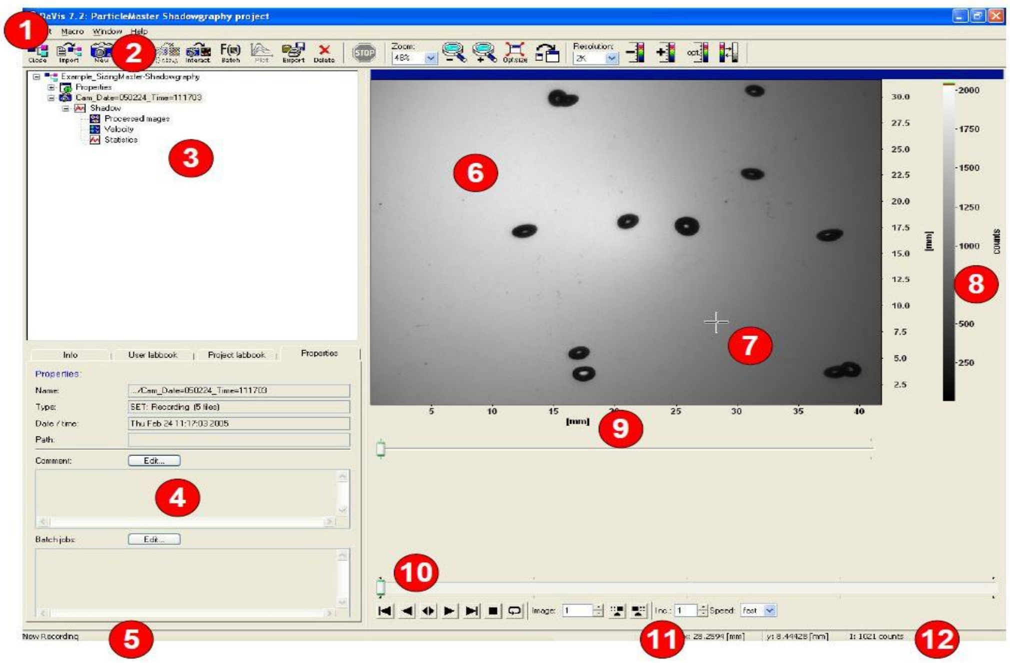

Figure 2-3: User interface in DAVIS

1- Menu Bar: Contains different option from managing files to window settings. One can access the inbuilt help tutorial using menu bar.
2- Tool Bar: Different tools options like calibration, scaling, zoom in, recording etc.
3- Tree View: Shows the structure of the stored results.

4- Info Box: Gives details about the undergoing process like recording, batch process etc.

5- Status Line: shows the information about the process of the task.

6- Show the real time images, gives visuals of the image to be captured or that which has been captured by the camera.

7- Cursor: Used to see the stored information of the captured image like coordinate, pixels etc.

8- Intensity Scaling: Give information about the counts, velocity, other data based on the assign color gradient. The same color gradient is also assigned to the image.

9- Camera Scaling: shows the field of view and image dimensions.

10- Movie Slider: This slider can be used to display the individual images of the image sequence.

11- Scaled x/y position: it shows the value of one pixel in real coordinates and also the frame information.

12- Pixel Intensity: It gives information about the counts assigned to the pixel. The count should not be more than 4000 at any point in the captured image.

2.2 Materials

The different materials used during the course of the study are given below

2.2.1 Solids

Two solid particles are used during the study. The detail is given in below sub sections.

2.2.1.1 Sand

Table 2-1 and Table 2-2 are the reported properties of the sand particles. Note that the most important property in these experiments is the specific gravity of both sand particles. The sand particles of size 0.35 -1.2 mm procured from Sil Inc. were used in this study.

Table 2-1: Physical properties of fine sand

Property	**Test Method**	**Unit**	**Typical values**
Mineral	Petrographic	………	Quartz
Shape and hardness	Visual	Mohr	Sub Angular/6.5
pH	AFS	……….	7.2-7.4
Specific gravity	ASTM C-128	……….	2.65
Bulk Density, aerated	ASTM C-29	Lbs/Ft^3	92-95
Compacted	ASTM C-29	Lbs/Ft^3	98-100

Table 2-2: Physical properties of coarse sand

Property	**Test Method**	**Unit**	**Typical values**
Mineral	Petrographic	………	Quartz
Shape	Krumbein	………	Sub Angular
Hardness	Moh	6.5	
Specific gravity	ASTM C-128	……….	2.65
Bulk Density, aerated	ASTM C-29	Lbs/Ft^3	92-95
Compacted	ASTM C-29	Lbs/Ft^3	98-100

2.2.1.2 Glass Sphere

Four different sizes of glass sphere (Corposular’s Glass Spacers Millibeads) have been used in the study. These spheres have high precision in dimensions and shape. The specification of the glass sphere used in the study is given in table 2-3.

Table 2-3: Specification of glass spheres as given by manufacturer

Diameter (Manufacturer Data) (mm)	Specific Gravity
0.71±0.02	2.51
2±.04	2.51
1.18±0.02	2.51
1.5±0.03	2.51

2.2.2 Fluids

2.2.2.1 Water Glycerine Mixture

Glycerine ($C_3H_8O_3$), is transparent Newtonian fluid which readily dissolves in water. Glycerine for this study has been procured from Acros Organics ltd and the product specimen for it is given below in Table 2-1.The product specification is taken from the site of the manufacturer [9] and is given in table 2-4.

Table 2-4: Product specification for Glycerol

Appearance	Clear liquid
Color Scale	=<10 APHA
Separat. Techn.GC	>=99.5 %
Water	=<0.5 % (Coulometric)
UV	(0.5 M in water) at 260 nm A: =<0.06 at 280 nm A: =<0.02
Acidity (CH3COOH)	=<0.003 %
pH	6 to 7 (10% soln. at 25°C)
Dnase,Rnase,Protease act.	none detected
Aldehyde	=<0.001 %

2.2.2.1.1 Fluid Preparation

The mixing procedure for this is simple and requires a hand mixer of adjustable rpm to mix it. The water is poured inside the bucket and a vortex is created with the use of hand mixer. The entire setup is shown in the figure 2-4. The glycerine is poured in the vortex as slowly as possible so as to ensure proper mixing.

Figure 2-4: Mixing facility used for Water-Glycerine mixture

2.2.2.1.2 Fluid Rheology

Three different classes of Cannon Fenske Viscometers (SR25 135, SR100 461, and SR150 798) were used for measuring the kinematic viscosity of different concentration (0%-40% by volume) of glycerol in Glycerol water mixture. The mixtures properties are given in Table 2-5.

Table 2-5: Water-Glycerine mixture properties

Fluid Type	Density (kg/m^3)	Viscosity (cSt)
Glycerine_Water (10% Glycerine)	1028	1.26
Glycerine_Water (20% Glycerine)	1037	1.65
Glycerine_Water (30% Glycerine)	1068	2.69
Glycerine_Water (40% Glycerine)	1180	5.93

2.2.2.2 Carboxy Methyl Cellulose Mixture

Carboxy Methyl Cellulose is the sodium salt of carboxy methyl cellulose [10]. It is cellulose ether, produced by reacting alkali cellulose with sodium monochloroacetate under rigidly controlled conditions [11]. The structure of CMC is shown in figure 2-5.

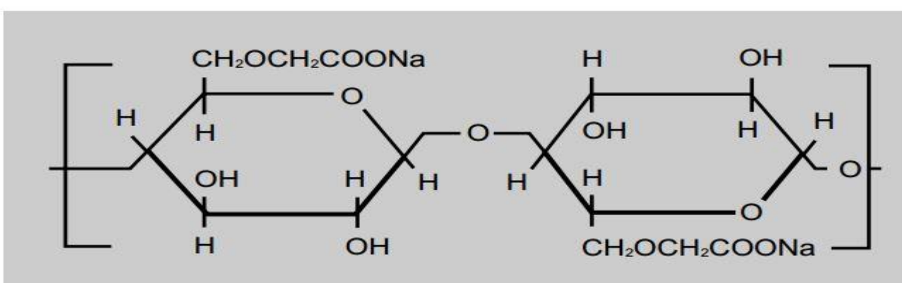

Figure 2-5: Idealized unit structure of Carboxy Methyl Cellulose [11]

2.2.2.2.1 Fluid Preparation

The CMC is not easy to dissolves and a good dispersion can be achieved by proper mixture procedure. The Hamilton beach three speed mixer has been used for the purpose (see figure 2-6). A 350 ml of water in the container is taken and at medium rpm mode of the mixer it is allowed to form the vortex. The quantity of CMC required to mix in the water is taken and is slowly introduced in the vortex. It takes around 6-7 minutes to introduce one gram of CMC in water. Once the entire polymer is poured into water it is allowed to mix for another one minute. Taking larger quantity of water at a time or lower rpm, or an increased rate of pouring can lead to the formation of a non- homogeneous fluid.

Figure 2-6: Hamilton Beach three speed mixture

2.2.2.2.2Fluid Rheology

The rheology of the polymer solution has been obtained using the controlled stress mode of Bohlin rheometer. Three different polymer solutions have been prepared following the above mentioned mixing procedure. The rheology curve measured for the mixture is shown in Figure 2-7. The measured rheological parameter (flow index 'n' and consistency index 'K') for CMC mixture is given in table 2-6.

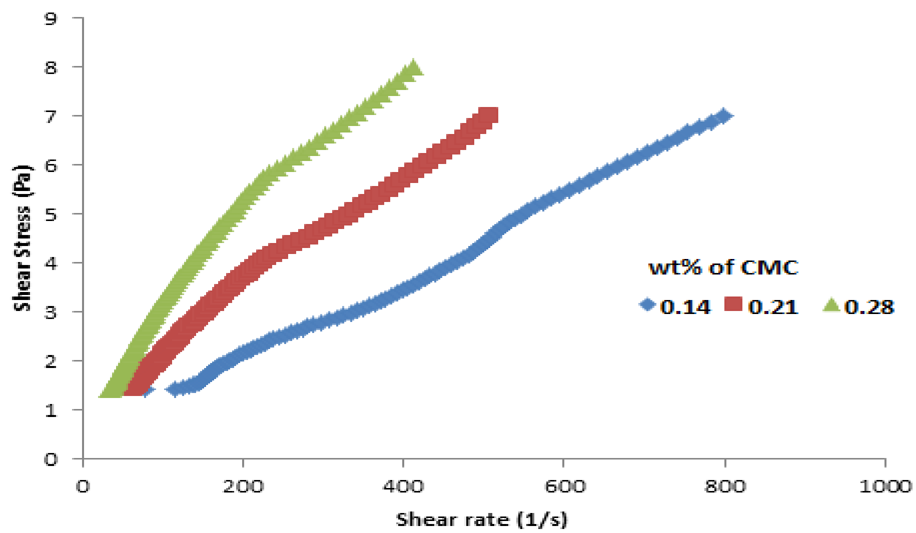

Figure 2-7: Shear stress vs shear rate for CMC

Table 2-6: CMC rheological parameter

Fluid	n	K (Pa s^n)
CMC 0.143 (wt%)	0.8177	0.0277
CMC0.2142 (wt%)	0.7407	0.0697
CMC0.2857 (wt%)	0.7142	0.1162

2.2.2.3 Carbopol

Carbopol is a polymer known to exhibit a yield stress [7]. The carbopol 940 used in the study has been procured from Acros organic ltd. The molecular structure of it is shown in figure 2-8. The average size of the Carbopol particle is 0.2µm and after absorbing the water yields a value of around 3.9 µm.

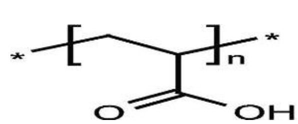

Figure 2-8: Carbopol molecular structure [13]

Carbopol mixture exhibits little or almost no thixotropy (manual). The very low wt% of carbopol mixture does not have a measurable yield stresses (16). The product specification has been taken from the Acros organic website and the details of the Carbopol 940 are given in table 2-7 [12].

Table 2-7: Product specification for Carbopol 940

Appearance	white powder
Infrared spectrometry	Authentic
Loss on drying	=<2 %
Heavy metals	=<10 ppm (Hg, Pb, As, Sb)
Viscosity	40000 to60000 cP (Brookfield,20rpm,25C) (neutralized soln.,420nm,0.5% dispersion)
Clarity of solution	>=85 % transmission (neutralized soln., 420 nm, 0.5% dispersion)
Residual solvents	=<0.5 % (benzene)

2.2.2.3.1 Fluid Preparation

It is difficult to dissolve this polymer into water because of the cross-linked structure and low density. A magnetic stirrer (see figure 2-9) with rpm 800-1200 is suggested to mix the polymer into the water. The polymer has been mixed with water at 950 rpm.

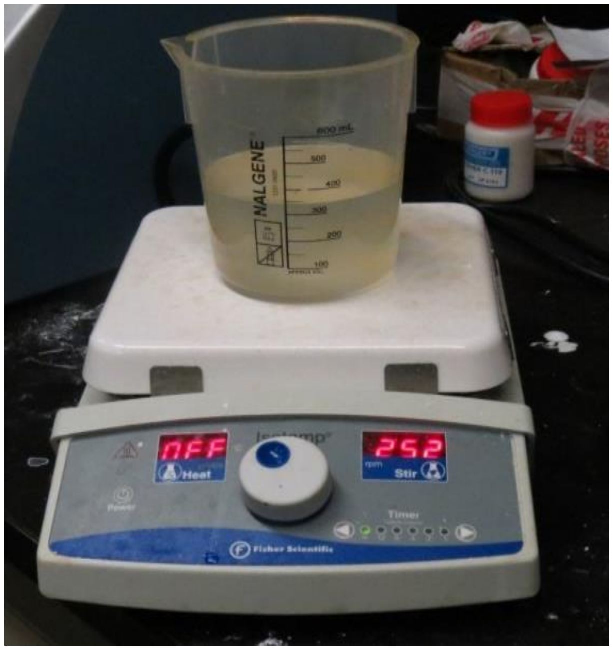

Figure 2-9: Magnetic stirrer

A small quantity of water (350 ml) was taken and put on the magnetic stirrer till a proper vortex is formed. Now the carbopol is introduced with a very slow rate to the agitating water. While introducing it in water one has to make sure that its lump free. It took around 23-25 minute to introduce 1 gm of carbopol in the water.

2.2.2.3.2 Fluid Rheology

Carbopol molecules consist of some linear chain polymer impurities which are responsible for a network like structure for the polymer when dissolved in solvent. Gutowski (2010) Rheological properties of the carbopol mixture exhibit a drastic change in yield value with change in pH. The yield values found to be drastically changing with the solution pH. The measured rheological properties of the sample Carbopol solution with NaOH added to it is shown in figure 2-10 and 2-11.

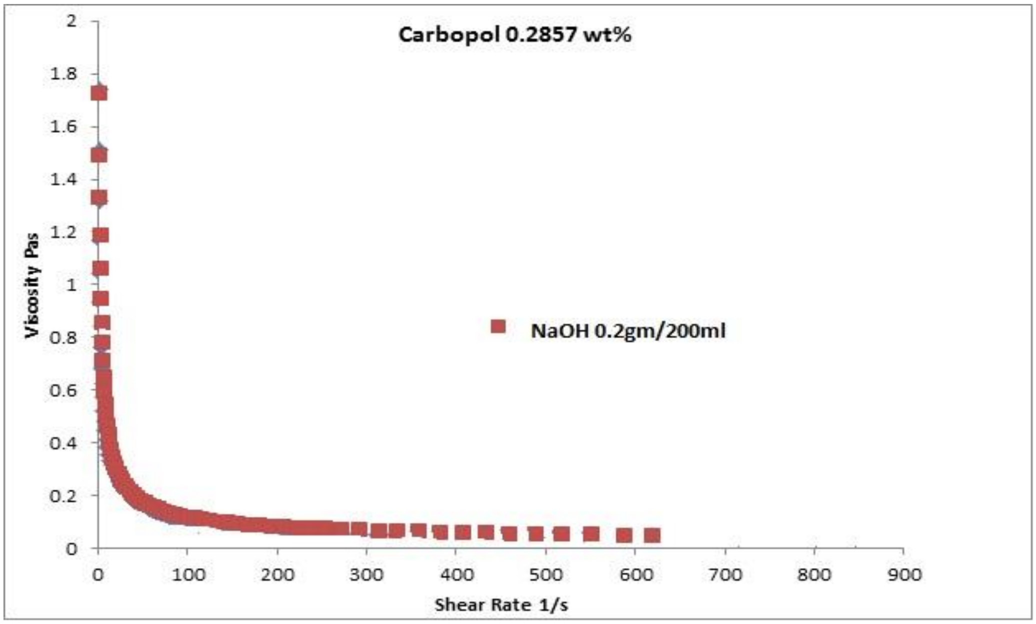

Figure 2-10: Viscosity versus shear rate for Carbopol solution

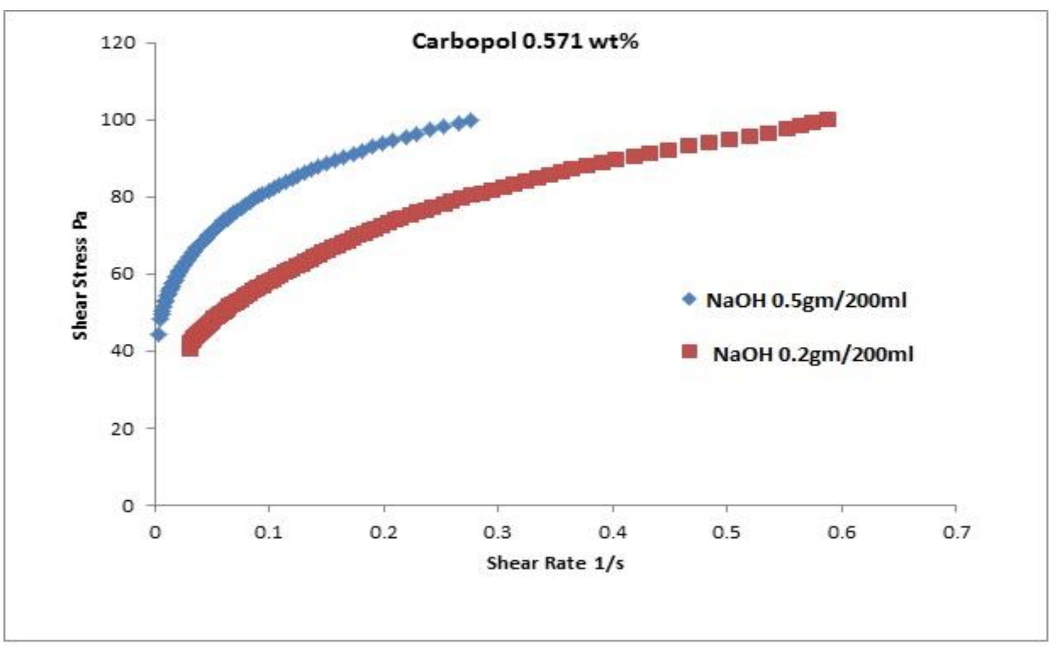

Figure 2-11: Shear stress versus shear rate for Carbopol solution

2.3 Rheology Measurement Tools and Techniques

The important component of the experimental procedure is to accurately measure the rheology of the fluid. Different instruments like BOHLIN rheometer, Fanning Viscometer, and Canon-Fenske viscometer has been used for the rheological measurement.

2.3.1 BOHLIN Rheometer

The rheology of the CMC and Carbopol mixture used in the study has been tested by a BOHLIN C-VOR 150 modular rheometer. The rheometer (figure 2-12) is equipped triple motor controls which allow for the controlled stress, strain, and shear rate measurements [6]. The two different facility the plate and High Temperature High Pressure (HTHP) chamber have been used based on the fluid's behavior. For the highly viscous fluids the normal plate method has been used, while for the low viscous fluid HTHP chamber is prefered. The controlled stress mode has been used in this study. The temperature and pressure for HTHP chamber has been maintained at room condition.

Figure 2-12: Bohlin rheometer with two different modes

The Bohlin rheometer is operated remotely by using the software provided by the manufacturer as shown in figure 2-13. At the start of the software one need to select the type of mode going to be used i.e. plate or high pressure cell. The next is to select the type of study going to be conducted, here in this study viscometry is selected. Once the viscometry mode is active one need to make sure that the measuring system is CP 4^0/40 mm for peltier i.e. plate mode and Titanium bob for high pressure mode. Another important factor to be considered is to enter the temperature at which the fluid needs to be tested; in this study 22^OC is used. The final step is to enter the range of values (i.e. the maximum and minimum) for stress or rate and click on the table of stress option from the drop down menu. In this study the controlled stress option has been deployed for measuring the rheology of the fluid. Once the process starts the values of stress, strain viscosity, temperature are recorded by the software which can be exported to excel. The readings with 1 remark should be neglected while processing the data.

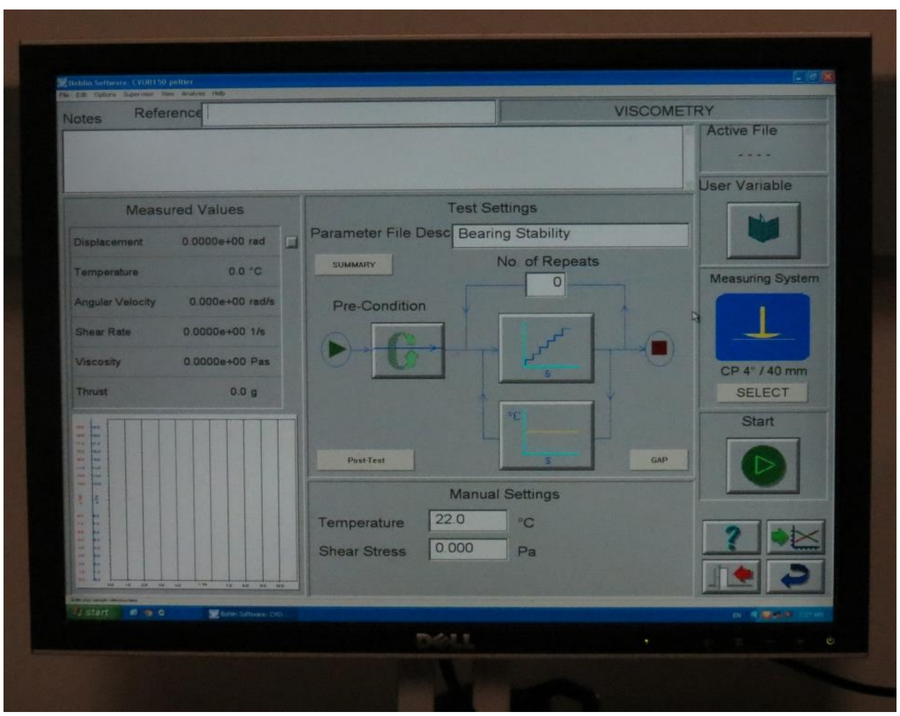

Figure 2-13: User interface for Bohlin rheometer software

2.3.2 Cannon-Fenske Viscometer

Rheology measurement for Glycerine-Water mixture is done using the Cannon-Fenske viscometer (see figure 2-14). This viscometer is used for measuring kinematic viscosity of transparent Newtonian liquids, particularly petroleum products or lubricants, according to ASTM D 445 and ISO 3104 [8] **(**figure 2-15). Three different class of Cannon Fenske Viscometer (SR25 135, SR100 461, and SR150 798) are used for the measuring the rheology of different concentration of glycerol and water mixture. The important property of this class of viscometer is that as the SR number decreases it becomes more suited for measuring lower viscosities. The Fischer Scientific traceable Stopwatch which is accurate to microsecond is used for measuring the time for the experiment.

Figure 2-14: Cannon-Fenske viscometer

2.3.3 Fann Viscometer

The Fann viscometer 35A/SR12 (see figure 2-15) has been used to monitor any change in the fluid's property during the course of experiments. It is used to provide quick information on the fluid's rheology. This instrument is equipped with 12 speed mode and twelve readings of shear stress can be measured at different rpms.

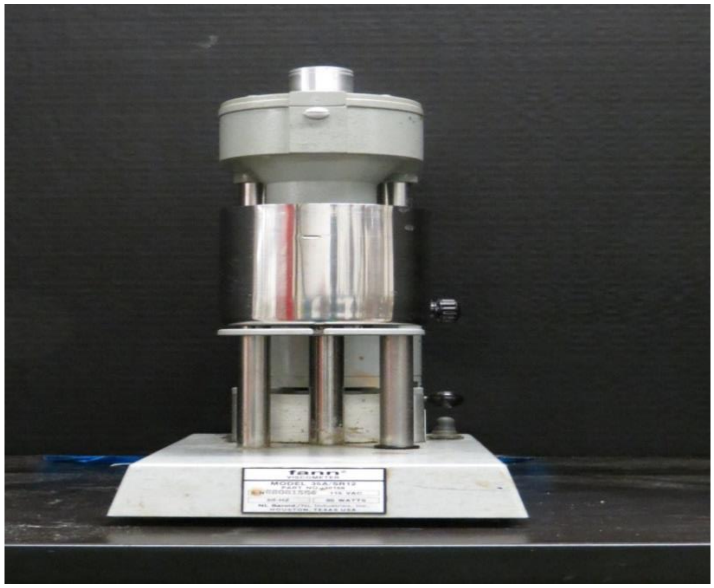

Figure 2-15: Fann 35 A 12 speed viscometer

2.4 Shadowgraph

The Shadowgraph technique is based on a simple optical principle in which a light source and a recording device are required. Since the light source is unable to pass through solid or opaque objects, light must refract around the object allowing for the formation of shadows, which is captured by the recording instrument. The general principal associated with this phenomenon is that a shadow is casted whenever there exists significant change in the densities of medium in which the light is passing through. This technique generates a series of shadow images from the focal plane of the camera to be projected on screen; allowing particles to be visualized. As some light rays are refracted, the ones remaining un-deflected will appear as dark marks captured by the instrument.

The modern Shadowgraph technique, which is being used for visualizing microscopic droplets from spray or particle of micron size in fluids, is based on high resolution imaging with pulsed backlight illumination. This technique is independent of the shape and material (eg. Transparent, translucent or opaque) of the particles, and allows for the investigation of sizes down to 5µm when using the appropriate imaging system and light source [1]. The typical hardware setup for the shadowgraph is shown in figure 2-16.

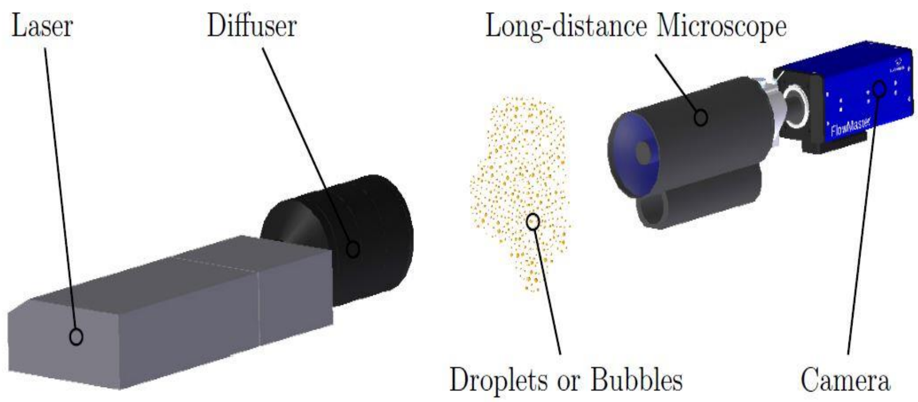

Figure 2-16: Typical hardware setup of the particle master shadowgraph[1]

The light source and camera type depends on the type of use. The light source could be a pulsed laser with special illumination optics or a flash lamp. Using a short laser pulse as illumination it is possible to freeze motions of more than 100m/s. A double-pulse laser combined with a double frame camera enables the investigation of size dependent velocities [1].

[1] The image is taken from product manual for Davis 7.2, 2010

2.4.1 Working Principle of LaVision Shadowgraph

Shadowgraph follows different algorithms to measure size and velocity. For size measurement the software follow the two steps; the first is to locate the particles in the box i.e. area of interest (generally the dimension of it is given based on the field of view) second step is the particles in this box are analyzed separately for size, shape and position. Recognition is based on the difference between the intensity of the image.

Generally a double pulse source and a double frame camera are used for measuring the velocities of individual particles. Before proceeding for the calculation of particles' velocities the sizing algorithm is applied to each frame of the source image [1]. The sizing algorithm is applied to each frame of source images before the velocity calculation. The velocity is calculated based on the x and y shift between the two consecutive frames and Δt. Where, Δt is the time difference between the two frames (see Fig. 2-17).

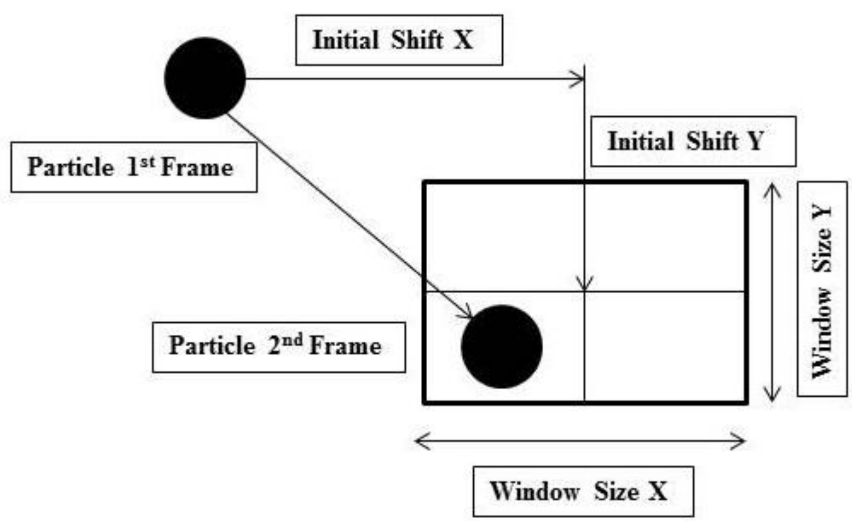

Figure 2-17: Illustration of interrogation window used to determine velocities of particle

2.4.2 Shadowgraph Components: Description and Details

2.4.2.1 CCD Camera and Lenses

A double frame CCD camera has been used for image acquisition (figure 2-18). A CCD (charge coupled device) camera converts photons to electric charge based on the photoelectric effect. The unique feature i.e. the double frame mode of the camera allows taking two separate exposures within a very short time delay in different frames. The acquisition of two frames usually needs to be synchronized to a pulsed light source as the exposure times for both frames are quite different [5]. A double impulse Solo III Laser has been used and synchronized with the camera for image acquisition. The time interval between two images is adjusted depending on the field of view and velocity of particle.

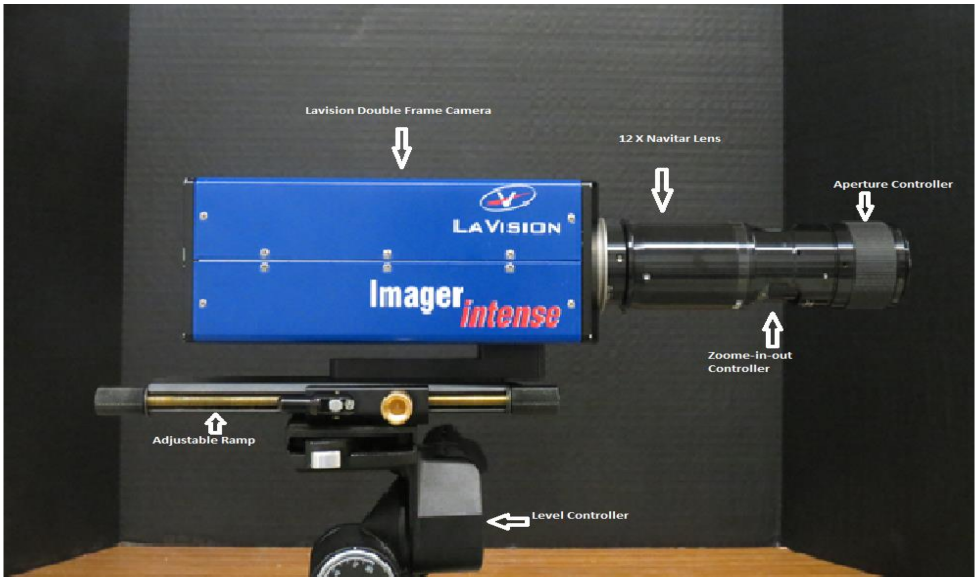

Figure 2-18: Lavision double frame camera and lens

Here in this study a 12 X Navitar is used. The field of view with the current setup is between 3x3 to 15x15 mm. The use of 2 X adapter along with the lens leads to more zoom in and can be used to capture very small particles. This lens is suitable for working distance of 32mm-341mm with maximum magnification of 12.

2.4.2.2 Double Pulsed Laser

A double pulsed Nd:YAG solo laser from New Wave Inc. is used as the illumination source for shadowgraph experiments. The laser is capable of emitting two pulses of light in adjustable assigned time period. The wavelength of the laser light is 532 nm with 15 Hz frequency. The laser is connected to the Lavision circular diffuser at the end [14].

2.4.2.3 Lavision Diffuser

The circular Lavision diffuser is used for strobe background illumination purposes as required in shadowgraph. The wavelength conversion facility located inside the diffuser provides a speckle free backlighting with ultra-short light pulses of high intensity. Diffuser has an input aperture of 9 mm and an output aperture of 120 mm. The minimum recommended laser power for the diffuser is 100 mJ or 527-532 nm with output wavelength of 574-580 nm and pulse duration of 20 ns [15].

2.4.3 Calibration of the Camera

Calibration is the process of assigning a pre known distance value between two points, and scaling the captured image accordingly. This is essential to convert the image's pixel into a real coordinates. One should note that the position of camera should not be disturbed during the course of calibration and image acquisition [2], [3]. There are different methods for the calibration but in this study a designed calibrated target has been used. The experimental setup is calibrated using a specially designed spherical dots pattern using MS Visio. Each circle printed at diameter of 0.8mm with spacing of 1.5mm as seen in figure 2-19. One of the basic requirements for the designed target sheet is that the dots should be black in color with a white background. The dots can be replaced with any known shape but of fixed dimension but it is always convenient to use circle. This calibration technique which is done with respect to x and y axis leads to less image distortion and better accuracy as compared to ruler or scale [4].

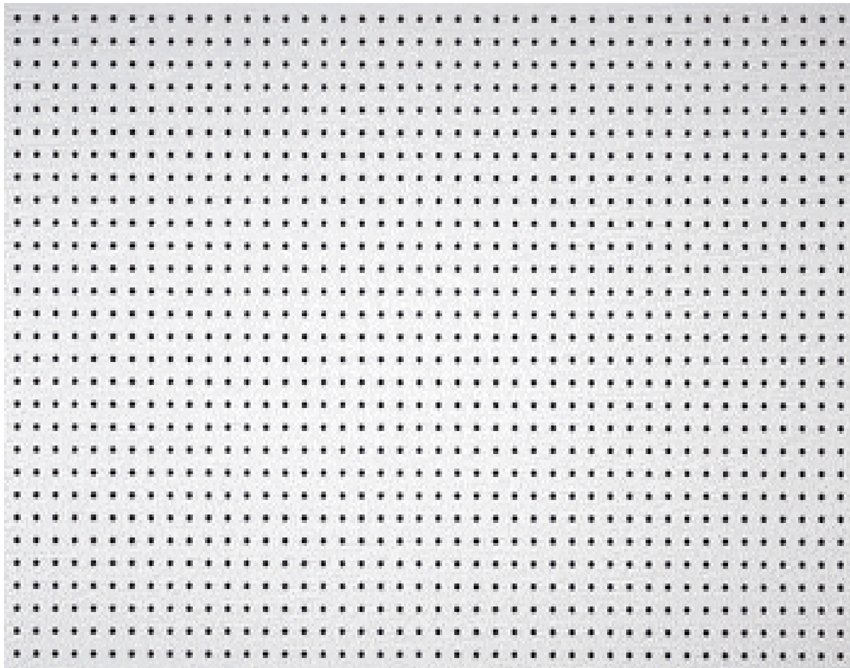

Figure 2-19: Calibration target used for calibrating the camera

The calibration is conducted in the real fluid medium and a plate with the printed sheet of dot pattern is inserted in the cubical container containing fluid. Adjust the camera lens in such a way that complete focussed image of the calibration sheet can be captured. Once the image of the calibration sheet is captured the 2 dimensional calibration process given in the Davis7.2 software is followed. In the calibration process, the distance between the circle and the diameter value is entered. Now in the next step a centre circle is chosen, generally it should be the one in the centre of the sheet (see the marked blue colour circle in figure 2-20). Next, two adjacent circles (i) right side circle (ii) top circle with respect to the centre circle are selected. The next step is performed by Davis software to find 25 circles in 5 by 5 square grid block to have a better calibration efficiency. The last step, i.e. the scaling up of the image and axis is automatically performed by the software using the dimensions assigned previously [5].

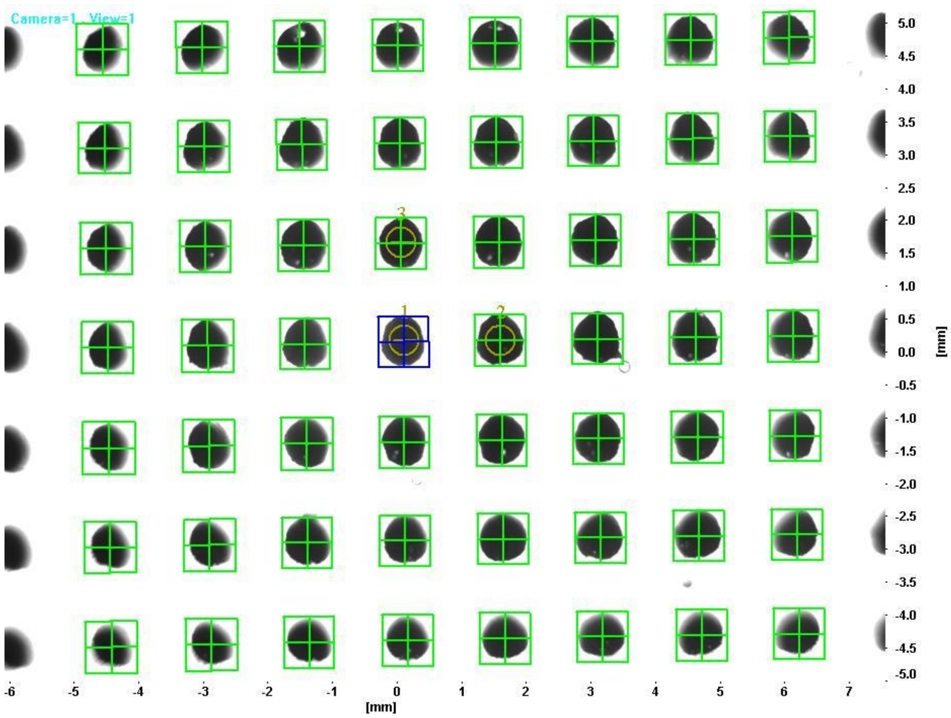

Figure 2-20: Calibration target after the calibration process from Davis software

2.5 Experimental Procedure

- The procedure for obtaining empirical data was split into two components; the physical setup of the experiment and the processing of data.
- Approximately 7l of water was transferred to a plexi glass cubical container (8cm x 8cm x 70cm) as depicted in Figure1. Let water settle for 24 hours or stir gently to minimize the air bubbles, which would result in image noise.
- Position the double frame camera, and laser and diffuser on opposite sides of container. Insert glass with calibration sheet attached.
- Connect camera to LaVision computer, then open Davis 7.2 processing software.

- Adjust the camera with 12X lens to focus on the points on the calibration sheet in a box of 10mm by 10mm. Distance between the points is 1.5mm, points have diameter of 0.8mm.
- Create a new file with Particle Master Shadowgraph as the type of project.
- Check that camera temperature is -11°C or lower before turning on laser.
- Press down both buttons for external, followed by internal and lastly turn the knob for load to high on the processor. The activated mode with all the switched ON is shown in figure 2-21.

Figure 2-21: Shows the double pulsed laser system with required mode swtiched ON

- In device settings on DAVIS 7.2, turn on laser and change power of laser to no more than 20% with a 2% difference between Power 1A and Power 1B.
- Choose timing between two images as somewhere between 500 to 3000 ms depending on the size of the particle. (Larger size means lower timing). At this point, the physical setup was complete, and the first step to recording and

processing data was to scale the Imaging System. When calibrating system, first choose option define scale, no image distortion.

- Turn on laser then record image with calibration plate inside the container.
- Enter values for the distance from center to center of the dots on the calibration plate. Before removing the calibration plate from the container, mark the position of the plate as this will be the plane of focus when particles are placed in.
- Record reference image by choosing recording mode as reference images, start/end condition is start immediately, followed by start recording. Wait till about 10 to 20 images have been taken before clicking stop.
- Process the reference images by selecting the folder: Properties/Reference and start batch processing. Under parameter, choose only average. This will produce a reference image based on the previously recorded images with less image noise in the background. One of the recorded images for the fine sand particles has been given in Figure 2-22. This is the image recorded using shadowgraph setup. As shown in the image, the particles which only fall in the focal plane of the lens will appear sharp.
- Change recording mode to Experiment Images, click start recording.
- Return to the container and drop particles in the container from the position marked earlier. When particles pass through the field of focus, dark marks will appear on the screen of Davis 7.2. This shadow phenomenon was previously discussed as the density of the particles and the fluid varies significantly. Only particles that fall on the plane of focus will look sharp as shown in figure 2-22.

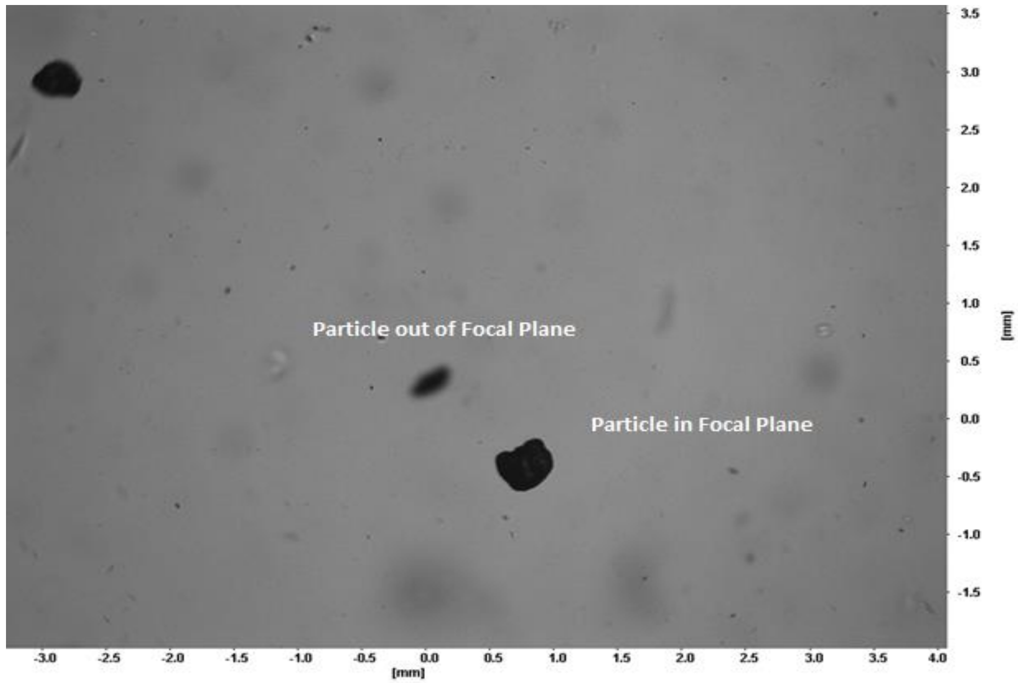

Figure 2-22: Shows the captured image from Lavision camera

- Process the experimental data by using Batch Processing. Select Shadowgraph from the operation, and go through the option list. In multi-frame selection, fill in 0 for number of 1st frame and 1 for number of 2nd frame. In image preprocessing, select no smoothing, and use the reference file previously processed to make comparisons with the experimental images. Enter 50, 40, 60 and 50 for global threshold, low level threshold, high level threshold and AOI expansion respectively. This was used to filter out other impurities from the fluid that have been recorded. Adjust recognition filter and velocity parameter to filter out the outliers of the experiment.

Once the experimental images have been processed, Davis 7.2 will display the particle size and velocity of all particles within the given range. The entire processed image look like the image shown in Figure 2-23. The image in Figure 2-23 is one of the processed images from shadowgraph for fine sands. The full process was repeated with four different sieve sizes of sands. For each sand type, experiments are performed thrice and the values are recorded. As depicted in Figure 2-17, the captured images from the double frame camera calculates the settling velocity of the particle based on knowledge of the distance travelled and the time difference between the two frames. The result for the velocity vectors for detected particles obtained after processing is shown in figure 2-24.

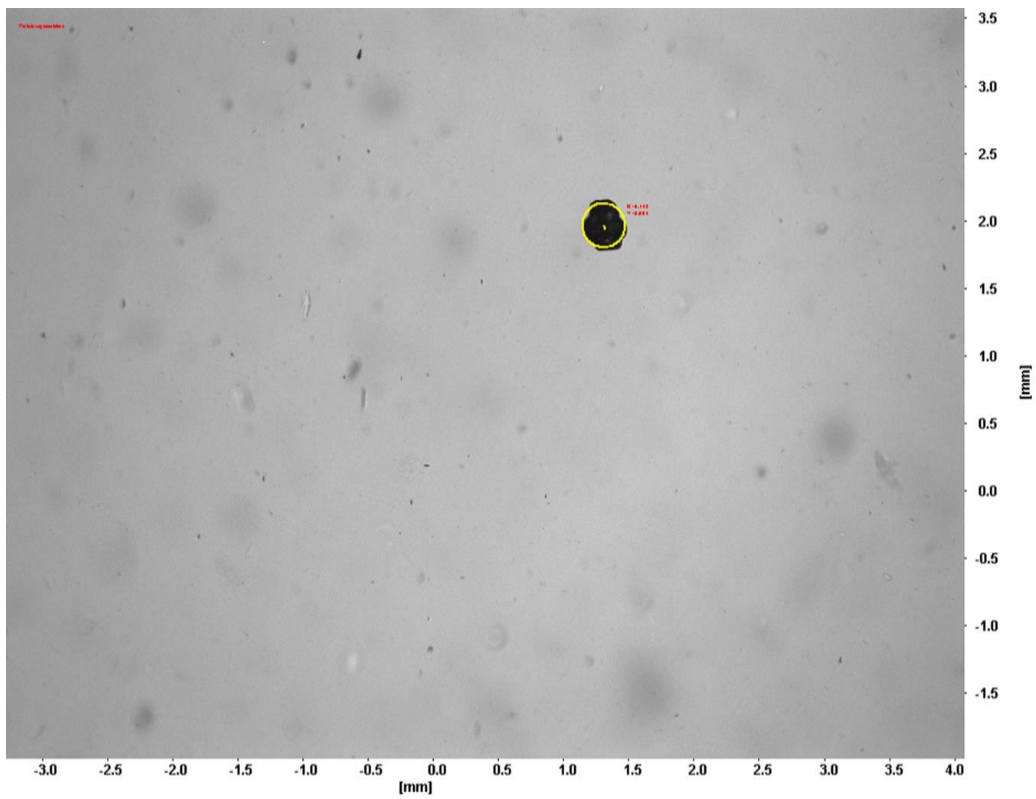

Figure 2-23: Shows the processed image from Davis software

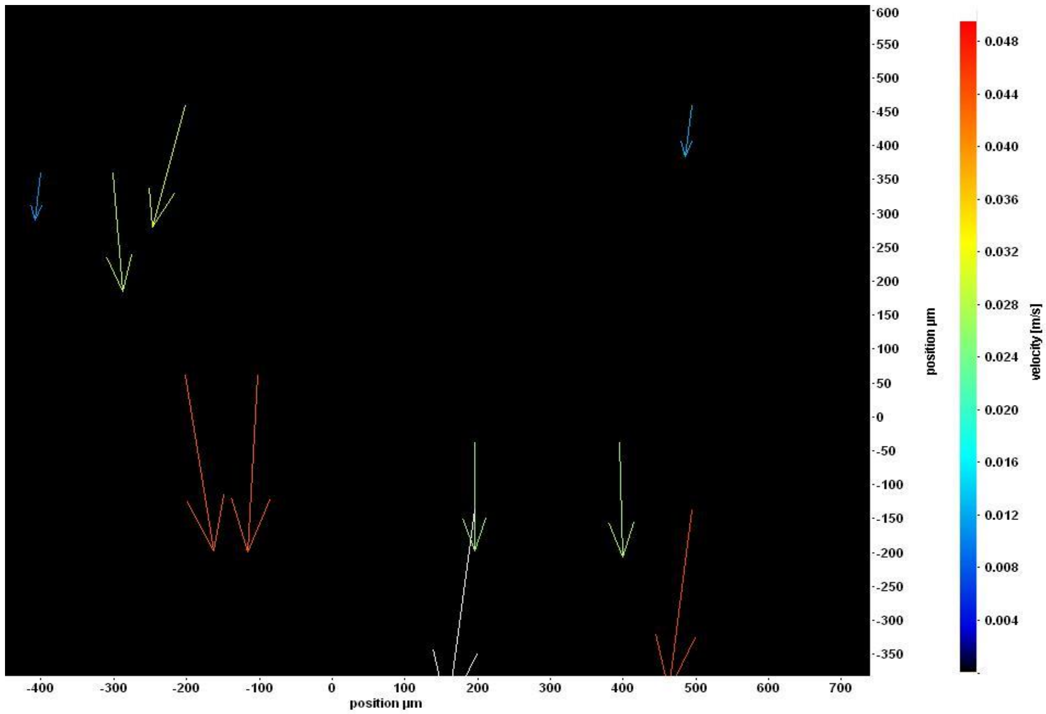

Figure 2-24: Velocity vector plot for the settling particles (after processing using Davis)

2.6 Precautionary Measures for PIS Experiment

2.6.1 Fluid Preparation

- Glycerine should be added exactly and in the middle of the vortex generated in the agitating water.
- CMC solution in water should be prepared in small batches. Preparation of concentrated batch and dilution of it with water to attain the target concentration should be avoided.
- CMC should be added at a very slow rate in the highly agitating water. It should be poured at a rate of 1gm CMC in 350 ml solution should take around 25-30 minute of time.
- Allow the mixer to mix it for about 3-5 minutes once the entire polymer has been added.

- Once the entire samples are prepared mix it gently with hand mixer to attain more homogeneity in the solution.

2.6.2 Fluid Rheology

- The samples used for the rheological study should be taken after shaking the sample container. Sometime the polymers in the stagnant solution may get segregated in layers and thus may lead to error.
- Use of controlled shear stress mode of the Bohlin rheometer is suggested. Since the solution is not very viscous the controlled rate mode does not give a smooth data.
- For highly viscous solution of more than 50 cp values should be measured using the Plate mode of the rheometer. While for the lower viscosity HTHP cell at room temperature and pressure is recommended.
- HTHP cell contains a spindle rotating in the fluid sample and at higher viscosity the spindle get stuck and thus leads to an erroneous rheological measurement.
- The value of the stress should be taken as the least available value given in rheometer and should not exceed 10 Pa. This is recommended because the study is conducted for the stagnant fluid and high shear rate or shear stress rheological will not be useful in this case.
- The HTHP cell should be assembled using the standard procedure mentioned in the rheometer manual. An improper installation may lead to error or even damage the instrument.
- The water pump should be connected with the rheometer during the measurement. It circulates the water so as to maintain the temperature of the rheometer. Without the use of water pump during the measurement leads to

increased temperature and thus affect the readings of the rheology. It can also damage the instrument due to overheating.

- Taking three and more readings for the same sample is recommended so as to reduce the experimental error.

2.6.3 Shadowgraph

- Allow the fluid to be in the measuring container for few hours so as to make it free of any trapped air bubbles.
- Try mixing the fluid in the container gently before the start of the experiment.
- Mark the plain in which the calibration sheet has been put in the container. This will give the knowledge of the focal plane and while adding the particle one can get more particles in focus if it is marked and known.
- Diffuser should be kept at distance of 5-10 cm from the container. This leads to better illumination even at low power level. Increasing the distance of the diffuser may lead to more scattered light source.
- X adapter with 12 X Navitar lens is recommended when seeing the particle less than 300 μm. For the particle size of greater than 300 μm the 12 X Navitar lens work well.
- Check the balance level bubble in the stand. Proper centering of the bubble leads to a good levelling. An inclined camera may lead to error.
- Never switch on the laser with diffuser directly facing the camera. This can damage the camera.
- Wait till the camera temperature has reached -11 ^{0}C, don't start using the camera until the specified temperature is reached.

- Gradual increase of the laser power is recommended. Never increase the power all of a sudden. Generally for the transparent liquid laser power of 15-30 works well. Always keep in mind the counts shown in the captured image should not go beyond 4000.
- While increasing the laser power it is recommended to take an image at every step of increasing power and should keep watch on the counts in the image.
- Working at 2K-4K resolution is recommended.
- During the calibration use of 2D scaling is recommended and while proceeding with the step in the calibration checks the entered distance between the dots. It should be 0.8 mm and 1.5 mm.
- During the calibration at least the calibrated image should have a 4X4 dots detected around the marked dot used as a reference in the calibration.
- Always use the average of the captured reference image in the processing, skipping this step will lead to automatically select the reference image from the last conducted experiments which leads to a severe error.
- In the particle recognition step in the processing enter the range of values which you have estimated for the particle. Sometime giving the value starting from zero leads to even processing of the small polymer molecule which can affect the overall results obtained from the shadowgraph.
- During the experiments on the spherical particle enter the centricity value >90%. This reduced the error in the processing and the unwanted particles will not appear in the particle list.
- During the sand experiment keep in mind to check the centricity value. Try keeping it below 50% so as to have better accuracy in the results.

- Once the particle list has been obtained never forget to check the details of it. It may contain some out of focus particle or noise with completely different values.
- Switching off the any room light is recommended, this leads to less noise generation in the measurement.
- Taking three or more trials on same fluid and particle system could lead to better efficiency and reduced experimental error.

2.7 References

1. Lavision Davis 7.2 Product Manual, 2010.
2. Adrian R. J., 2005, “ Twenty Years of Particle Image Velocimetry”, Experiments in Fluids, Vol. 39, pp. 159-169
3. Wieneke B., 2005, “Stereo-PIV Using Self-calibration on Particle Images”, Experiments in Fluids, Vol. 39, pp. 267-280.
4. Bizhani, Majid., 2013, “Solid transport with turbulent flow of non-newtonian fluid in horizontal annuli,”, Master Thesis, University of Alberta.
5. LAVision, Flow Master, Product Catalogue, 2006
6. Malvern Instruments Limited, 2005, “Bohlin C-VOR”, Product Catalogue
7. Japper-Jaafar,A., Escudier, M.P., and Poole, R.J., 2010, “Laminar, transitional and turbulent annular flow of drag-reducing polymer solutions”, J. of Non-Newtonian Fluid Mech., Vol. 165, pp.1357-72.
8. http://www.cannoninstrument.com/cfr.htm cited on March 21, 2014.
9. http://www.acros.be/DesktopModules/Acros_Search_Results/Acros_Search_Results.aspx?search_type=Specifications&SearchString=327255000 cited on March 23, 2014.
10. http://www.modernistpantry.com/carboxymethyl-cellulose.html cited on March 23, 2014.
11. http://www.brenntagspecialties.com/en/downloads/Products/Multi_Market_Princ ipals/Aqualon/Aqualon_CMC_Booklet.pdf cited on March 24, 2014.
12. http://www.fishersci.com/ecomm/servlet/fsproductdetail_10652_803022__-1_0# cited on March 24, 2014.

13. http://www.acros.be/DesktopModules/Acros_Search_Results/Acros_Search_Results.aspx?search_type=Specifications&SearchString=27838 cited on March 24, 2014.

14. Lavision Product Manual for double pulse Nd:YAG Laser, 2007.

15. Lavision Product Manual for Diffuser, 2008.

16. Gutowski, Iris., 2010, “The effect of pH and concentration on the rheology of Carbopol gels”, Master of Science Thesis, Simon Fraser University.

Chapter 3

Size and Shape Measurement for Sand Particle Using Particle Image Shadowgraph

The chapter contains the detail study on the shape and size characterization of natural sand particles. The first section discusses the importance of particle size distribution and associated literature. Different techniques used for particle size distribution in the past are discussed and compared with the shadowgraph technique. Next sections delineate different diameters generally used for particle characterization. Measurement techniques used in the study have been explained in detail. Different diameter and shape parameter for sands particles measured using PIS are given in the results and discussion section. Conclusions of the study are given at the end of the chapter.

3. 1 Introduction

The modern civilization is heavily dependent on minerals. Minerals in their raw form are not readily usable and their processing becomes imperative and inevitable. Particles are thus dealt in a large scale to meet the ever increasing demand of chemicals. Most of the industrial processes handle particles ranging from a few microns to big rocks spanning hundreds of centimeters on a daily basis. Understanding the bulk behaviour of particles and the impact of the particle properties on the process parameters is important. Particle characterization in several respects is required for optimal and safe operation of the equipment. The size of the particle plays an important role in determining the quality and performance of particulate material. The particle's size and shape greatly influences the flow and compaction properties [1]. The rheological properties of polymers are directly related to the particle size distribution of the polymer [2]. The clear information about the constituent particle's size play an important role in soil texture and soil mechanics related application [3]. There exist several applications in industries wherein accurate information about the size and shape of the particles control the process and their output. The settling velocity, particle size, and shape are important parameter in understanding the transport efficiency of vertical well. The critical velocity for an efficient bore hole cleaning and proper drilling operation is generally determined with the knowledge of single particle settling velocity in stagnant fluid [10]. Cuttings' slip velocity, hydraulic fracturing, drilling mud rheology, pump capacity, designing borehole, and shaker design are amongst the few application of particle size, shape, and velocity in drilling and petroleum industry.

Particle size is probably the first property that comes to mind when particle characterization is thought of. The most primitive technique for particle size measurement in industrial era is the use of meshes/sieves which had apertures of known dimensions. In this way, a rough estimate of the average size of the particles can be determined. Naturally, the use of sieve technology is restricted to the order of microns as manufacturing sieves for such small sizes becomes expensive. To substitute this shortcoming, a hydrometer is used for the small particles which exploit the settling velocity of the particles as a property for the size determination. Sieve-Hydrometer method for the estimation of particle size has been the most popular method used ever since. However, the inherent disadvantages involved in the estimation, viz, the dependence of the hydrometer measurements on the particle properties like density and sphericity introduce uncertainty into the size measurement which have to be taken into account in cases where a high accuracy of particle size determination is required [4]. Out of all the new technologies for the measurement of particle size like laser diffraction, microscopic imaging, speed photography, laser diffraction method, shadowgraph, phase-doppler particle analysis, light diffraction and adsorptive techniques, laser diffraction has been found to be most accurate and is thus widely accepted ([5] and [6]).

Wen et.al [7] compared the efficiency of Sieve Hydrometer Method (SHM) and Laser Diffraction Method (LDM) for particle size analyses on granitic Saprolites and volcanic Seprolites. It has been concluded that there are clear discrepancies between PSD by the two methods; there can be no universal correlation between two kinds of analyses for all soils because mineral content may affect the PSD to great extent. The analysis by Wen et al [7] on Saprolites concluded that LDM has various advantages over the classical SHM method and LDM should be adopted as standard practice in geotechnical engineering.

The use of manual methods, viz., sieving, sieve hydrometer among others, is more tedious and non-efficient as compared to image processing technique. Rogerio [6] had studied the different optical techniques in detail and found that shadowgraph technique have a great advantage over other techniques. The laser diffraction method which has been commonly used in the past for PSD is found to be erroneous when the particle numbers increased because of the multiple scattering phenomenon. In case of high particle population, the light gets multiple diffractions before reaching the detector and thus introduces an error in the measurements. The similar limitation exists for Phase Doppler Particle Analyzer (PDPA) technique and is not recommended to use for dense spray or near the nozzle outlet [6]. In Planar Droplet Sizing (PDS), a group of small droplets and a large droplet provide the same intensity in the image and thus one cannot differentiate between the two cases [6].

The shadowgraph (backlighting) technique is a point measurement method and uses a non-intrusive optical image for measuring particle's velocity and size. This technique is independent of the material and shape of the particle being observed [6]. The Davis Particle Master shadow software used for data processing is found to be an efficient image processing tool for estimating particle shape, velocity, size and other related statistical properties [8].

The sieve analysis emphasize on the second smallest diameter because of the way particle must orient to pass through the sieve opening [1]. The estimation of particle's size based on it leads to erroneous conclusion. Moreover, in sieve analysis, no information about the shape of the particles can be obtained. The particle image shadowgraph has been used to study the sand shape and size in detail. A geometrically identical particle like spheres requires a single dimension to define the size. While a non-spherical particle need multiple width and length to define the particle's geometry. Many measuring techniques make the general assumption that the particles are spherical in shape and thus represent non-spherical particle in terms of equivalent spherical or equivalent volumetric spherical diameter. This assumption can lead to an error in the efficiency of various industrial processes. The literature lags a detailed study about the Sand's shape and size and the main objective of this part of study is to analyze the sand's geometrical parameters using a highly efficient shadowgraph technique.

The two most important reasons for industries to perform the particle characterization is to have a better control on product quality and have a better understanding of products, ingredients and processes [9]. In particle characterization, the two most important and easy to measure properties are particle shape and size. The particle shape and size directly influence the reactivity or dissolution rate, efficiency of delivery, texture and feel, viscosity, packing density, stability in suspension, flow ability and handling; because of this, it is important to measure the two parameters accurately [9].

Shadowgraph is found to be more effective image processing tool. The shape and size of the particles play a major role in determining its settling velocity. Sand being an important material to handle in the petroleum, mining and transportation industry requires a detail investigation of its size and shape. Until now, no such detailed investigation or data is available in the literature where in one can find detailed measured values for the natural sands. The study provides a scope to measure the margin of error in settling velocity calculation by using the complete size distribution knowledge associated with a particular sieve size. This study when used properly with the settling velocity calculation would lead to a better judgment criterion in designing pipeline and also finds useful in transportation industry. One would have a better idea of the range of settling velocities of sand particles which might not have been possible by using a single sieve diameter. Moreover these are the diameters for the settling sand when it has achieved the settling velocity, making it more useful and accurate.

3.2 Equivalent Diameters for Non-Spherical Particles

The ParticleMaster Shadow software models each particle as an ellipse and quantifies the major and minor axis (the ratio of these numbers is a "shape factor" or centricity). The reported diameter of each particle is derived from a circle that has the equivalent number of pixels as the ellipse. For all particle statistics (e.g. D10, D32, etc), the equivalent diameter of each particle is used and all particles are assumed to be spherical.

3.2.1 Arithmetic Mean (D10)

It is a one dimensional measurement. It can be defined as the number length mean or the arithmetic mean. It is of more importance where the number of particles is of interest [9]. The number length mean is given by equation 3-1.

$$D_{10} = \left(\sum_{i=1}^{N} D_i\right) / N \qquad \textbf{Eq. (3-1)}$$

Where D_i is the particle diameter and N is the total number of detected particle

3.2.2 Sauter Mean Diameter (D32)

It is defined as the diameter of a sphere with the same volume/surface area ratio as that of particle of interest. This diameter is most sensitive to the presence of fine particles in the size distribution because of the impact of surface area on its value. The equation for the Sauter mean diameter is given by the relation eqn. 3-2.

$$D_{32} = \sum_{i=1}^{N} D_i^3 / \sum_{i=1}^{N} D_i^2 \qquad \textbf{Eq. (3-2)}$$

Where D_i is the particle diameter and N is the total number of detected particle

3.2.3 Volumetric diameter (DV10, DV50, and DV90)

These representative diameters are extracted from the cumulated volume of all particles. DV10 represents the maximum particle size below which 10% of the sample volume exists. Similarly DV50 and DV90 represent the maximum particle size below which 50% and 90% of the sample volume exists respectively. These are three very common volume diameter values used to monitor any significant change in the particle size, any changes in the extremes of the distribution, which probably could be the effect of presence of fines or oversized particles [9].

3.2.4 Equivalent Circular Diameter (D_C)

The diameter is of a circle with the area equivalent to the actual projected area of the particle image. This diameter takes care of the shape effect and is found to be an effective tool to define the sand's diameter.

3.3 Measurement Technique

It is widely accepted that the Particle Image Shadowgraph is an efficient technique to measure the size, shape, and velocity of a particle. In this study, the experimental setup designed for measuring the particle's settling velocity, as discussed in the Chapter 3, has been used for detailed characterization of sand's shape and size.

The validation of the setup has been done by measuring the size of four spheres of known diameter. The difference between measured values and manufacturer values were less than 4%. The fine and coarse sand from Sil Inc. Ltd. has been used in the study. The physical properties of sands used in the study is given in Table 3-1 and 3-2

Table 3-1: Physical properties of fine sand

Property	**Test Method**	**Unit**	**Typical values**
Mineral	Petrographic	………	Quartz
Shape and hardness	Visual	Mohr	Sub Angular/6.5
pH	AFS	……….	7.2-7.4
Specific gravity	ASTM C-128	……….	2.65
Bulk Density, aerated	ASTM C-29	Lbs/Ft^3	92-95
Compacted	ASTM C-29	Lbs/Ft^3	98-100

Table 3-2: Physical properties of coarse sand

Property	**Test Method**	**Unit**	**Typical values**
Mineral	Petrographic	………	Quartz
Shape	Krumbein	………	Sub Angular
Hardness	Moh	6.5	

Specific gravity	ASTM C-128	……….	2.65
Bulk Density, aerated	ASTM C-29	Lbs/Ft^3	92-95
Compacted	ASTM C-29	Lbs/Ft^3	98-100

The sieve analysis on the coarse sand has been performed and the sample has been segregated into three parts. The first one is the sand with sieve size in between 0.71 mm-0.85 mm; second is of size between 0.85-1.18mm while the third part consists of sand with sieve size of 1.18mm-1.7mm. The fine sand sieve size range is between 0.3 to 0.4 mm.

The sand particles are dropped in CMC-water mixture (test fluid) and the images are captured using the Lavision double frame camera with a double pulse backlight illumination from the diffuser. The images are then processed using the Davis Particle Master Shadow software. The process is repeated four times for each set of sand so as to reduce the manual and experimental error that may have occurred during the experiments. This also permits validating the repeatability of the experiments. The different diameter and geometrical parameters measured for sand are then analysed individually using the descriptive statistical tool available in Microsoft excel.

3.4 Results and Discussion

Different diameters for natural sands have been measured using the PIS technique. The different diameter values for a particular sieve size are given in table 3-3 to table 3-8. Correlations for predicting these diameters from the given sieve size were developed using the shadowgraph results. The different correlations developed for estimating equivalent diameters for natural sands are given by Equation 3-3 to 3-7. The regression coefficient values for the correlations were found to be very good with the minimum value of 0.93 observed for D10 diameter. Seeing the irregularity and nature of sands the suggested regression coefficients are acceptable.

$$S_{DV90} = 1.4217d_s + 0.0003 \quad \textbf{Eq. (3-3)}$$

$$S_{D10} = 0.8416d_s^{1.1396} \quad \textbf{Eq. (3-4)}$$

$$S_{DV10} = 0.9058d_s - 0.0525 \quad \textbf{Eq. (3-5)}$$

$$S_{D32} = 1.0766d_s + 0.0028 \quad \textbf{Eq. (3-6)}$$

$$S_{DV50} = 1.0544d_s + 0.0088 \quad \textbf{Eq. (3-7)}$$

$$S_{D_c} = 1.2489d_s - 0.1267 \quad \textbf{Eq. (3-8)}$$

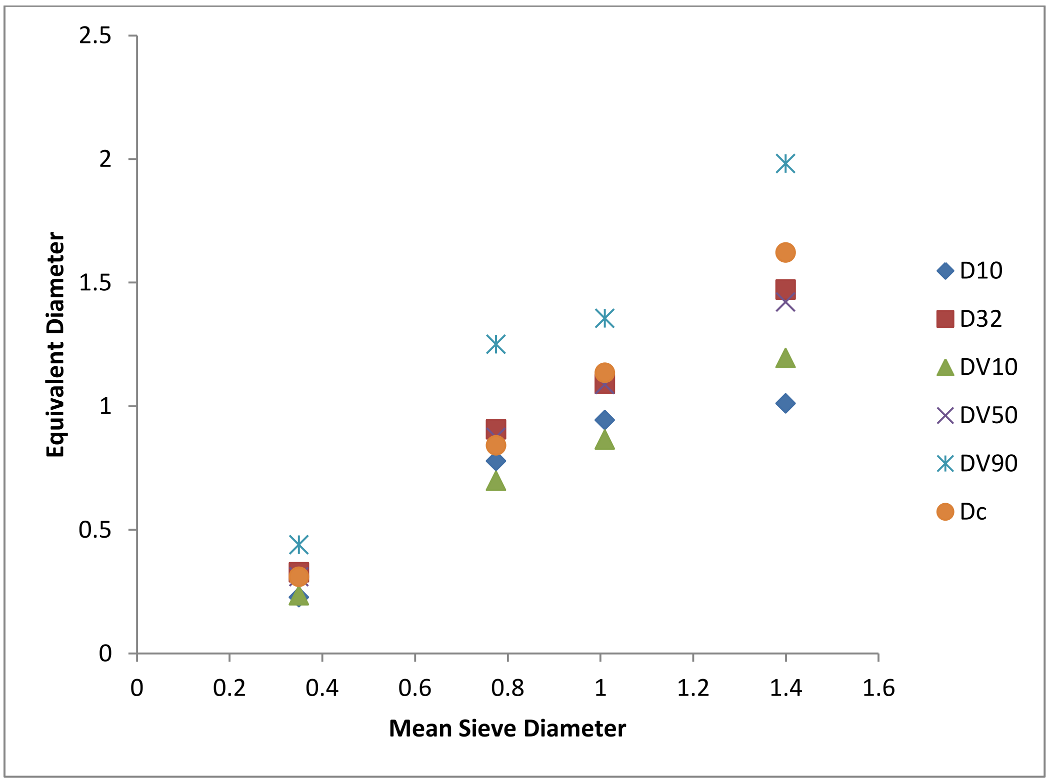

Figure 3-1: Equivalent diameter versus mean sieve diameter for natural sand particles

Table 3-3: D10 diameter data for natural sand

Sieve Size (mm)	Mean (mm)	Median (mm)	Standard deviation	Minimum (mm)	Maximum (mm)	Confidence Level (95.0%)
0.3-0.4	0.227	0.234	0.024	0.164	0.246	0.017
0.71-0.85	0.778	0.814	0.086	0.649	0.833	0.137
0.85-1.18	0.944	0.938	0.056	0.883	1.017	0.089
1.18-1.58	1.011	0.995	0.078	0.937	1.116	0.125

Table 3-4: D32 diameter data for natural sand

Sieve Size (mm)	Mean (mm)	Median (mm)	Standard deviation	Minimum (mm)	Maximum (mm)	Confidence Level (95.0%)
0.3-0.4	0.328	0.330	0.0088	0.312	0.339	0.006
0.71-0.85	0.906	0.905	0.0078	0.897	0.916	0.012
0.85-1.18	1.090	1.090	0.0077	1.082	1.098	0.012
1.18-1.58	1.471	1.472	0.1045	1.368	1.571	0.166

Table 3-5: DV10 diameter data for natural sand

Sieve Size (mm)	Mean (mm)	Median (mm)	Standard deviation	Minimum (mm)	Maximum (mm)	Confidence Level(95.0%)
0.3-0.4	0.235	0.233	0.014	0.218	0.255	0.010
0.71-0.85	0.697	0.702	0.011	0.681	0.705	0.018
0.85-1.18	0.864	0.863	0.014	0.849	0.883	0.023
1.18-1.58	1.195	1.191	0.082	1.117	1.279	0.131

Table 3-6: DV50 diameter data for natural Sand

Sieve Size (mm)	Mean (mm)	Median (mm)	Standard deviation	Minimum (mm)	Maximum (mm)	Confidence Level (95.0%)
0.3-0.4	0.309	0.313	0.011	0.294	0.323	0.008
0.71-0.85	0.874	0.876	0.009	0.861	0.883	0.015
0.85-1.18	1.087	1.088	0.015	1.071	1.103	0.024
1.18-1.58	1.421	1.425	0.100	1.312	1.522	0.159

Table 3-7: D90 diameter data for natural sand

Sieve Size (mm)	Mean (mm)	Median(mm)	Standard deviation	Minimum(mm)	Maximum (mm)	Confidence Level (95.0%)
0.3-0.4	0.439	0.441	0.021	0.391	0.466	0.015
0.71-0.85	1.250	1.247	0.024	1.225	1.283	0.038
0.85-1.18	1.355	1.375	0.056	1.272	1.396	0.089
1.18-1.58	1.981	1.986	0.109	1.875	2.076	0.174

Table 3-8: D_c and Centricity for natural sand

Sieve Size (mm)	Mean (mm)	Range (mm)	Avg. Centricity	Avg. Large axis (mm)	Avg. Small axis (mm)
1.18-1.6	1.3746	1.0-1.9	0.5735	0.9899	1.7593
0.85-1.18	0.8225	0.5-1.2	0.5675	0.5827	1.0618

0.71-0.85	0.5632	0.4-1.1	0.4572	0.4023	0.7242
Fine	0.3612	0.1-0.6	0.5968	0.2684	0.4539

2.5 Conclusions

Different equivalent diameters (D10, D32, DV10, DV50, DV90, and Dc) for natural sands have been defined and their values determined successfully using PIS technique. Correlations between the mean sieve diameter and equivalent diameters have been developed. Statistical analyses were conducted on each diameter values obtained from the shadowgraph. This analysis gives a better insight of the size distribution of the sand particle. Apart from different equivalent diameter the average centricity values for different sieve diameters have also been measured and reported.

3.6 References

1. A guide book to particle size distribution by Horiba Scientific Ltd. cited from internet on April 1, 2014.
2. Hosseini, Alireza., Oshaghi, Milad., and Engell, Sebastian., 2013, “Control of the particle size distribution in emulsion polymerization by mid-course correction using a hybrid model”, Proceedings of the 23rd European symposium on Computer aided process engineering.
3. Taguas, F.J., Martin, M.A., and Perfect, E., 2000, “Simulation and testing of self-similar structures for soil particle-size distributions using iterated function system”, Fractals in Soil Mechanics, pp. 101-113.
4. Cooper, L. R., Haverland, R. L, Hendricks, D. M., and Knisel, W.G., 1984, “Mircotrac Particle Size Analyzer: An Alternative Particle-Size Determination Method for Sediment and Soil,” Soil Science, Vol. 138, pp.138–146.
5. Pabst, W., Gregorová E., 2007 “Characterization of Particles and Particle systems-1”, ICT Prague.
6. Pimentel,Gomes Rogerio., 2006, “Measurement and prediction of droplet size distribution in sprays”, PhD, Faculty of science and engineering, Laval University, Quebec.

7. Wen B., Aydin .A, Duzgoren-Aydin, N.S, 2002, "A comparative study of Particle size analyses by Sieve-Hydrometer and Laser-Diffraction methods", Geotechnical Testing Journal, Vol. 25, No. 4.
8. Fountain, M.S., Blanchard, J., Erikson, R.L., Kurath, D.E., Howe, D.T., Adkins, H., and Jenks, J., 2012, "Design of a particle shadowgraph velocimetry and size (PSVS) system to determine particle size and density distributions in Hanford nuclear tank wastes – 12280", WM2012 Conference, Phoenix, Arizona, USA.
9. Malvern Instruments Worldwide, 2012, "A basic guide to particle characterization", cited from the Malvern website on April 2, 2014.
10. http://petrowiki.org/Cuttings_transport cited on April 3, 2014.

Chapter 4

Experimental Investigation of Settling Velocity of Spherical Particle in Newtonian Fluid [2]

[2] A version of this chapter has been already presented.
Shahi, Shivam., and Kuru, Ergun. 2014, "An experimental investigation of settling velocity of spherical particles in Newtonian fluid using Particle Image Shadowgraphy," 2014 Spring Meeting & 10th Global Congress on Process Safety, New Orleans, US, 106(a).

The settling velocity is a fundamental requirement and key variable for modeling sedimentation processes and particle transport. The Particle Image Shadowgraph (PIS) experimental technique used here is unique in its kind and very efficient in measuring the size, shape, and settling velocity of the particles, simultaneously. Experiments are conducted using different sizes of glass and plastic spheres (0.5-2 mm) with five different Newtonian fluids. Mixtures of water and different concentrations of glycerol (10-40% by volume) have been used as the fluid medium in the experiments. Different models to predict the settling velocity present in the literature have been critically analyzed and based on the experimental results from the shadowgraph a new dimensionless model for predicting settling velocity for a wider range of particle size and flow regime has been developed.

4.1 Introduction

The earliest literature to determine the relationship between settling velocity and particle moving through fluid could be traced back to the Stokes' [1], which was derived by equating the effective weight of a spherical particle to the viscous resistance. Stokes' Law applies only for small rigid spheres settling within an infinite and viscous fluid column. Since early 20th century, numerous studies have been conducted and several empirical formulae were established to estimate the setting velocity of a particle. Rubey [2] combined Stokes' law and the Impact law into a general equation, which considers not only the viscous resistance but also the fluid impact. Gibbs et al. [3] derived the empirical equation to estimate the relationship between settling velocity and grains of sphere size. Peden and Luo [4] proposed the drag coefficient correlations for spheres within a limited particle Reynold's number range, which when compared with the experimental results gave an error of ±16%. Mordant and Pinton [5] experimentally investigated the motion, physics and factors governing the setting of solid spheres using acoustic models and signal processing. Furthermore, they also proposed that the density is an important control parameter for Reynolds number. Later on, Brown and Lawler [6] studied different settling velocity correlations and experiments available in the literature and suggested two different correlations for spheres.

In the case of non-spherical particles, there are several reports in literature that examine the settling velocities through analytical, empirical or phenomenological models ([7] to [10]). However, in most of them, the settling velocities were developed based on settling of spheres. Thus, there emerges a need to accurately estimate and understand the settling of spheres in real-world industrial applications. Although the factors influencing the settling velocity are well known, there is always a need for simulating the functional relationships among settling velocities, particles and the influencing parameters more accurately through modern experimental techniques.

This work is an attempt to develop a more accurate empirical model for settling velocity of spheres based on an advanced laser based image processing techniques, PIS for measuring size, shape, and settling velocity. Experiments are conducted using different sizes of glass and plastic spheres (0.5-2 mm) with five different Newtonian fluids. Mixtures of glycerol and water and different concentrations of glycerol (10-40% by volume) have been used as the fluid medium in the experiments. Further, based on measured experimental values a dimensionless model of particle settling velocity has been has been developed and compared with the existing models in literature for spheres in Newtonian fluid.

4.2 Experimental Design

The PIS technique, which is being used for visualizing settling of fine particles in fluids, is based on high resolution imaging with pulsed backlight illumination. The general principle associated with this phenomenon is that a shadow is casted whenever there is a significant change in the densities of medium through which the light is passed. This technique generates a series of shadow images from the focal plane of the camera to be projected on screen; allowing particles to be visualized. Most light rays are refracted and the ones un-deflected will appear as dark marks captured by the instrument (Davis 8.0 Manual). This technique is independent of the shape and physical properties (e.g. density, size, transparency) of the particles. It allows for the investigation of sizes down to 5µm and freeze motions of more than 100 m/s when using the appropriate imaging system and light source [17]. The experimental setup designed for measuring the settling velocity using PIS is shown in Figure 4-1.

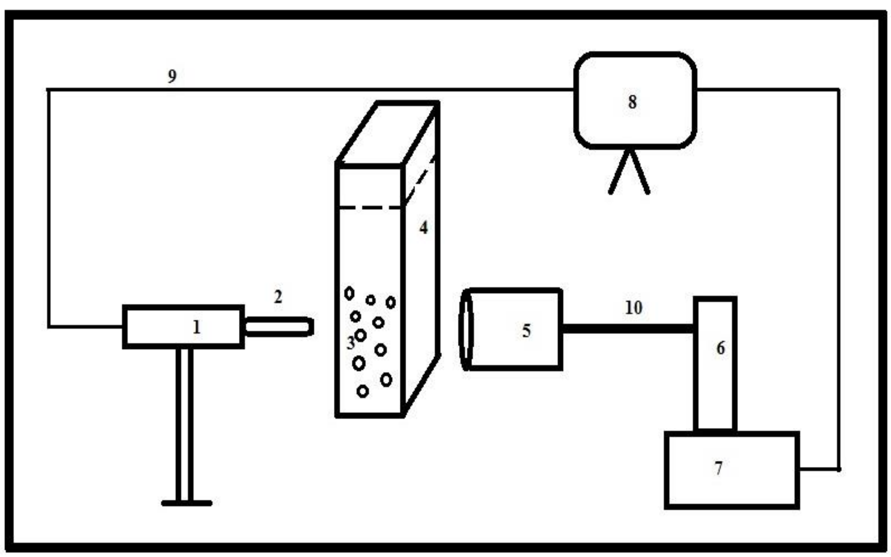

Figure 4-1: Schematic of the experimental setup for measuring settling velocity using PIS [1. Lavision image intense camera 2. 12 X Navitar lens 3. Particles 4. Plexi glass container with fluid 5. Diffuser 6. Lavision illumination high efficiency diffuser 7.New Wave Research laser solo III 15Hz] 8. Lavision Davis 8.0 9. Connecting wire 10. Optical fibre cable

4.3 Experimental Detail

The experiments have been carried out with four different glass spheres (Corposular's Glass Spacers Millibeads) and two different sizes of plastics beads. All the experiments were performed at room temperature. The rheological properties of the fluids were measured using Cannon-Fenske viscometer. Experiments begin with the calibration of the camera, which is done using a rectangular plate with printed circle of size (0.8 mm) spaced at 1.5 mm distance from each other. Once the particle start descending, the double frame camera starts capturing the images at a particular time step (usually 500-3000 ms) that depends on the size of the particle. The recorded images are processed using Davis 8.0 software which detects the particle based on the intensity difference and calculates the settling velocity.

4.3.1 Validation of Experimental Measurement

The validation of the particle size measurements using PIS technique has been carried out by comparing the measured size and settling velocities of four different glass spheres (Corposular's Glass Spacers Millibeads) with the data provided by the manufacturers. The comparative results of the actual and experimentally measured diameters of glass beads are shown in Table 4-1.

Table 4-1: Measured and actual diameter of glass spheres

Diameter (Manufacturer Data) (mm)	Diameter (Measured) (mm)
0.71±0.02	0.71
2±.04	2.002
1.18±0.02	1.175
1.5±0.03	1.52

In addition, measured settling velocity values from shadowgraph experiments were validated by first determining the drag coefficient (eqn. 4-1) using the measured values of settling velocities of spheres in water by using the equation 4-1 and introducing these values into the universal drag coefficient versus particle Reynolds number plot for Newtonian fluid as shown in Figure 4-3**.** It was found that the measured drag coefficients were within acceptable limit of 5% to the theoretical values.

$$C_D = \frac{4gD(\rho_s - \rho_f)}{3\rho_f V_s} \qquad \textbf{Eq. (4-1)}$$

Where, C_D is drag coefficient, ρ_s is density of solid, ρ_f is density of fluid, V_s is settling velocity, g is acceleration due to gravity, d is particle's diameter

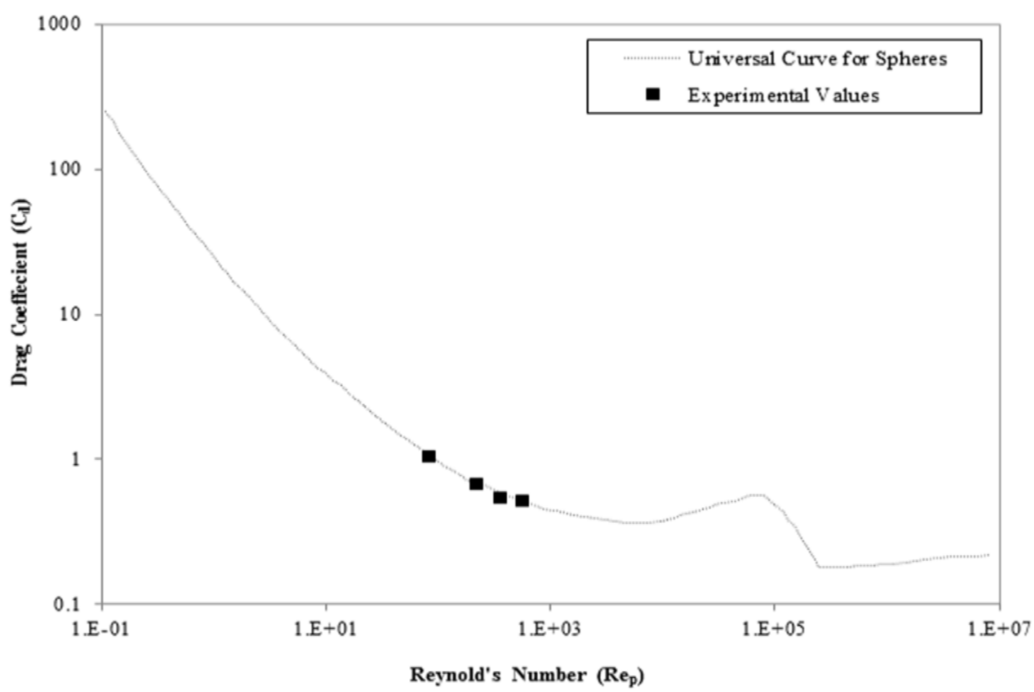

Figure 4-2: Shows the experimental values on C_D vs Re_p universal plot

4.3.2 Fluid and Particle Characteristics

Three different classes of Cannon Fenske Viscometers (SR25 135, SR100 461, and SR150 798) were used for the measuring the kinematic viscosity of different concentration (0%-40% by volume) of glycerol in glycerol water mixture. The kinematic viscosity values of four different water-glycerol mixtures are shown in figure 4-3. The measured values of the viscosity for water-glycerol mixtures are given in table 4-2. The densities of the fluids were determined by using direct mass and volume measurements. A 10 ml measuring jar and highly precise weighing machine was used for these measurements. The measure values are given in figure 4-3.

Table 4-2: Measured viscosity of Glycerine-Water mixtures

Fluid Type	Cannon-Fenske	Viscometer Constant	Time (min:sec)	Viscosity (Cst)	Average Viscosity (Cst)
Type 1	SR 25	0.001404	14:59.53	1.26299	1.2597
		0.001007	20:47.85	1.25658	
Type 2	SR 100	0.01948	1:24.97	1.6552	1.6463
		0.0123	2:10.91	1.6102	
	SR 25	0.001404	19:44.72	1.6634	
		0.001007	27:25.19	1.6567	
Type 3	SR 150	0.04071	1:5.97	2.6856	2.6885
		0.02764	1:36.38	2.6639	
	SR 25	0.001404	31:55.87	2.6898	
		0.001007	44:56	2.7148	
Type 4	SR 150	0.04071	2:26.55	5.9660	5.93
		0.02764	3:33.65	5.9052	

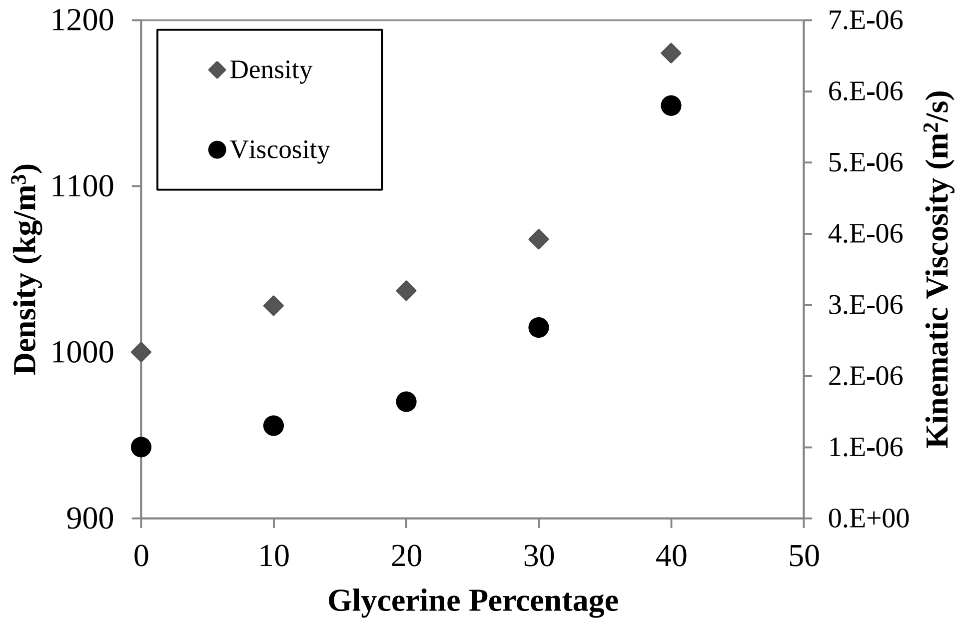

Figure 4-3: Shows the kinematic viscosity and density values for Water–Glycerol mixture

4.3.4 Density Measurement

Density measurement of different water-glycerine mixture is done using intelligent weighing technology weighing machine which can measure till 0.1 mg and Pyrex Vista no. 70024 10 ml measuring jar which can measure volume till 0.1 ml accuracy. Five different reading for the same sample is taken and the average value of density is used in the analysis.

The results for the average density for the fluids are reported in table 4-3.

Table 4-3: Measured fluid density

Fluid Type	Density (kg/m3)
Water	998
Fluid type 1	1028.5
Fluid Type 2	1037.2
Fluid Type 3	1068.6
Fluid Type 4	1105

The specific gravity of the glass spheres were found to be 2.523 which, compares well with manufacturer's value of 2.510. Considering the possible errors in measurements, we have decided to use the manufacturer's data in our analyses.

4.4 Results and Discussion

4.4.1 Measured Settling Velocities

Experiments were performed using four different sizes of glass spheres (0.71, 1.18, 1.5 and 2.0 mm) in five different glycerol-water mixture (0-40% glycerol by volume in water). With each fluid and sphere experiments were triplicated to verify repeatability better accuracy for the measurement. The average settling velocities of a sphere in each fluid are reported in Figure 4-4. It can be seen that the settling velocity increases steadily with the particle diameter. In addition, the settling velocity is inversely proportional to the viscosity of the solution for all particle sizes. Obviously, this is consistent with the physics of settling particles and many other experimental results available in literature [3], [5], and [6]. The measured value of the settling velocities in different fluids (water-Glycerin mixture) using PIS is given in Table 4-4.

Table 4-4: Measured settling velocity of spheres

Fluid Type	Density of Fluid (Kg/m^3)	Kinematic Viscosity (m^2/s)	Particle's Density (Kg/m^3)	Diameter (mm)	Settling Velocity (m/s)
Glycerine_Water (10% Glycerine)	1028	1.30E-06	2510	2.0	0.26
				1.5	0.201
				0.71	0.104
				1.18	0.1777
Glycerine_Water	1037	1.64E-06	2510	2.0	0.254
				1.5	0.21

(20% Glycerine)				0.71	0.0911
				1.18	0.16
Glycerine_Water (30% Glycerine)	1068	2.68E-06	2510	0.71	0.083
				1.18	0.14
				1.5	0.187
				2.0	0.22
Glycerine_Water (40% Glycerine)	1180	5.80E-06	2510	1.18	0.097
				2.0	0.17
				0.71	0.05
				1.5	0.12
Water (0% Glycerine)	1000	0.000001	2510	0.71	0.1141
				1.5	0.2347
				2.0	0.274
				1.175	0.1845

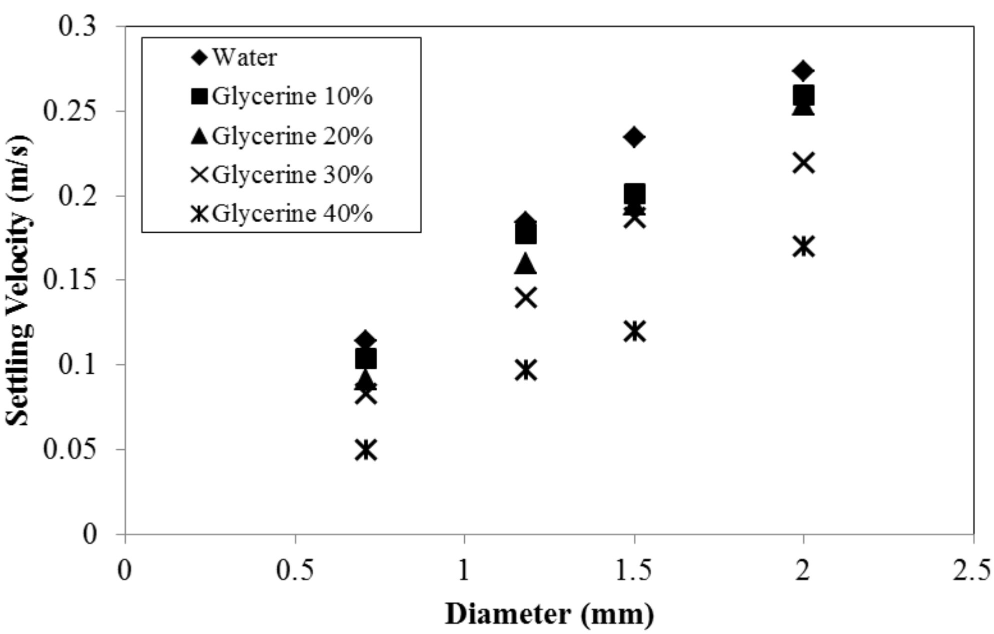

Figure 4-4: Measured settling velocity of glass beads in different water-glycerol mixture

4.4.2 Review of Available Models in the Literature

Moreover, the settling velocity obtained from the PIS experiments have been compared with the prediction of a few well accepted models. The models include, Rubey [2], Ahrens [10], Darby [11], Hallermeir [7], Julien [12], Soulsby [13], Van Rijn [14], Zanke [15], Sha [16], and Cheng [8] for predicting settling velocity of a particle in Newtonian fluid. The detail descriptions for these models are given in table 4-5. The model predictions as compared to the measured experimental results have been summarized in Figure 4-5. Furthermore, the same model predictions were compared with some of the experimental data from Gibbs [3] and the results are shown in Figure 4-6. The analysis shows that all the considered models are underestimating the settling velocities. One can observe a similar trend in both the plots, the difference in the predicted and experimental values are increasing as the diameter of the particles increase. In other words, as the size of the particles reduces, efficacy of these models improves. It can also be noticed that no two models are giving the same results for particle's settling velocity.

Table 4-5: Commonly used settling velocity models

Originator	Main Relation	Comments
Ahrens [10]	$w = C_1 \Delta g d^2 / \upsilon + C_t \sqrt{(\Delta g d)}$ $C_1 = 0.055 \tanh\left[12 A^{-0.59} \exp(-0.0004 A)\right]$ $C_t = 1.06 \tanh\left[0.016 A^{0.50} \exp(-120 / A)\right]$ $A = \Delta g d^3 / \upsilon^2$ $\Delta = \dfrac{\rho_s - \rho}{\rho}$	

Cheng [8]	$\frac{wd}{\upsilon}=(\sqrt{25+1.2d_*^2}-5)^{1.5}$ $d_*=(\frac{\Delta g}{\upsilon^2})^{1/3}d$	CSF = 0.7
Dietrich [9]	$w_s=\frac{1}{18}\frac{1}{\mu}(\rho_s-\rho)\,\mathrm{g}\,D_n^{\ 2}E^{0.28}$ $E=c\left[\frac{(a^2+b^2+c^2)}{3}\right]^{-1/2}$	
Hallermeier [7]	$\mathrm{R}_e=\frac{D_{gr}^{\ 3}}{18}$ $\mathrm{R}_e=\frac{D_{gr}^{\ 2.1}}{6}$ $\mathrm{R}_e=1.05D_{gr}^{\ 1.5}$	$D_{gr}<3.42$ $3.42<D_{gr}<21.54$ $D_{gr}>21.54$
Julien [12]	$w=\frac{8\upsilon}{d}\left[(1+0.222\frac{(s-1)gd^3}{16\upsilon^2})^{0.5}-1\right]$	
Rubey [2]	$w=F\left[dg(s-1)\right]^{0.5}$ $F=\left[\frac{2}{3}+\frac{36\upsilon^2}{gd^3(s-1)}\right]^{0.5}-\left[\frac{36\upsilon^2}{gd^3(s-1)}\right]^{0.5}$	
Sha [16]	$w=\frac{1}{24}\frac{\Delta gd^2}{\upsilon}$ $w=1.14\sqrt{\Delta gd}$ $(\log\frac{R}{d_*}+3.790)^2+\log d_*-5.777)^2=39$ $d_*=(\frac{\Delta g}{\upsilon^2})^{1/3}d$	$d<0.01cm$ $d>0.2cm$ $d=0.01\sim0.2cm$
Soulsby [13]	$w=\frac{10.36\upsilon}{d}\left[(1+0.156\frac{(s-1)gd^3}{16\upsilon^2})^{0.5}-1\right]$	
Van Rijn [14]	$w=\frac{1}{18}(s-1)\frac{gd^2}{\upsilon}$ $w=1.1\sqrt{(s-1)gd}$ $w=10\frac{\upsilon}{d}\left[\sqrt{(1+0.01d_*^{\ 3})}\right]$ (Zanke 1977)	$d<0.01cm$ $d>0.1cm$ $d=0.01\sim0.1cm$

Zanke [15]	$w=\frac{10\upsilon}{d}\left[(1+0.01\frac{(s-1)gd^{3}}{\upsilon^{2}})^{0.5}-1\right]$	

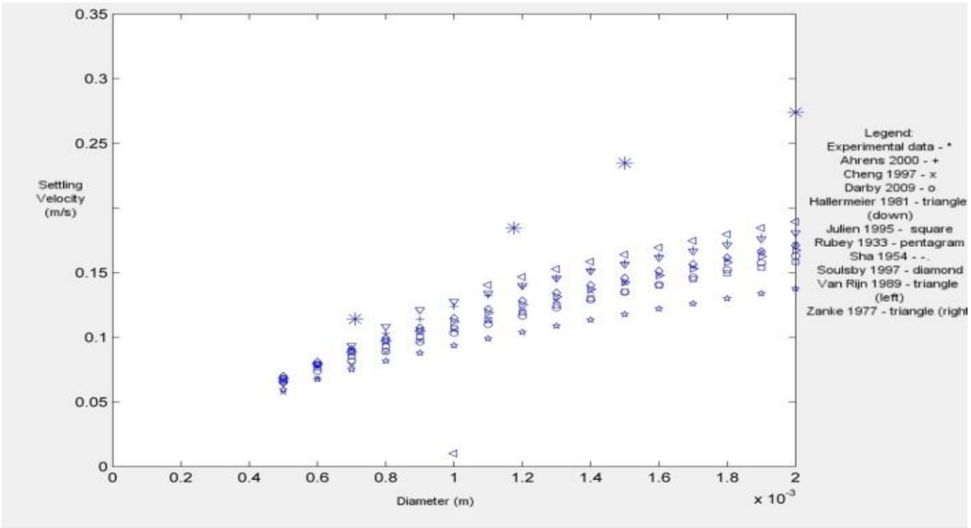

Figure 4-5: Shows the predicting capability of available models compared with shadowgraph's result

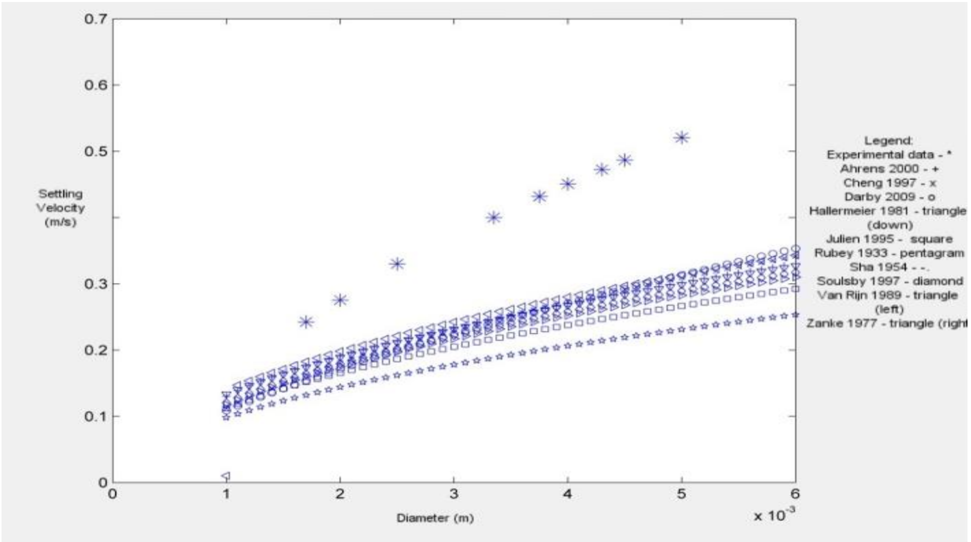

Figure 4-6: Shows the predicting capability of available models with Gibbs experimental result

4.4.3 Development of the Settling Velocity Model

The empirical model developed here is based on the dimensionless diameter and dimensionless velocity. In the current analysis, extended version of numbers Hallermeir's [7] Archimedes Buoyancy Index is used. Similar parameters have also been used by Cheng [8] and Dietrich [9]. The two dimensionless numbers used in this study are given by the equations 4-2 and 4-3.

$$D_d = \left(\rho_s - \rho_f\right) * D^3 * \frac{g}{\rho_f * \upsilon^2} \qquad \textbf{Eq. (4-2)}$$

$$V_d = V^3 * \rho_f / ((\rho_s - \rho_f) * g * \upsilon \qquad \textbf{Eq. (4-3)}$$

The measured values of settling velocities from the shadowgraph experiments as given in Figure 5were fit to a power law model (See equation 4-1). The regression coefficient value comes out to be 0.991 for the experimental data. Due to the limited range of experimental data the equation 4-4 predicts the settling velocity values very efficiently in 1.18 E+02 < D_d < 1.2 E+06. This is a major limitation for the empirical models in general.

$$V_d = 0.2269\mathrm{D}_\mathrm{d}^{0.7497} \qquad \textbf{Eq. (4-4)}$$

When analyzed and compared with the other experimental values from the literature ([3], [5], and [6]) on a dimensionless scale, all the values are found to be lying on the same curve as shown in Figure 4-7. This not only verifies the consistency with the dimensionless number but also the accuracy of the measured results obtained from the shadowgraph setup. To have greater scope for the model, experimental results from the literature ([3], [5], and [6]) were also included in the regression fit (see eq. 4-5). The proposed curve fit model yield a regression coefficient (R^2) of 0.9991.

$$V_d = 0.404 D_d^{0.695}$$ **Eq. (4-5)**

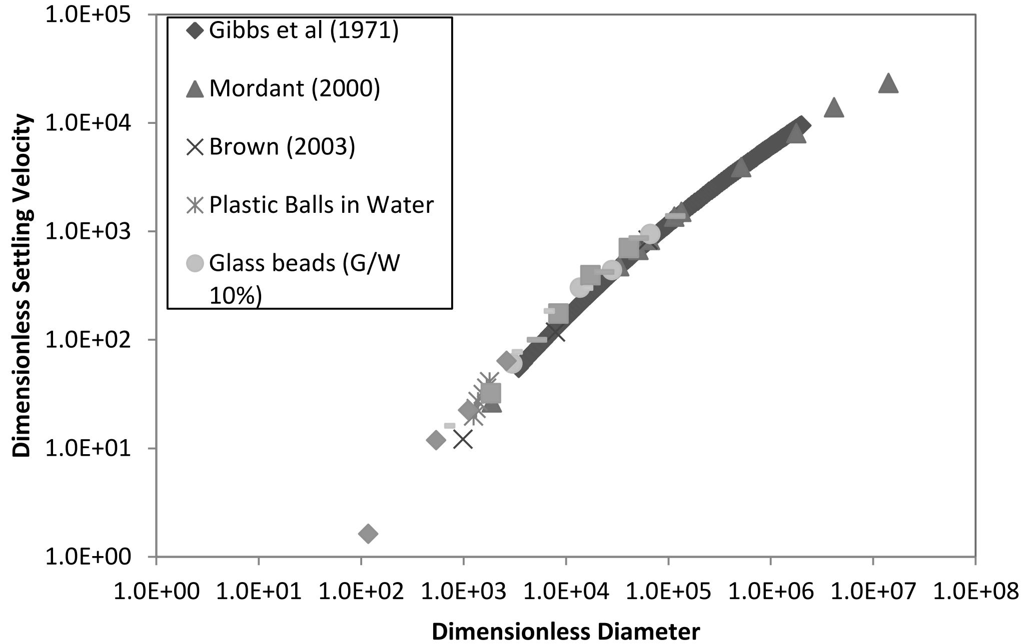

Figure 4-7: Dimensionless settling velocity curve for settling velocity of spheres in Newtonian fluid

4.5. Conclusions

A new experimental technique for measuring the settling velocity, size, and shape of the particle has been developed. The measurement technique (PIS) is found to be very accurate in terms of size, shape, and velocity measurements. The experimental technique used in this work also describes a new application of shadowgraph technique in fluid particle systems. Different settling velocity predicting models available from the literature have been analyzed. It was found that most of the models underestimate the settling velocity values. In a quest for more accurate predicting model, a new empirical model has been developed using dimensionless diameter and settling velocity. Based on the value of dimensionless diameter value one can either use equation 4-4 or equation 4-5 to predict the dimensionless settling velocity. And subsequently can predict the settling velocity of spheres in Newtonian fluid.

4.6. References

1. Stokes, G. G., 1851, "On the effect of the internal friction on the notion of pendulums", Cambridge Philo. Trans., Vol. 9, No. 2, pp. 8-106.
2. Rubey, W., 1933, "Settling velocities of gravel, sand, and silt particles", American Journal of Science, 225, pp.117-119.
3. Gibbs, R.J., Matthews, M.D. and Link, D.A., 1971, "The relationship between sphere size and settling velocity", Journal of Sedimentary Petrology, Vol. 41, No. 1, pp. 7-18.
4. Peden, M James., and Luo, Yuejim., 1987, "Settling velocity of variously shaped particles in drilling and fracturing fluid", Document ID SPE-16243-PA, SPE Drilling Engineering, Vol. 2, No. 4, pp.337-343.
5. Mordant, N. and Pinton, J. F., 2000, "Velocity measurement of a settling sphere", The European Physical Journal B, Vol. 18, pp. 343–352.
6. Brown,P. Phillip.,and Lawler, F. Desmond., 2003, "Sphere drag and settling velocity revisited", Journal of Environmental Engineering, Vol.129, pp.222-231.
7. Hallermeier, R.J., 1981, "Terminal settling velocity of commonly occurring sand grains", Sedimentology, Vol. 28, No. 6, pp.859-865.
8. Cheng, N.S., 1997, "Simplified settling velocity formula for sediment particle", Journal of Hydraulic Engineering, Vol.123, No. 2, pp.149-152.
9. Dietrich, E William., 1982, "Settling velocity of natural particles", Water Resources Research, Vol. 18, No. 6, pp.1615-1626.
10. Ahrens, J.P., 2000, "A Fall-velocity equation", Journal of Waterway, Port, Coastal, and Ocean Engineering, Vol.126, pp.99-102.

11. Sadat-Helbar, S.M., Amiri-Tokaldany, E., Darby, S., and Shafaie, A., 2009, “Fall velocity of sediment particles”, in IASME/WSEAS International Conference on Water Resources, Hydraulics and Hydrology, pp.39-45.
12. Julien, Y.P., 1995, “Erosion and Sedimentation”, Cambridge University Press, Cambridge, United Kingdom.
13. Soulsby, R.L., 1997, “Dynamics of Marine Sands”, Thomas Telford, London.
14. Van Rijn, L.C., 1989, “Handbook: Sediment Transport by Currents and Waves”, Rep. No. H 461, Delft Hydraulics, Delft.
15. Zanke, U., 1977, “Calculation of settling velocities of sediments,” Mitt Des Franzius Institute of hydraulic engineering, Technical University Hannover.
16. Sha, Y.Q., 1956, “Basic principles of Sediment Transport”, Journal of Sediment Research, Vol. 1, No. 2, pp. 1-54.
17. “Product Manual: ParticleMaster Shadow,” Item Number: 1105032, Lavision GmBh Germany.

Chapter 5

Experimental Investigation of Settling Velocity of Natural Sands in Water

Considering the extensive industrial usage of sands, a detailed experimental study on settling of quartz sands in water has been conducted. In this study, 980 quartz sands particles under four sieve sizes in the range of 0.35mm-1.18mm have been used. Particle Image Shadowgraph (PIS), an accurate and efficient technique, is employed for the first time to determine the settling velocity of the particles. Moreover, using PIS the particle dimensions are characterized in terms of centricity, major/minor axes, and equivalent circular diameter. Using the Shadowgraph results, an empirical model for settling velocity has been developed based on a dimensionless diameter and Reynolds number. The dimensionless diameter has been calculated from the equivalent circular diameter (D_c) for the actual projected area of the particle. Further, a simplistic empirical model based on equivalent circular radius (R_{ce}) is also proposed in which the particles are considered to be elliptical. Both models require only two- dimensional size parameters that can be easily measured. In this work, drag coefficient (C_d) versus Reynolds number curve for sand particles in the intermediate regime has also been presented. It is observed that C_d attains a constant value of 0.95 at $Re_p > 160$. Also, for particles within a particular sieve diameter range, a large variance (16.35% to 92.35%) in settling velocity is observed. Based on the experimental measurement a correlation between mean sieve diameter and equivalent circular diameter (D_c) is developed which helps in predicting the settling velocity more accurately. The new empirical models when compared with the literature data predict the settling velocity with an average absolute error of 4.1 % and 6.5%, respectively for sieve sizes of 0.35-1.18 mm.

5.1 Introduction

Sand particles are widely encountered in the mining, petroleum and transportation sectors for major applications like hydraulic fracturing, slurry and cutting transport**.** Therefore, understanding the characteristics of sand particles is important for the design and smooth operation of such industrial processes. Among the various characteristics, settling velocity plays a major role in behavior of fluid particle systems. The settling velocity of a particle is defined as the constant velocity attained by a particle when the forces acting on it are in equilibrium. Accurate estimation of the settling velocity increases the efficiency of various fluid particle systems likes cuttings' transport in oil and gas well drilling, gravity settling vessel, slurry transport in pipeline, hydro-cyclone, mixing tank, and sediment's transport to a great level. Naturally occurring sands are different from the other non-spherical particle like discs, cubes, spheroids, and cylinders, because of their high irregularities in terms of shape and size [1]. There are numerous studies done on non-spherical particles, however, the understanding on the settling behavior of sand particles is limited**.** This paper summarizes the results of a novel experimental technique, Particle Image Shadowgraph (PIS) for the estimation of settling velocities of sand particles. In addition, empirical models have been developed and validated by using the data from current experimental study as well as the data from literature.

The nature of sand is unique as it possesses highly irregular particle shape and size parameters. The shape plays a vital role in estimating the drag force acting on the particles during settling. Moreover, in case of irregular particles, the surface irregularities lead to increased drag force and greater flow separation, and thus reducing the settling velocity compared to spherical particles [2] and [3]. The shape of non-spherical particles is generally expressed in terms of centricity, elongated factor, hydrodynamic sphericity, Corey shape factor, circularity index, shape parameters, rectangularity, ellipticallity, elongatedness, eccentricity, and perimeter based convexity ([2], [4] to [9]). However, the comparison of particles based on different characteristic dimensions is difficult and there has been no common acceptance on the best parameter to be used for estimating settling velocity of non-spherical particles.

Numerous empirical and semi-empirical models for the determination of settling velocity of irregular particles have been reported in literature. Hallermeier [10] applied a segmented relationship between Reynolds number and the Archimedes buoyancy index, and developed relatively accurate empirical relations for the settling velocity of sediment particles without using any specification of exact grain shape. Dietrich [2] proposed a complex, empirical formula to determine the settling velocity of sediment by considering sediment size, density, shape factor, and roundness factor. Later, Cheng [11] proposed a simple relationship between Reynolds number and a dimensionless particle diameter for sand particles and calculated the settling velocity in different flow regimes for an assumed shape factor of 0.7. Ahrens [12] expanded on the method developed by Hallermeier [10] by plotting Reynolds number (Re_p) against Archimedes buoyancy index; this however, gave significant errors in predicted settling velocities.

Ahrens [13] also studied previous models ([12] to [15]) and stated that the Archimedes buoyancy index is the fundamental independent variable for both Reynolds number and the normalized sediment scale parameter. In another study by Fentie et al [16], the seven most commonly used models for predicting settling velocity in Newtonian fluid were compared against the experimental data from Raudkivi [17] and Van Rijn [18] with an error varying from 6% to 65 %. Wu and Wang [19] studied the existing models of Dietrich [2], Swamee and Ojha [20], and Jimnez & Madson [22], They found that the models gave mean relative error of 10.9%, 12.8%, and 10.7 % respectively. Wu's model, which is an improved version of the U.S. Interagency Committee [22] model gives an error of 9.1% and requires complex inputs like shape factor and three different correlations constant. Holtzer [23], in his study, showed that there exists a smooth curved correlation between drag coefficient and Reynolds number for almost all the non-spherical particles. Holtzer and Sommerfeld's gave their own correlation model which predicts the drag coefficients with mean relative deviation of 9.2% to 29 % and maximum relative deviation of 88%. Sadat-Helbar et al. [24] re-examined 22 relationships published by 17 researchers from 1933 to 2007 then developed a new relationship with a better agreement between observed and predicted data.

Almost all early theoretical formulas for estimating sediment settling velocity were developed by assuming grains as spheres, which is proven to be not true. The nature of sand is unique in its kinds possessing highly irregular particle shapes. Various studies present in the literature have used mean sieve diameter as the characteristic diameter to predict the settling velocity of sands. After analyzing various sand particles experimentally, it was found that the mean sieve diameter is not a good presentation of sand's shape and size. But none of the authors had presented a universally accepted analysis on the naturally available sands, which can be used to estimate the settling velocity of sands accurately. Out of all the models available, Hallermeier's [10] empirical model was found to be more suitable for sands; however, the model results in an absolute average error of 14.7%.

In the current study, PIS technique has been used, for the first time, to accurately determine the settling velocity of sand particles in water. This modern technique is based on high resolution imaging with a resolution of 5µm and capability to freeze motions of more than 100 m/s. The experimental setup has been calibrated using the glass beads in the size range of 0.7-2.0 mm. Four different sieve sizes of sub angular quartz sand particles have been used for experimental investigations. Apart from settling velocity, shadowgraph technique has been used to measure centricity, project area, major and minor axes of individual sand particles. Based on the experimental results an empirical model for the prediction of settling velocity was developed using equivalent circular diameter (D_c) obtained from shadowgraph. In addition, a simplistic model was also proposed based on equivalent circular radius (R_{ce}) considering the particles to be an ellipse. Both models have been compared with the literature data ([22], [25] to [28]).

5.2 Experimental Details

5.2.1 Experimental Program

The experimental setup discussed in chapter 2 in details has been used for this study. All settling velocity measurements are carried using sand particles in water at room temperature. The calibration of the experimental technique has been carried out by measuring the size and settling velocities of four different glass spheres (Corposular's Glass Spacers Millibeads) and comparing with the data provided by the manufacturers as well as the predictions by using the universal drag curve available for spheres.

5.2.2 Experimental Procedure

The procedure for obtaining empirical data was split into two parts; the physical setup of the experiment and the processing of data. The procedure is the same as the one presented in the Chapter 2. One of the captured image from Lavision double frame camera and the double pulse laser is shown in figure 5-1. This is the image recorded using shadowgraph setup. As shown in the image, the particles which only fall in the focal plane of the lens will appear sharp (basic principle of optics). The entire processed image after processing using Davis 8.0 software look like the image shown in Fig.5-2. The image in Fig. 5-2 is one of the processed images from shadowgraph for fine sands. The full process was repeated with four different sieve sizes of sands. For each sand type, experiments were performed thrice and the values were recorded.

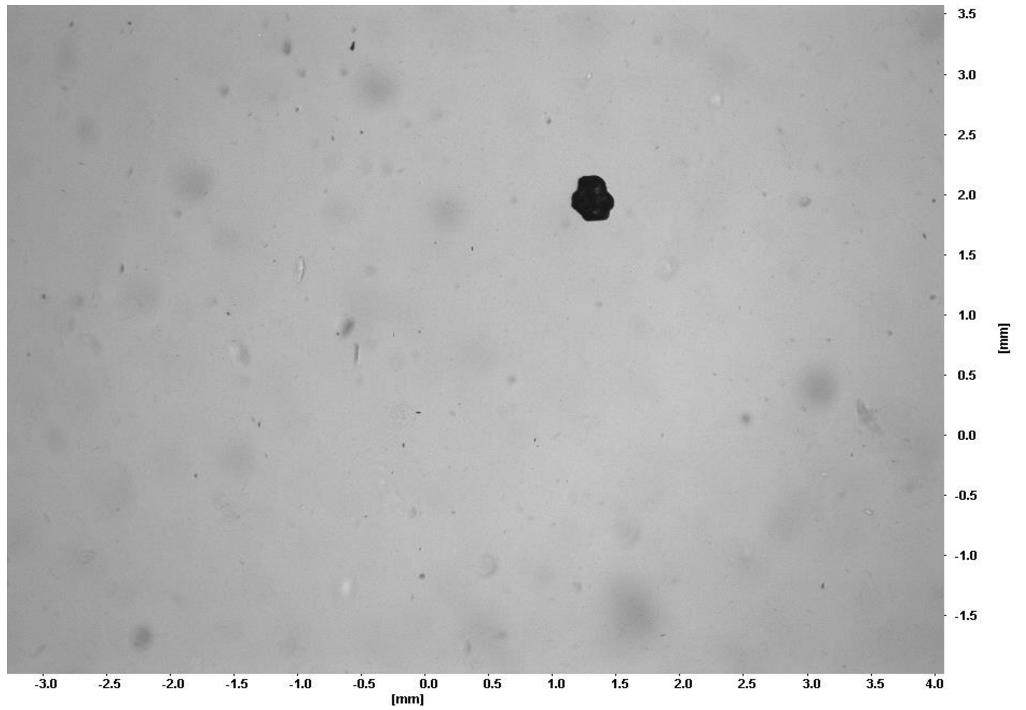

Figure 5-1: Image of fine sand particle recorded by shadowgraph

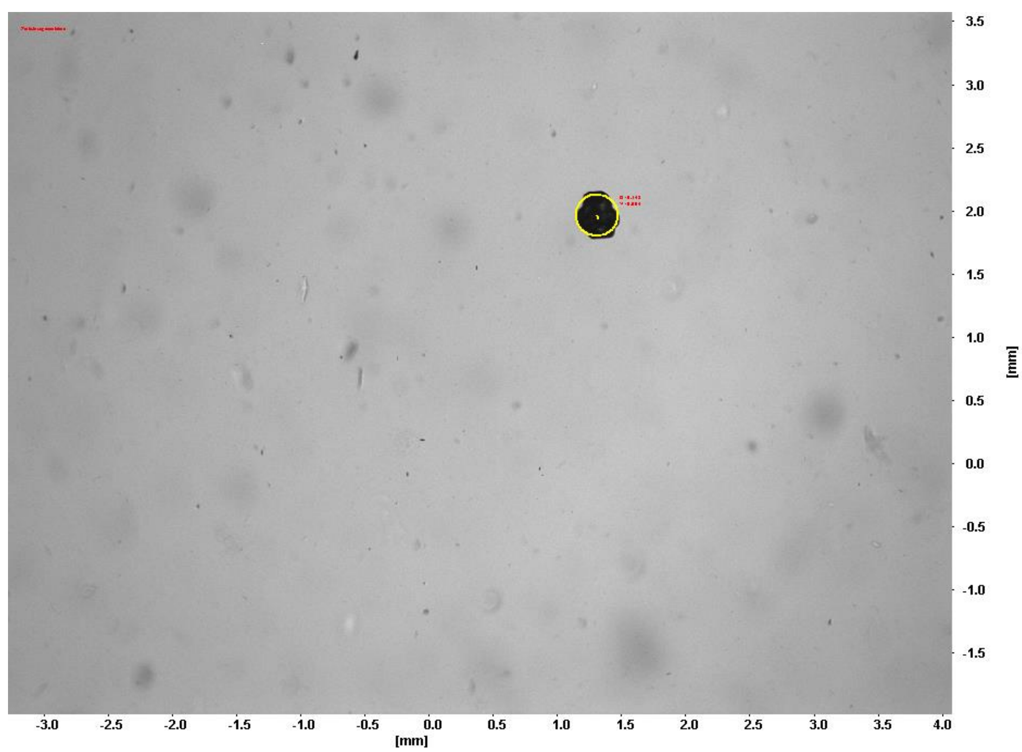

Figure 5-2: The processed image from Davis 8.0 for fine sands

5.2.3 **Physical Properties of Sand Particles**

Table 5-1 and Table 5-2 are the reported properties of the sand particles. Note that the most important property in these experiments is the specific gravity of sand particles. The sand particles of size 0.35 -1.2 mm procured from Sil Inc. were used in this study.

Table 5-1: Physical properties of fine sand

Property	**Test Method**	**Unit**	**Typical values**
Mineral	Petrographic	………	Quartz
Shape and hardness	Visual	Mohr	Sub Angular/6.5
pH	AFS	……….	7.2-7.4
Specific gravity	ASTM C-128	……….	2.65
Bulk Density, aerated	ASTM C-29	Lbs/Ft^3	92-95
Compacted	ASTM C-29	Lbs/Ft^3	98-100

Table 5-2: Physical properties of coarse sand

Property	**Test Method**	**Unit**	**Typical values**
Mineral	Petrographic	………	Quartz
Shape	Krumbein	………	Sub Angular
Hardness	Moh	6.5	
Specific gravity	ASTM C-128	……….	2.65
Bulk Density, aerated	ASTM C-29	Lbs/Ft^3	92-95
Compacted	ASTM C-29	Lbs/Ft^3	98-100

5.3 Error analysis for available settling velocity models

There exist multiple correlations developed empirically and analytically to predict the settling velocity of sand. An important parameter known as dimensionless diameter (d_d) given by eqn. 5-1 [12] has been frequently used to develop the correlation. Several models for sand settling velocity published in the literature from 1956 to 2009 have been critically reviewed. The applicability of the models and there predicting capability has been discussed below in details.

$$d_d = d\left(\left(\frac{g\left(\frac{\rho_p-\rho_O}{\rho_o}-1\right)}{v^2}\right)\right)^{\frac{1}{3}} \qquad \textbf{Eq. (5-1)}$$

Shah [29] has also proposed a settling model for the sediment particles which is given below:

$$w = \frac{\frac{1}{24}(\rho_p-\rho_o)}{\rho_O} * g * \frac{d^2}{v} \quad \text{for d<0.01 cm} \qquad \textbf{Eq. (5-2)}$$

$$w = 1.14\left(\frac{\rho_p-\rho_o}{\rho_o} * g * d\right)^{0.5} \text{for d>0.2cm} \qquad \textbf{Eq. (5-3)}$$

$$\left(\log\left(\frac{R}{d_d}\right) + 3.790\right)^2 + (log d_d - 5.777)^2 = 39 \quad for\ 0.01 \le d \le 0.2 \qquad \textbf{Eq. (5-4)}$$

The sand particle used in this study is in the range of third correlation (Eq.5-4) proposed by Shah [29]. Iteration has been performed to get the settling velocity from the proposed equation. The equation5-4 gives an error of 14-38% with an average error of around 26%.

There are some simple relations (eqn. 5-5), which can predict the settling velocity of sand equally well as those of complicated relationships (eqn. 5-4, eqn. 5-6, eqn. 5-8). One of such equation has been proposed by Migniot [36], which is easy to use and just require a single input. The relation is valid for diameter 0.02-0.1 cm and fluid medium need to be water at room temperature. The model (eqn. 5-5) is found to be giving an error in the range of 1.39-23.6 % with an average of 9.6%.

$$w = 125d \qquad \textbf{Eq. (5-5)}$$

Hallermeier [10] developed a correlation between the settling velocity of sand and sphere of similar diameter as sieve diameter of sand. For the estimation of settling velocity of sphere with equivalent diameter as that of sand the proposed relation (eqn. 5-6) was used.

$$w_s = 0.11\left(\frac{\rho_p-\rho_O}{\rho_o}g\right)^{0.75} D^{1.25}\upsilon^{-0.5} \qquad \textbf{Eq. (5-6)}$$

And using the settling velocity of equivalent sphere the settling velocity of sand particle can be estimated using Eq.5-7.

$$w = 1.062(w_s)^{0.956} \qquad \textbf{Eq. (5-7)}$$

On comparison with the measured values, the model gives an average error of 14.7% with error varying from 1.9-27.64%.

Zhang [37] proposed yet another correlation for predicting the settling velocity of sand grain given by eqn. 5-8.

$$w = \left(\left(\frac{13.95\upsilon}{d}\right)^2 + 1.09 * \frac{\rho_p-\rho_O}{\rho_o} * d\right)^{0.5} - 13.95 * \frac{\upsilon}{d} \qquad \textbf{Eq. (5-8)}$$

The uniqueness of the correlation is that it is valid for all size ranges. When comparing with the experimental results, the model was found to be relatively more accurate and gives an error in the range of 2-16%, with a mean error of 10.6%.

Van Rijn [18] proposed similar correlations as that of Shah [29]. Based on the particle size three different correlations had been proposed and are given by eqn. 5-9 to eqn.5-11.

For the intermediate diameter the author had suggested the use of correlation proposed by Zanke [30] which is given by the Eqn. 5-11. The proposed models were found to give an error in the range of 4-26% with average error of 14.3% when compared with the measured experimental values from the shadowgraph.

$$w = \frac{\frac{1}{18}(\rho_p - \rho_o)}{\rho_O} * g * \frac{d^2}{\upsilon} \qquad \text{for d<0.01 cm} \qquad \textbf{Eq. (5-9)}$$

$$w = 1.1\left(\frac{\rho_p - \rho_o}{\rho_o} * g * d\right)^{0.5} \text{ for d>0.1 cm} \qquad \textbf{Eq. (5-10)}$$

$$w = 10 * \frac{\upsilon}{d}\left(\left(1 + 0.01 d_d^3\right)^{0.5} - 1\right) \qquad \text{for } 0.01 \le \text{d} \le 0.1 \text{ cm} \qquad \textbf{Eq. (5-11)}$$

Ibadzade [31] developed a unique relation for settling velocity of grains which had also included the effect of temperature in it. The model is similar to the one developed by Shah [29]. For particle size smaller than 0.01cm, the relationships from both authors are the same. The proposed relations are given by eqn. 5-12 to eqn. 5-14.

$$w = \frac{\frac{1}{24}(\rho_p - \rho_o)}{\rho_O} * g * \frac{d^2}{\upsilon} \qquad \text{for d<0.015cm} \qquad \textbf{Eq. (5-12)}$$

$$w = 1.068\left(\frac{\rho_p - \rho_o}{\rho_o} * g * d\right)^{0.5} \text{ for d> 0.15 cm} \qquad \textbf{Eq. (5-13)}$$

$$w = 67.6 * \frac{\rho_p - \rho_O}{\rho_o} * d + 0.52 * \frac{\rho_p - \rho_O}{\rho_o}\left(\frac{T}{26} - 1\right) \text{ for } 0.015 \le \text{d} \le 0.15 \qquad \textbf{Eq. (5-14)}$$

T is in Degree Celsius d in cm and w in cm/s

The predicting capability of the model is found to give error of 10-31%. The mean average error is found to be 18.69% when compared with the experimental results.

Cheng [11] developed a settling velocity model using dimensionless approach for natural grains and sediments. A simple correlation for natural sand grains in intermediate flow regime was proposed (eqn. 5-15).

$$\frac{wd}{\upsilon} = \left(\left(25 + 1.2d_d^2\right)^{0.5} - 5\right)^{1.5} \qquad \textbf{Eq. (5-15)}$$

The proposed model (eqn. 5-15) is found to give an error of 20-42% when compared with the experimental results on sands.

Another settling velocity model (eqn. 5-16) was proposed by Soulsby [32], when compared with the experimental results, the proposed model show a very high degree of deviation in prediction. The maximum error is found to be 75%. The proposed model is given as follows:

$$Re = 2.59\left(\left(16 + 0.156d_d^3\right)^{0.5} - 4\right) \qquad \textbf{Eq. (5-16)}$$

Jemnez and Madsen [21] proposed a correlation based on dimensionless diameter for predicting the settling velocity of sand particles. The predicting capability of the proposed model (eqn. 5-17) is found to be very poor and gives very high error when compared with the measured velocity.

$$Re = \frac{d_d^3}{0.954d_d^{1.5} + 20.48} \qquad \textbf{Eq. (5-17)}$$

She et al. [33] had tried to develop more accurate model for the settling velocity of sand. Authors proposed correlations (eqn. 5-18 and eqn. 5-19) using dimensionless diameter for predicting the settling velocity of particles.

$$Re = 1.05d_d^{1.5}((1 - \exp\left(-0.08d_d^{1.2}\right)) \qquad \text{for } d_d > 2 \qquad \textbf{Eq. (5-18)}$$

$$Re = 1.05 d_d^{1.5}((1 - \exp(-0.315 d_d^{0.765})) \qquad \text{for } d_d < 2 \qquad \textbf{Eq. (5-19)}$$

She et al. [33] correlation has been found to be more accurate than the previous models available in the literature, with an average error of about 9% when compared with the experimental results. The maximum deviation of 24% has been noticed.

In one of the recent study, Fergusson and Church [34] have proposed a settling velocity model for sand grains based on the sieve diameter. The model is simple and has been extensively referred in different related studies. The proposed relationship is given by eqn. 5-20.

$$\upsilon = \frac{rgd^2}{C\upsilon + (0.75Brgd^3)^{0.5}} \qquad \textbf{Eq. (5-20)}$$

Where r=submerged specific gravity, g is acceleration due to gravity, d is the diameter in m, C and B are constants, υ is kinematic viscosity of the fluid.

For sand grains the recommended value for C is 18 and B is 1 when the d is the sieve diameter.

The proposed model when compared with the experimental results from Shadowgraph measurements gives an error in the range of 4.7 to 16% with a mean average error of 10.7%. While the maximum deviation is found to be less, the average error is slightly higher when compared to the other models from the literature.

In a very recent study conducted by Sadat and Tokaldany [24], the fall velocity of sediments is studied in detail. The proposed models in the study are given by eqn. 5-21 and eqn. 5-22.

$$w = \frac{0.033\upsilon}{d}\left(d^3 * g * \frac{\frac{\rho_P - \rho_O}{\rho_O} - 1}{\upsilon^2}\right)^{0.963} \qquad \text{for } d_d \leq 10 \qquad \textbf{Eq. (5-21)}$$

$$w = \frac{0.51\upsilon}{d}\left(d^3 * g * \frac{\frac{\rho_p-\rho_O}{\rho_o}-1}{\upsilon^2}\right)^{0.553} \qquad \text{for } d_d > 10 \qquad \textbf{Eq. (5-22)}$$

The authors had reported an average error of 11.7% for the proposed model. When compared with the experimental data from shadowgraph the average error is found to be nearly 11%, while the actual error varies between 3-23%.

The discussed model is no better than the previous model and author has failed to minimize the error in the predicted settling velocity.

The detailed error analysis of the models has shown that for the coarse sand of size greater than 1 mm, Migniot [36] is predicting the values best followed by Van Rijn[18], Fergusson and Church [34], Ibad Zade [31], ,Shah [29], Zhang [37], Hallermeir (1981), Sadat [24], She et al. [33], Cheng [11], Jimnez and Madsen [21] and Soulsby [32].

For fine sands She et al. [33] is found to be best followed by Sadat [24], Fergusson and Church [34], Zhang [37], Migniot [36], Van Rijn [18], Hallermeir (1981), Ibad Zade [31], Shah [29], Jimnez and Madsen [21], Cheng [11], and Soulsby [32]. One of the important observations that can be made is that the model which is suited for coarse sand has been found to be inefficient for fine sands. The deviation in the prediction of these models is found to be more in case of fine sands. One can conclude that even though the average error in different model is more than 10, none of them is applicable for both sand type at a time. An important observation which noticed during the study is that for higher Reynolds number the drag coefficient for natural sediment particles are found to be around 1-1.2 ([17], [18], [29], [35], and [37]).

5.4 Results and Discussion

5.4.1 Experimental Results

Settling velocity experiments using PIS technique are conducted using the four different sieve sizes of sands. Using the provision available in Davis 8.0 processing software, shape, size, velocity, and centricity values for the sand particles have been measured and tabulated in table 5-3. Within a particular sieve size, it is observed that there is a considerable variance in the settling velocity, major axis, and minor axis dimensions for the sand particles. For example, if the mean sieve diameter (D_s) of sand is 1.18 mm, the average settling velocity of the particle with this mean sieve diameter would be 0.1757 m/s. However, the actual velocities of particles with D_s = 1.18 mm, vary from 0.151 to 0.199 m/s. In this case, settling velocity calculated based on D_s can result a variance as high as 16.35 %. Similarly, the error can be 59%, 27%, and 92.35% for particles with D_s values of 0.775 mm, 0.60 mm, and 0.35 mm, respectively. Assuming a particular sieve size is valid for batch of sand sample means that all the sands particles in that batch are spheres with a particular diameter. These assumptions are not valid for sand particles and as shown from the results given in Table 5-3, D_s do not give accurate information about the size and shape of the particles. It has been observed from the captured image from shadowgraph (Fig. 5-1 and Fig. 5-2) that sand particles are not spherical in shape. An ellipse can define the sand particle shape better than a sphere. Even the centricity values of different sand particles lie within the range of 0.30-0.7, which is not even close to the centricity value of sphere. Most of the models presented in the literature define the settling velocity as a function of sieve diameter only (Migniot [36], Baba & Komar [1] and Hallermeir [10] and did not include the effect of centricity or shape of the sand particles. Based on the experiments conducted, a particle diameter (equivalent circular diameter (D_c)) is proposed for the sand particle. D_c is defined as the diameter of the circle which has same area as that of the actual projected area of the particle. Since this new diameter is based on the actual area of irregular sand particle, it contains the actual shape and size factor in it.

Table 5-3: Particle geometrical parameters and settling velocities measured from Shadowgraph experiments

Sand Size Sieve Diameter & Total Number of Particles	Dia Range (mm)	Average Diameter (mm)	Avg. Settling Velocity (m/s)	Avg. Centricity	Avg. Large Axis (mm)	Avg. Small Axis (mm)	No. of Particle
1.18 mm (274)	1.0-1.1	1.0661	0.1549	0.472	0.671	1.461	10
	1.1-1.2	1.1521	0.1510	0.552	0.814	1.489	28
	1.2-1.3	1.2502	0.1714	0.586	0.916	1.584	64
	1.3-1.4	1.3486	0.1768	0.600	0.991	1.706	62
	1.4-1.5	1.4420	0.1799	0.593	1.062	1.822	42
	1.5-1.6	1.5434	0.1826	0.554	1.084	2.003	35
	1.6-1.7	1.6356	0.1898	0.559	1.158	2.113	21
	1.7-1.8	1.7233	0.1989	0.598	1.269	2.176	8
	1.8-1.9	1.8502	0.1864	0.489	1.714	2.529	4
700µm<D_c<850 µm (240)	0.5-0.6	0.5890	0.0595	0.493	0.387	0.791	3
	0.6-0.7	0.6578	0.0707	0.6350	0.5066	0.809	30
	0.7-0.8	0.7582	0.0900	0.6132	0.5721	0.944	79
	0.8-0.9	0.8433	0.1057	0.5603	0.5980	1.088	70
	0.9-1.0	0.9445	0.0994	0.5123	0.6355	1.253	41
	1.0-1.1	1.0530	0.1034	0.3933	0.5860	1.520	13
	1.1-1.2	1.1231	0.1199	0.4510	0.6910	1.555	4

500µm<D_c<700 µm (241)	0.4-0.5	0.470	0.079	0.412	0.275	0.275	3
	0.5-0.6	0.564	0.094	0.567	0.404	0.403	37
	0.6-0.7	0.649	0.096	0.591	0.478	0.478	82
	0.7-0.8	0.744	0.105	0.580	0.541	0.540	78
	0.8-0.9	0.838	0.111	0.559	0.594	0.594	28
	0.9-1.0	0.928	0.107	0.487	0.596	0.596	9
	1.0-1.1	1.038	0.098	0.411	0.483	0.483	4
300µm<D_c<400 µm (226)	0.1-0.2	0.173	0.030	0.395	0.098	0.248	4
	0.2-0.3	0.257	0.046	0.593	0.203	0.348	36
	0.3-0.4	0.351	0.059	0.602	0.261	0.440	120
	0.4-0.5	0.433	0.064	0.599	0.323	0.544	62
	0.5-0.6	0.509	0.065	0.636	0.392	0.623	4

The Table 5-3 shows the equivalent circular diameter of each sample of sands. It is found that the particle diameter within a sieve size range is varying a great range and using the equivalent sieve diameter as one representative diameter for all particles in that sieve range is erroneous. For each sand group, around 250 sand particles are detected during shadowgraph experiments and average of these values are shown in Table 5-4. Averaging is done using the frequency distribution of the data. The correlation for settling velocity present in the literature with equivalent sieve diameter may look simple and easy to use but in reality without considering the effect of shape parameter, the predicted settling velocity may not be accurate. The centricity of a particle or any other parameter, which defines the shape of a particle, should be included in modeling to accurately estimate the setting velocity.

Table 5-4: Average values of particle geometrical parameters and Settling Velocities Measured from Shadowgraph Experiments

Sand Type	Mean D_c (mm)	Mean D_c (mm)	Range of D_c (mm)	Avg. velocity (m/s)	Avg. Centricity	Avg. Large axis (mm)	Avg. Small axis (mm)	Total no.of particles
Coarse	1.18	1.375	1.0-1.9	0.176	0.573	0.990	1.759	274
Coarse	0.775	0.822	0.5-1.2	0.095	0.568	0.583	1.062	237
Coarse	0.60	0.563	0.4-1.1	0.081	0.457	0.402	0.724	241
Fine	0.35	0.361	0.1-0.6	0.058	0.597	0.268	0.454	226

5.4.2 Relationship between Equivalent Circular Diameter and Sieve Diameter

The equivalent circular diameter, D_c, is more accurate way of measuring the size and shape of the sand. Based on the results tabulated in Table 5-5, a relationship (equation 5-23) between mean sieve diameter, D_s, and the equivalent circular diameter, D_c, has been developed.

$$D_c = 1.2489D_s - 0.1267 \qquad \textbf{(Eq. 5-23)}$$

This relationship can be used to convert the sieve diameter into D_c. The relationship between D_c and D_s is also shown in Fig. 5-3 graphically. Each point in the graph (Fig. 5-3) shows the average D_c values of all the sand particles measured for that particular sieve size of sand. Like for the first point, it is the average value of 226 particles detected for mean sieve diameter of 0.35 mm and D_c varying from 0.1mm to 0.6 mm. Therefore, the averaging which is shown by a single point incorporates all type of particle's shape and size occurring within that particular (sieve) group of sand. For each group of sand, the average D_c and the measured sieve diameter is shown in Fig. 5-3. The detailed values of these points plotted in Fig. 5-3 are given in Table 5-4.

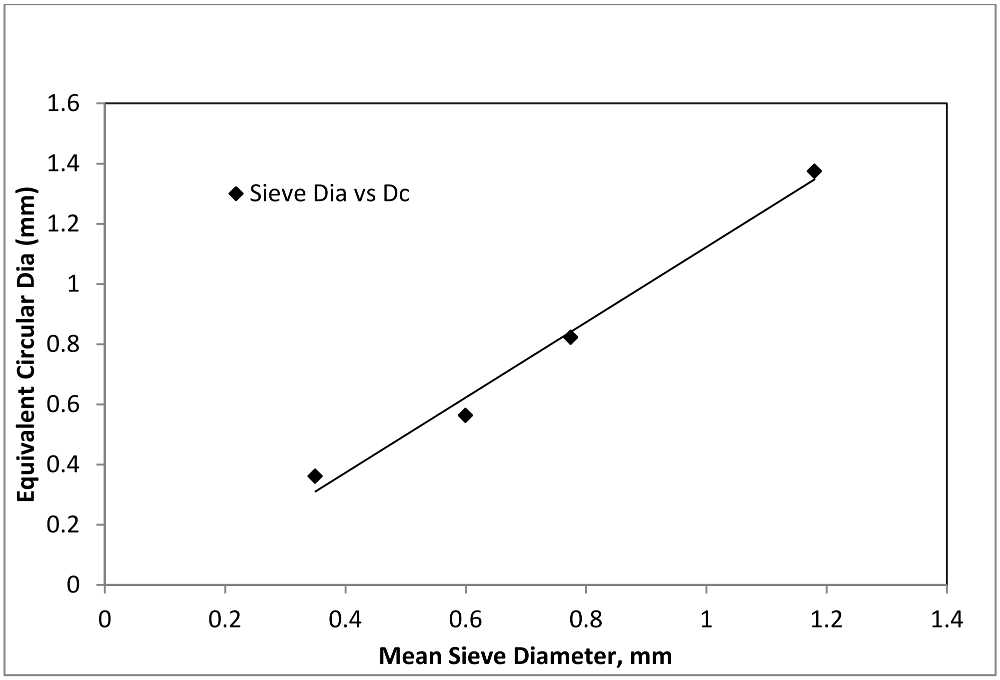

Figure 5-3: Data showing the relationship between D_c and D_s for natural sands.

5.4.3 C_d –Re_p Relationship for Sands

To present a better understanding of the settling velocity behavior, the drag coefficient versus Reynolds number is calculated. To see the relation between the C_d vs Re_p for sands, data from different authors (listed in table 5-5) and measured values from shadowgraph experiments are shown in Fig. 5-4. The drag coefficient values for spheres in Newtonian fluid obtained from universal C_d vs Re_p curve are also plotted in Fig. 5-4. It is noticed that sand data differ from the spheres because of the fact that sand do not have a fixed shape and has varying centricity. It is observed that there is significant deviation in drag coefficient values of sands when compared with the regular sphere. An important observation that can be made from the plot is the significant effect of centricity which leads to different drag values for the same particle Reynolds number. Another important fact observed from the plot is that for Reynolds number greater than 160, C_d attains a constant value of ~ 0.95. When this drag coefficient value is used for calculating the settling velocity of actual sand particles of different D_c and centricity as measured from shadowgraph experiments, it gives an absolute average error of around 8.80% for 276 sands particles with Re >160. The result of the curve fitting of drag coefficient vs Reynolds number data is shown by equation 5-24. The regression coefficient value is found to be 0.91 for 95% confidence level.

$$C_d = 21.87 * Re_p^{-0.8679} + 1.105 \qquad \textbf{Eq. (5-24)}$$

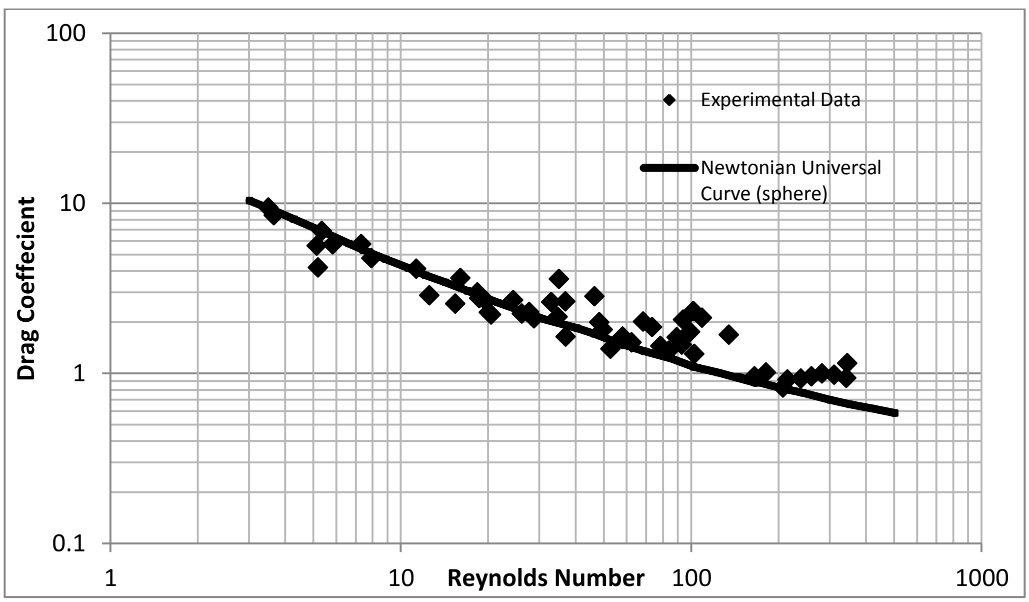

Figure 5-4: Comparison of Reynolds number vs C_d plot for natural sands

5.4.4 Settling Velocity Model for Sand

Considering that there are significant irregularities in the shape of sand particles, a model based on the measured values of settling velocity and equivalent circular diameter has been developed. The equivalent circular diameter, D_c, used in the analysis takes care of the shape factor because it is derived from the actual projected area of the irregular sand particles. The current analysis is the extended version of numbers given by the Hallermeier [10] as Archimedes Buoyancy Index. Dietrich [2] had used the same number with the name dimensionless diameter. Cheng [11] had also used the same number as D* and named it as dimensionless diameter. In the current analysis, we also used the same dimensionless number used by Hallermeier [10], Dietrich [2], and Cheng [11]. The two numbers used in this study are given by the equations 5-25 and 5-26.

$$D^{*} = D^{\prime}\ g D_s^3 / v^2 \qquad \textbf{Eq. (5-25)}$$

$$R_s = V_s * D_c / v \qquad \textbf{Eq. (5-26)}$$

The measured data from shadowgraph experiments listed in table 5-3 were used for the analysis. Here D_c has been used for the dimensionless number D*. The values of the dimensionless number are calculated and plotted as shown in Fig. 5-5. Regression analysis has been performed and a simple power law correlation given by equation 5-27 represents the relation between these two dimensionless parameters. The regression coefficient (R^2) for the fit comes to be 0.9826, showing the nature of the correlation is acceptable.

$$R_s = 0.3623 D^{*0.6008} \qquad \textbf{Eq. (5-27)}$$

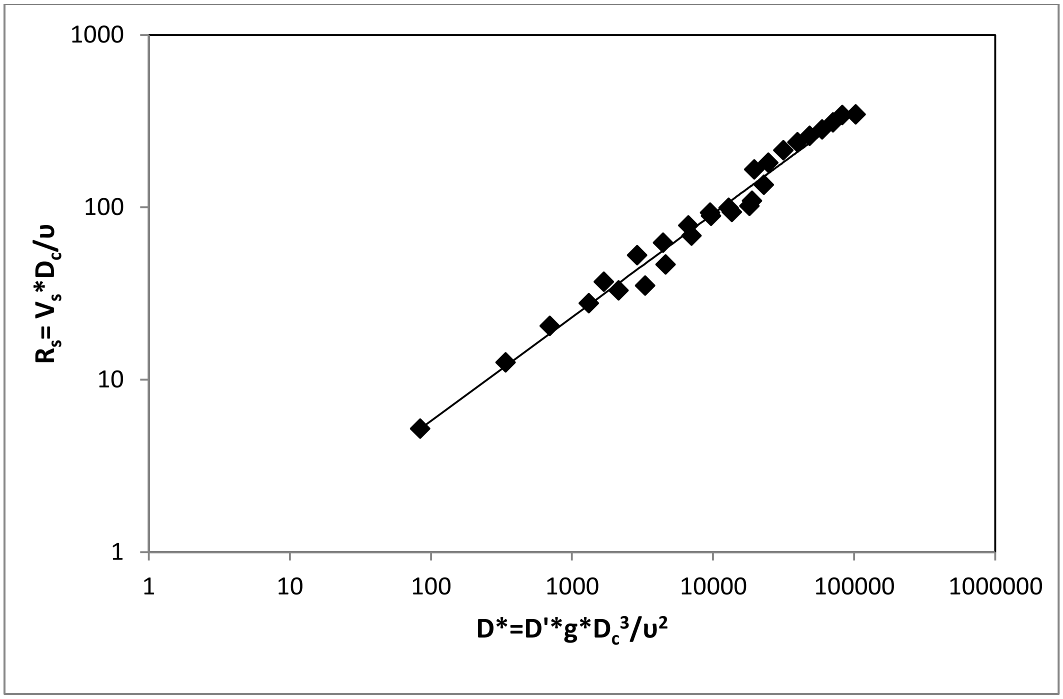

Figure 5-5: Relationship between R_s and D* for natural sands

5.4.5 Steps to Calculate Particle Slip Velocity, Vs, Using the Regular Model

- Measure the D_c for sand particle, in case if D_c cannot be measured because of lack of availability of measuring technique, one can use the D_c and D_s relationship given by equation 5-23.
- Calculate the D* using the relationship given by eqn. 5-25.
- Once D* is calculated, one can use the R_s and D* relationship given in the equation 5-27 to calculate R_s
- Using the definition of R_s the settling velocity can be calculated from eqn. 5-26.

5.4.6 Sample Calculation

The detailed sample calculation regarding how to use the model is given below.

Problem: To estimate the settling velocity of sand grain with following properties:

Specific gravity: 2.65

Fluid: Water (density 1000)

Fluid's Viscosity: $1.00*10^{-6}$ m^2s^{-1}

Mean Sieve Diameter: 0.59 mm

All the above data has been taken from Engelund and Hansen [26]

Solution:

Here the steps mentioned in the results and discussion section is followed to estimate the settling velocity.

Step 1: Calculate Dc

Since in this example Dc is not given, one needs to estimate it with the relation given by equation 5-23

$$Dc = 1.2489Ds - 0.1267$$

Substituting the value of Ds = 0.59 in the above equation

$$\text{Dc} = 0.59*1.2489\text{-}0.1267\text{=}0.611 \text{ mm=}.0611*10^{-3} \text{ m}$$

Step 2: To calculate D*

Using the relation given in eqn. 5-25

$$D^* = D'gDc^3/v^2$$

D'=S.G. of Sand –S.G. of Fluid = 2.65-1.0

$D^* = (1.65*9.81*(.611*10^{-3})^3)/(1.00*10^{-6})^2 = 3676.57$

Step 3: Using the equation 5-27 the R_s value can be predicted

$$R_s = 0.3623 D^{*0.6008}$$

Substituting D* calculate in part two to the relation given above

Rs = 0.3623 * $(3676.57)^{.6008}$ = 50.257

Step 4: To estimate Vs

In this final step using the relation given in eqn. 5-26 and substituting the R_s and D_c value estimated in the step 3 and Step 1

$$R_s = V_s * D_c / \nu$$

Vs= $(50.27*1.00*10^{-6})/(0.611*10^{-3})$ = **0.0824 m/s**

The measured value for the same particle was reported by Engelund [26] as 0.084 m/s.

5.4.7 Comparison of Predicted Results with Literature

There are several previous works reporting measured settling velocities of different sizes of sand grains in Newtonian fluid. Experimental results from Engelund and Hansen [26],Dalrymple and Thompson [25], U.S Inter-Agency Committee (1957), Vincent [27], and Nielsen [28] were compared with the settling velocity values predicted by using the model developed by the current study. The detailed comparison of the results is shown in Table 5-5.

Table 5-5: Comparison of the predicted vs experimental sand settling velocity values in water

Source	D_s (mm)	D'	υ	V (m/s)	D_c (mm) (eqn 4-23)	D* (eqn 4-25)	R_s (eqn.4-27)	V_s (eqn.4-26)	Absolute Error %
Engelund and Hansen [26]	0.76	1.65	1.00	0.11	0.82	9005.4	86.09	0.105	4.80
	0.76	1.65	1.31	0.10	0.82	5328.6	62.81	0.100	0.04
	0.59	1.65	1.00	0.08	0.61	3676.7	50.26	0.082	1.94
	0.59	1.65	1.31	0.08	0.61	2175.6	36.67	0.078	2.24
	0.42	1.65	1.00	0.06	0.39	1019.3	23.25	0.055	0.76
	0.42	1.65	1.31	0.05	0.40	593.9	16.81	0.055	10.69
	0.29	1.65	1.31	0.03	0.24	123.2	6.53	0.036	10.11
	0.29	1.65	1.00	0.04	0.24	211.4	9.04	0.038	1.61
	0.25	1.65	1.31	0.03	0.19	60.2	4.25	0.030	7.17
	0.208	1.65	1.31	0.02	0.13	22.2	2.33	0.023	0.06
	0.208	1.65	1.00	0.03	0.13	38.1	3.23	0.024	13.31
Dalrymple & Thompson [25]	0.4	1.65	1.20	0.06	0.37	582.7	16.61	0.054	4.33
	0.4	1.65	1.16	0.06	0.37	623.5	17.31	0.056	2.11
	0.4	1.65	0.95	0.06	0.37	929.7	22.00	0.056	9.58
	0.4	1.65	0.89	0.06	0.37	1059.2	23.79	0.057	11.25
U.S Inter-Agency Committee(1957)	0.425	1.65	1.65	0.06	0.40	1067.9	23.91	0.059	1.04
	1.2	1.65	1.65	0.14	1.37	57857	263.2	0.163	15.65
Vincent [27]	0.24	1.65	1.00	0.03	0.17	83.8	5.19	0.029	9.19
	0.46	0.46	1.00	0.06	0.45	1453.4	28.78	0.064	7.10
	1.1	1.65	1.00	0.06	1.25	7230.1	75.45	0.060	8.03
	1.2	0.38	1.00	0.07	1.37	9627.1	89.61	0.065	10.53

	0.39	0.38	1.00	0.02	0.36	211.19	9.03	0.025	19.33
Nielsen [28]	0.175	1.65	1.00	0.02	0.09	12.545	1.66	0.018	9.86
	0.19	1.65	1.00	0.03	0.11	21.893	2.31	0.021	22.51
	0.36	1.65	1.00	0.05	0.32	544.97	15.96	0.049	3.07
	0.55	1.65	1.00	0.07	0.56	2845.5	43.09	0.077	14.79

5.5 An Alternative Approach to Calculate D_c and V_s (Elliptical Model)

Results of the current study have shown that sieve diameter is not a good way for representing proper size and shape characteristics of sand particles. Therefore, a new model based on the equivalent circular diameter, D_c, of the projected area has been developed. The D_c used here can be measured accurately with image processing technique, which can give the area for an irregular shape, however, in case the imaging technique is not available an alternative method of estimating D_c is proposed here. Sand particles are assumed to be represented by elliptical geometry. The measured data of small (a) and big (b) axis for different sand particles using shadowgraph have been used to calculate the area of the ellipse and later on area estimated from ellipse is used to calculate the equivalent circular radius i.e., R_{ce} . The equation 5-28 defines as a function of a and b.

$$R_{ce} = (ab)^{0.5} \qquad \textbf{Eq. (5-28)}$$

When the calculated values of R_{ce} (using equation 5-28) are compared with the measured values from shadowgraph experiments (980 sand particles used in the analysis), it gives an absolute average error of 4.45%.

The actual D_c values measured by the shadowgraph are now replaced with the R_{ce} calculated by assuming particle to be an ellipse. The revised equation for converting sieve diameter to R_{ce} is given by equation 5-29. The regression coefficient (R^2) for the relationship was found to be 0.9867.

$$R_{ce} = 1.865 D_s - 0.118 \qquad \textbf{Eq. (5-29)}$$

Using the same step as that has been used in the section 3 for developing equation 5-27, a modified version of the equation was obtained by replacing D_c with R_{ce}. The alternate relationship between the R_s and D* is given by equation 5-30. The regression coefficient (R^2) for this relation is found to be 0.9837.

$$R_s = 0.3766 D^{*0.6018} \qquad \textbf{Eq. (5-30)}$$

5.5.1 Comparison of Elliptical Models with Literature

The equation 5-30 can then be used to determine sand particle settling velocity using the same steps mentioned in the above section, Comparison of the predicted V_s values using eqn. 5-30 (elliptical model) and the experimental values measured by different authors are given in Table 5-6. The maximum absolute average error for this case was found to be 9.16% while with the previous model it was 7.7%. The particles are the same as the ones given in Table 5-5.

Table 5-6: Comparison of the predicted (Elliptical model) vs experimental sand settling velocity values in water

Source	D_s (mm)	D'	υ	V (m/s)	R_{ce} (mm) eqn 4-29	D* (eqn 4-25)	R_s (eqn. 4-30)	V_s (eqn. 4-26)	Absolute Error
Engelund and Hansen [26]	0.76	1.65	1.0	0.11	0.78	7792.36	82.8	0.105	3.98
	0.76	1.65	1.3	0.10	0.78	7792.36	82.8	0.106	5.61
	0.59	1.65	1.0	0.08	0.58	3191.54	48.4	0.083	1.06
	0.59	1.65	1.3	0.08	0.58	3191	48.4	0.083	7.93
	0.42	1.65	1.0	0.06	0.38	890	22.4	0.059	1.71
	0.42	1.65	1.3	0.05	0.38	890	22.4	0.059	17.98
	0.29	1.65	1.3	0.03	0.23	187	8.8	0.039	17.58
	0.29	1.65	1.0	0.04	0.23	187	8.8	0.038	0.50
	0.25	1.65	1.3	0.03	0.18	92	5.7	0.032	14.63
	0.208	1.65	1.3	0.02	0.13	34.6	3.2	0.025	7.23
	0.208	1.65	1.0	0.02	0.13	34.6	3.2	0.024	11.91
Dalrymple & Thompson[25]	0.4	1.65	1.2	0.06	0.36	582.7	16.0	0.054	3.45
	0.4	1.65	1.1	0.06	0.36	623.5	16.7	0.054	4.49
	0.4	1.65	0.9	0.06	0.36	929.7	21.2	0.057	8.71
	0.4	1.65	0.9	0.06	0.36	1059.3	23.0	0.057	10.38
U.S Inter-Agency Committee [22]	0.425	1.65	1.6	0.06	0.39	1067.9	26.5	0.062	2.28
	1.2	1.65	1.6	0.14	1.31	57857	252.0	0.165	16.79
Vincent [27]	0.24	1.65	1.0	0.03	0.17	75.1	5.06	0.030	7.97
	0.46	0.46	1.0	0.06	0.43	1267.2	27.7	0.065	8.09
	1.1	1.65	1.0	0.05	1.19	6236.9	72.4	0.061	8.89
	1.2	0.38	1.0	0.07	1.31	8300	85.9	0.065	9.80
	0.39	0.38	1.0	0.02	0.34	184.9	8.7	0.025	20.33

Nielsen [28]	0.175	1.65	1.0	0.02	0.09	11.7	1.6	0.018	7.90
	0.19	1.65	1.0	0.03	0.11	20.0	2.30	0.021	21.06
	0.36	1.65	1.0	0.05	0.31	478.1	15.4	0.049	2.10
	0.55	1.65	1.0	0.07	0.53	2472	41.5	0.077	15.82

5.6 Conclusions

The PIS technique was found to be very efficient and accurate in capturing the shape, size, and settling velocity of the sand particles. It was noted from the experimental results that for a particular sieve diameter, there exists a range of sizes, centricity, and settling velocity values. Considering this observation, 'equivalent circular diameter of the projected area' D_c is incorporated in the models as it was found to be more accurate in predicting the settling velocity of a single particle.

Alternatively, a 'more practical' approach correlating the sieve diameter to D_c was proposed. This correlation was tested by using the literature data for particle size greater than 0.1 mm. Settling velocity values calculated by incorporating the predicted D_c in the regular model yielded satisfactory results.

It was also found that the drag coefficient vs Reynolds number plot exhibit a unique curve. For $Re_p > 160$ the C_d value attained a constant value of 0.95.

The predicted values from regular model compared with the literature data resulted in an absolute average error of 7.7% for sieve size 0.19-1.22 mm. The model is even more effective and gives 4.1% error for particles within the size range of $0.35<D_s<1.18$ mm.

By observing all the images of 980 different sand particles, it was found that an ellipse could define the sands' shape precisely. In light of this, the developed simplistic elliptical model predicts the settling velocity using the major and minor axes of the particles with an absolute average error of 9.2 % and 6.5% for sieve size of 0.19-1.22 mm and 0.35-1.18 mm respectively. Considering the irregular nature of sand particles, the error in both models seem to be acceptable and the error magnitude is lower than other empirical models for sand particles till date.

The study is solely focuses on the industrial sand and it may not be related to other irregular particles.

5.7 References

1. Baba, Jumpei., and Komar, D Paul., 1981, “Measurements and analysis of settling velocities of natural quartz sand grains”, Journal of Sedimentary Petrology, Vol. 51, No. 2, pp. 631-640.
2. Dietrich, W.E., 2009, “Settling velocity of natural particles”, Water Resources Research, Vol. 18, No. 6, pp.1615–1626.
3. Middleton, G. V., J. B, Southard., 1978, “Mechanics of sediment movement”, Lecture notes for Short Course 3, 248, Eastern Section of the Soc. of Econ. Paleontol and Mineralog, Binghampton, NewYork.
4. Cox, E.P., 1927, “A method of assigning numerical and percentage values to the degree of roundness of sand grains”, Journal of Paleontol, Vol. 1, pp. 179-183.
5. McNown, S John., and Malaika, Jamil., 1956, “ Effects of particle shape on settling velocity at low Reynolds number”, Transactions American Geophysical Union, Vol. 31, No. 1.
6. Concha,F., and Christiansen, A., 1986, “Settling velocities of particulate systems, settling velocities of suspensions of particles of arbitrary shape”, International Journal of Mineral Process, Vol. 18, pp. 309-322.
7. Hartman, Miloslav., Trnka, Otakar., and Svoboda,Karel., 1994, “Free settling of non-spherical particles”, Ind. Eng. Chem. Res, Vol. 33, pp. 1979-1983.
8. Ghaemi, Sina., Rahimi, Payam., and Nobes, S. Nobes., 2008, “Measurement of droplet centricity and velocity in the spray field of an effervescent atomizer”, 14th Int. Symp on Application of Laser Technologies to Fluid Mechanics, Portugal.
9. Davaadorj, Bat-Erdene., Kim,Youngjin., and Lee, Jaeryeong., 2013,“Settling velocity of irregularly shaped particles in Newtonian fluids”, Geosystem Engineering, Vol. 16, No.3, pp. 225-230.

10. Hallermeier, R.J., 1981, “Terminal settling velocity of commonly occurring sand grains”, Sedimentology, Vol. 28, No.6, pp.859-865.

11. Cheng, N.S., 1997, “Simplified settling velocity formula for sediment particle”, Journal of Hydraulic Engineering, Vol.123, No. 2, pp. 149-152.

12. Ahrens, J.P., 2000, “A fall-velocity equation”, Journal of Waterway, Port, Coastal, and Ocean Engineering, Vol. 126, pp.99-102.

13. Ahrens, J.P., 2003, “Simple equations to calculate fall velocity and sediment scale parameter”, Journal of Waterway, Port, Coastal and Ocean Engineering, Vol. 129, No. 3, pp.146-150.

14. Rubey, W., 1933, “Settling velocities of gravel, sand, and silt particles”, Am. J. Sci., Vol.225, pp. 117-119.

15. Chang, H.K. and Liou, J.C., 2001, “Discussion of a free-velocity equation, by John P. Ahrens”, Journal of Waterway, Port, Coastal and Ocean Engineering, Vol. 127, No. 4, pp. 250–251.

16. Fentie,B., Yu, B., and Rose, C.W., 2004, “Comparison of seven particle settling velocity formulae for erosion modeling”, 13th International Soil Conservation Organization Conference, Brisbane.

17. Raudkivi, A.J., 1990, “Loose boundary hydraulics”, Pergamon Press, Inc., New York.

18. Van Rijn, L.C., 1997, “Sediment transport and budget of the central coastal zone of Holland”, Coastal Engineering, Vol. 32, pp. 61-90.

19. Wu, Weiming, M., and Wang, S.Y, Sam., 2006, “Formulas for sediment porosity and settling velocity”, Journal of Hydraulic Engineering, pp. 858-862.

20. Swamee, P.K., and Ojha, C.S.P., 1991, “Drag coefficient and fall velocity of non-spherical particles”, journal of Hydraulics Engineering, Vol. 117, No.5, pp. 660-667.

21. Jimenez, J. A., and Madsen, O.S., 2003, “A simple formula to estimate the settling velocity of natural sediments”, J. of waterway, port, coastal, ocean engineering, ASCE, Vol. 129, No. 2, pp. 70-78.

22. U.S. Interagency Committee on Water Resources, 1957, “The development and calibration of the visual accumulation tube”, rep. No. 11, Washington.

23. Holtzer, Andreas., and Sommerfeld, Martin., 2008, “New simple correlation formula for the drag coefficient of non-spherical particles”, Powder Technology, Vol. 184, pp. 361-65.

24. Sadat-Helbar, S.M., Amiri-Tokaldany, E., Darby, S., and Shafaie, A., 2009, “Fall Velocity of Sediment Particles”, IASME/WSEAS International Conference on Water Resources, Hydraulics and Hydrology, pp.39-45.

25. Dalrymple, R.A., and Thompson, W.W., 1976, “Study of equilibrium beach profiles”, Proceeding 15th Coastal Engineering, Hawaii, pp. 1277-1296.

26. Engelund, F., and Hansen, E., 1967, “A monograph on sediment transport in alluvial streams”, Published by Technical Publishers Skelbrekgade 4 Copenhagen V, Denmark.

27. Vincent, C.E., 1958, “Contribution to the study sediment transport on a horizontal bed due to wave action”, Proc. 6th Coastal Engineering Conference, Florida, pp. 326-355.

28. Nielsen, P., 1979, “Some basic concepts of wave sediment transport”, Series paper 20, Institute of Hydrodynamics and Hydraulic Engineering, Technical university of Denmark, Lyngby.

29. Shah, Y.Q., 1956, “Basic principles of sediment transport”, J. of Sediment Research, Vol. 1, No. , pp. 1-54.

30. Zanke, U., 1977, “Calculation of settling velocities of sediments”, Mitt Des Franzius Institute of hydraulic engineering, Heft 46, Seite 243, Technical University Hannover.

31. Ibad-Zade, Y A., 1992, “Movement of sediment in open channels”, translated by S.K. Gosh, Russian Translator series, Vol. 4.

32. Soulsby, R.L., 1997, “Dynamics of marine sands”, Thomas Telford, London.

33. She., K., Trim, L., and Pope, D., 2005, “Fall velocities of natural sediment particles: a simple mathematical presentation of the fall velocity la”, J. of Hydraulic Research, Vol. 43, No. 2, pp. 189-195.

34. Ferguson, R I., and Church, M., 2004, “A simple universal equation for grain settling velocity”, Journal of Sedimentary Geology, 74, pp. 933-937.

35. Zhu, L.J., and Cheng, N S., 1993, “Settlement of sediment particles”, Res. Rep., Department of River and Harbor Eng., Nanjing Hydraulic Research Inst., Nanjing, China.

36. Migniot, C., 1977, “Action of currents, waves and wind on the sediments”, White coal, Vol.1, pp. 9-47.

37. Zhang, R.J., 1989, “Sediments dynamics in rivers”, Water Resources press.

Chapter 6

Experimental Investigation of the settling velocity of spherical particles in Power Law fluids using Particle Image Shadowgraph

An experimental investigation of the settling velocity of spherical particles in Power law fluids has been conducted. The study starts with a brief summary of available literature on the topic and the scope of possible improvement related to it. The Shah and Chhabra [1] method which is found to be the most accurate technique has been discussed in detail. In the next section experimental procedure and the results of the fluid rheology have been presented. Next, the measured experimental results from the shadowgraph experiments are explained and the effects of flow index and consistency index on the settling velocity are presented. Based on the observations, a new model for predicting the settling velocity has been proposed, which is an improved version of the Shah's model. The last section consists of the major conclusions observed in the study.

6.1 Introduction

There exists a wide and diversified opinion amongst different investigators for power law fluid and unlike Newtonian model there is no universally accepted general model for determining the settling velocities of spherical particles for these fluids. Two different opinions prevail amongst the authors regarding the use of Newtonian drag curve for non-Newtonian fluid and on the dependency of drag coefficient on flow behaviour index 'n'. Authors ([1] to [9]) have observed the strong dependency of drag coefficient on 'n'. On the other hand, authors [10] to [13]) have the opinion that even the use of Newtonian drag curve for power law fluid gives equally good results.

Different correlations for drag coefficient developed during various studies have all been found to give an average error of more than 23% for the settling velocity of spherical particles in power law fluids. Some of the well-known correlations available in the literature like Acharya et al [14], Darby [15], Ceylan et al[16], Matijasic and Glasnovic [17], and Graham and Jones [18] resulted in a mean error of 26.7%, 31.55%, 63.73%, 26.0%, 31.3%, 23.28% respectively [13]. Moreover, the use of Newtonian drag curve for predicting the settling velocities also led to an error of about 30%. Taking the complex nature of the correlations into consideration, use of Newtonian curve is generally the preferred choice.

Since the average error involved in the case of power law fluid is large, the incorporation of settling velocity of spherical particles for pumping energy calculation, critical lift velocity, and other design parameters can potentially lead to significant errors in calculation. The failure of correlations and the Newtonian drag curve led to a significant study conducted in 2007 by Shah [1], wherein a new and more accurate model was proposed. This model is found to be more accurate than any other correlations in the literature and predicts the values with an average error of around 17% with maximum deviation of up to 29%. The issue on variability in the results from one author to other was also noticed during the course of the study.

Taking into account the high error in the predicted settling velocity values and the discrepancies in the measured experimental values of the literature, a detailed and accurate study is required. Very little research has been conducted in the recent time to explain or examine the accuracy of Shah's hypothesis in detail. This work aims at checking the accuracy of the available models in the literature which one can use with confidence in the future.

The rheology of the fluid which plays a vital role in determining the settling velocity has been measured using a highly advanced and multifunctional Bohlin rheometer. The correlation developed by Shah (2007) has been enhanced to increase its efficiency. The newly suggested model has been found to give an average error of 10%

with maximum deviation of around 21%. It is improved version of Shah's original model with an up-gradation performed using a highly accurate experimental technique.

6.2 Shah and Chhabra [1] Approach

By utilizing the observed dependency of drag coefficient on 'n', a new relation between $\sqrt{C_d^{(2-n)}Re^2}$ vs Re has been plotted as compared to C_d vs Re which is used for Newtonian curve. Experimental results from the literature had been used and curve for the below mentioned relation was plotted (See equation 6-1). The value of coefficients was obtained empirically using the available data from the literature. The relations between the coefficients with flow index are given by equations 6-2 and 6-3.

$$\left(C_d^{2-n}Re^2\right)^{0.5} = XRe^Y \qquad \textbf{Eq. (6-1)}$$

$$X = 6.9148(n^2) - 24.838(n) + 22.642 \qquad \textbf{Eq. (6-2)}$$

$$Y = -0.5067(n^2) + 1.3234(n) - 0.1744 \qquad \textbf{Eq. (6-3)}$$

The surface average shear rate ($2v_t/d_p$) of the particle has been used to define the effective viscosity of the shear thinning fluid. The relation for the effective viscosity is given by equation 6-4.

$$\mu_a = K\left(\frac{2v_t}{d_p}\right)^{n-1} \qquad \textbf{Eq. (6-4)}$$

The general drag coefficient equation is used for the calculation (equation 6-5). With the modified Reynolds number given by equation 6-6 the term $\sqrt{C_d^{(2-n)}Re^2}$ gets converted to a function which is independent from settling velocity (See equation 6-7).

$$C_d = \frac{4}{3}\left(\frac{d_p g}{v_t^2}\right)\left(\frac{\rho_p - \rho_o}{\rho_o}\right) \qquad \textbf{Eq. (6-5)}$$

$$Re = \frac{d_p^n v_t^{2-n} \rho_o}{2^{n-1} K} \quad \textbf{Eq. (6-6)}$$

$$\left(C_d^{2-n} Re^2\right)^{0.5} = \left(\frac{13.08^{2-n}}{2^{2(n-1)}} \left(\frac{d_p^{n+2} \rho_o^n \left(\rho_p - \rho_f\right)^{2-n}}{K^2}\right)\right)^{0.5} \quad \textbf{Eq. (6-7)}$$

6.2.1 Steps for Calculation

- Based on the particle diameter and fluid rheological parameter $\sqrt{C_d^{(2-n)}} Re^2$ is calculated using equation 6-7.
- With the measured flow behaviour index ‘n’ the coefficients X and Y are estimated using equations 6-2 and 6-3.
- On completion of step 1 and step 2, Reynolds number is calculated using the relation given in equation 6-1.
- Settling velocity is then calculated using equation 6-6.

6.3 Experimental Procedure

The Carboxy Methyl Cellulose (CMC) mixture in water has been used as fluid medium. Different concentrations of CMC-water mixture were prepared and used in the experiments. Polymer solution was prepared by slowly mixing the polymer in the agitating mixture. The key to prepare the homogeneous mixture is to add the polymer as slowly as possible. Addition of 1 gm in 350 ml takes around 35 minutes duration. Moreover, the polymer particles are poured into the middle of the vortex generated in water because of the agitation. Seven litres of each concentration has been prepared with a sample size of 350 ml.

The experimental procedure and detail of measurement technique are the same as mentioned in chapter 2.

6.4 Fluid Rheology

Rheology of CMC solutions has been measured by using the four different modes available in the rheometer.

Plate Controlled Stress Mode (Plate SS)

Plate Controlled Rate Mode

HTHP Controlled Stress Mode (HTHP SS)

HTHP Controlled Rate Mode

For each mode, three different readings are taken for individual concentration of CMC. The repeatability of the three readings for each individual concentration is found to be excellent and therefore only one data set has been used in the analysis.

Controlled rate mode readings are ignored because they resulted in few off data points and are relatively less consistent as compared to controlled stress mode. Three different wt% (0.143%, 0.2142%, and 0.2857%) mixtures CMC have been prepared in water. The shear stress vs shear rate for different mixtures have been obtained using the Bohlin rheometer controlled stress mode. The plots are shown in figure 6-1.

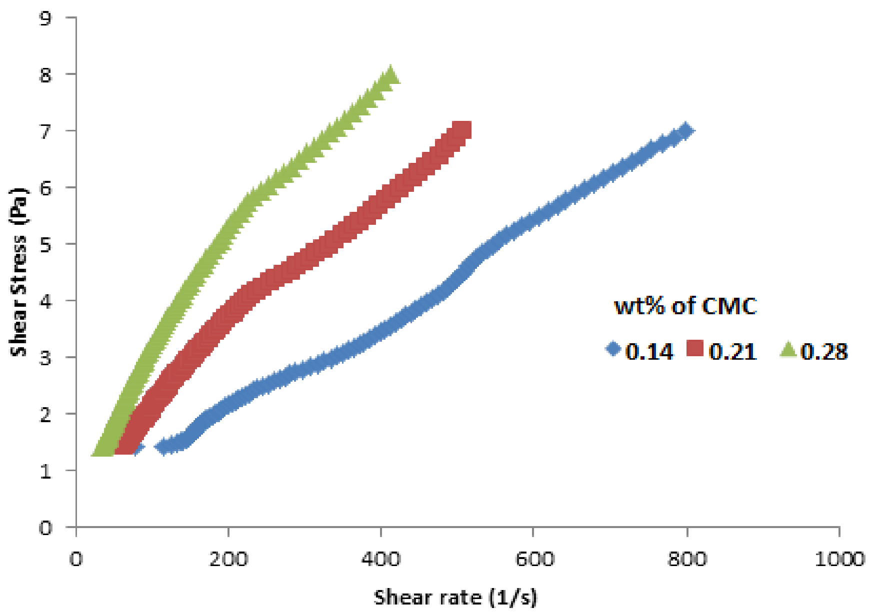

Figure 6-1: Shear stress versus shear rate for different mixture of CMC

The flow behaviour index ‘n’ and the consistency index of the fluids have been calculated using the power law fit for the stress-strain curve. The values for different fluids are given in table 6-1.

Table 6-1: Measured values of n and K for CMC solutions

Fluid	N	K (Pa s^n)
CMC 0.143 (wt%)	0.8177	0.0277
CMC0.2142 (wt%)	0.7407	0.0697
CMC0.2857 (wt%)	0.7142	0.1162

6.5 Results and Discussion

Experiments are conducted using three different power law fluids and four different sizes of glass spheres. The properties of glass beads used in this study are given in table 6-2. The measured values of settling velocity by shadowgraph for four different sizes of glass spheres in power law fluids are given in table 6-3.

Table 6-2: Properties of glass spheres

Diameter (Manufacturer Data) (mm)	Specific gravity
0.71±0.02	2.51
2±.04	2.51
1.18±0.02	2.51
1.5±0.03	2.51

Table 6-3: Measured settling velocity (m/s) of spheres in CMC

Diameter (mm)	CMC(0.14 wt%)	CMC 0.21(wt%)	CMC 0.28(wt%)
0.71	0.030	0.013	0.013
1.18	0.069	0.032	0.022
1.5	0.077	0.054	0.033
2	0.151	0.070	0.049

The measured values of settling velocities are compared with the predicted values by Shah and Chhabra [1] model given in section 6.2. The result obtained with error percentage in the prediction is shown in table 6-4.

Table 6-4: Comparison of measured settling velocity with Shah and Chhabra

Fluid type	Diameter (mm)	A	B	$(C_d^{(2-n)}Re^2)^{0.5}$	Re	Predicted velocity (m/s)	Measured velocity (m/s)	error (%)
CMC (0.14 wt%)	0.71			8.75	1.50	0.027	0.0298	10.9
	1.18			17.90	5.27	0.054	0.069	21.1
	1.5			25.11	9.55	0.076	0.077	1.02
	2.0	6.955	0.569	37.66	19.5	0.114	0.152	24.7
CMC (0.2142 wt%)	0.71			5.44	0.48	0.017	0.013	27.9
	1.18			10.91	1.79	0.036	0.032	11.6
	1.5			15.16	3.33	0.052	0.054	3.65
	2.0	8.038	0.528	22.49	7.02	0.079	0.070	12.7
CMC (0.2857 wt%)	0.71			3.80	0.21	0.013	0.013	4.45
	1.18			7.58	0.81	0.027	0.022	20.6
	1.5			10.50	1.54	0.0387	0.033	16.2
	2.0	8.430	0.512	15.52	3.29	0.059	0.049	21.9

6.5.1 Effect of n and K on Settling Velocity

There exists a significant effect of flow behaviour index 'n' on the drag coefficient and has been discussed by various authors in the literature. This effect forms the basis of developed model by Shah and Chhabra [1]. However, the nature in the change of settling velocity has not been discussed. In this work, the proposed model with variation in 'n' and K are studied in detail. It has been observed that error graphs attain a minima at a particular value of 'n' and 'K', beyond which the error increases (see figures 6-2 and 6-3). The rate of increase in the error has been observed to surge with decreasing 'n' values. In other words, more the concentration of non-Newtonian fluid, the effect of flow index is higher. Similar trend is observed for the flow consistency index, K as shown in figure 6-3. It can be observed that the K values have less effect on the percentage as compared to n values. The extent of maximum error with varying k values is found to half of what is observed in case of varying flow index.

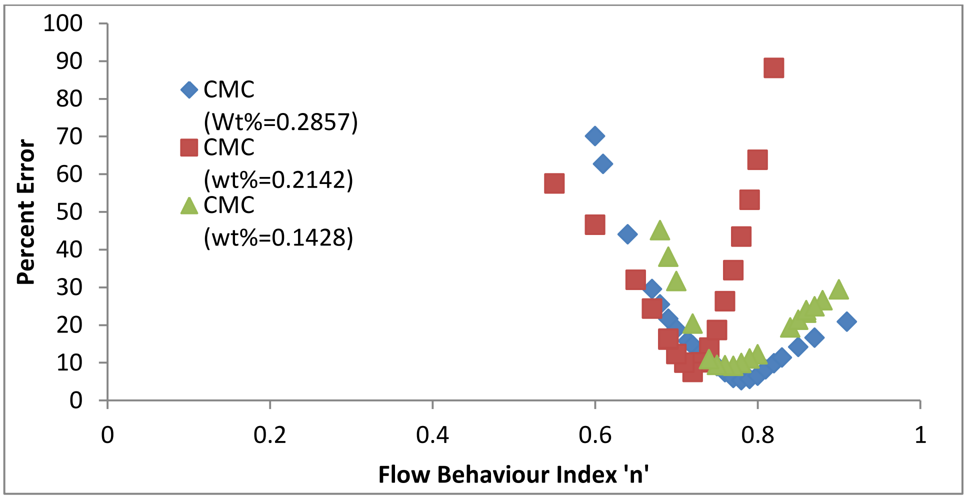

Figure 6-2: Percent error in settling velocity with flow behaviour index 'n'

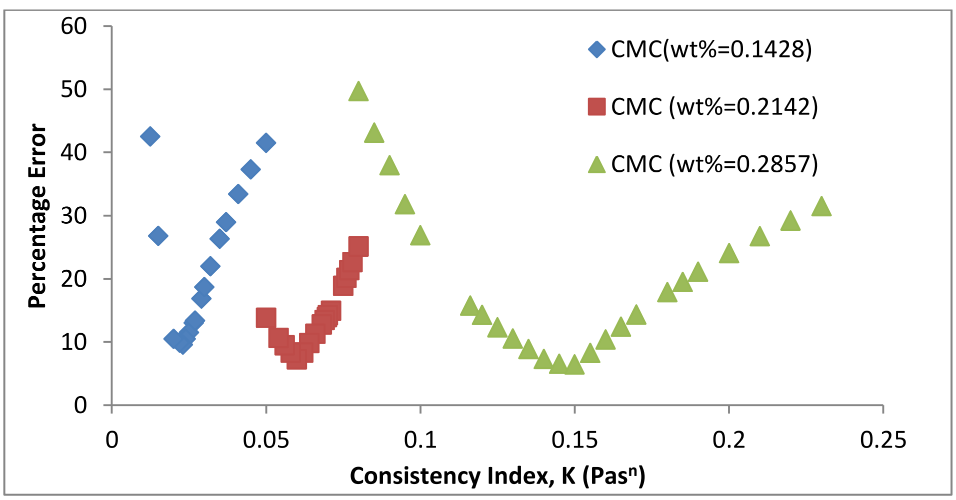

Figure 6-3: Percent error in settling velocity with consistency Index 'K'

6.6 Development of Model

The model discussed before in the section 6.2 was an empirical model developed by using experimental measurements from five different authors. The relationships between 'n' and the coefficients X (eqn.6-2) and Y (equation 6-3) are proposed by using the experimental data from the literature. The regression coefficient of the experimental data for X and n is 0.9157 while it is just 0.88 for Y and n. These relatively low values for regression might have occurred due to different experimental errors associated with measurements by different authors. In other words, there is an issue of variability in the results from one author to other which was noticed during the study. Therefore, there always exists a room for an improvement in any such correlations.

The shadowgraph technique which can measure settling velocity up to seven decimal places is a highly accurate image processing technique. Experiments using four different sizes of spheres are conducted with increased precision. At least three different trials are conducted to reduce any experimental error which might have occurred during the experiment. The results are plotted in the form of $\sqrt{C_d^{(2-n)}} Re^2$ versus Re as shown in figure 6-4. It is observed that power law relation exists between these two measured parameter. The power curve fit coefficient of these curves give the X' and Y' values.

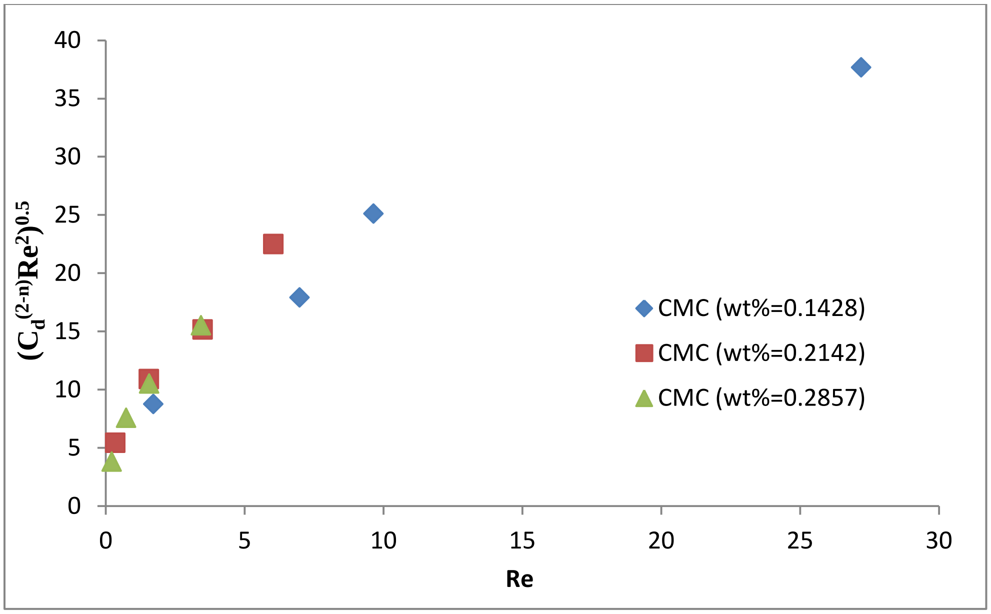

Figure 6-4: $\sqrt{C_d^{(2-n)}} Re^2$ versus Re plot using the data from Shadowgraph experiments

The coefficients X' and Y' obtained from shadowgraph experiments are compared with the original proposed model by Shah and Chhabra [16]. The plots are shown in figure 6-5 and 6-6. The correlation between X and X' has been obtained by using the linear regression tool and is given by equation 6-8. The observed correlation between Y and Y' is given by equation 6-9. The new developed equation when used in the original model gives an average error of 10.7% as compared to average error of 14.9% given by the original model of Shah and Chhabra [16]. The detailed comparison between the measured values of settling with the predicted value from both the models is given in table 7-4.

$$X' = 1.5269X - 3.9375 \qquad \textbf{Eq. (6-8)}$$

$$Y' = 0.892Y + 0.0326 \qquad \textbf{Eq. (6-9)}$$

Where X and Y is calculated using the equation 6-2 and 6-3.

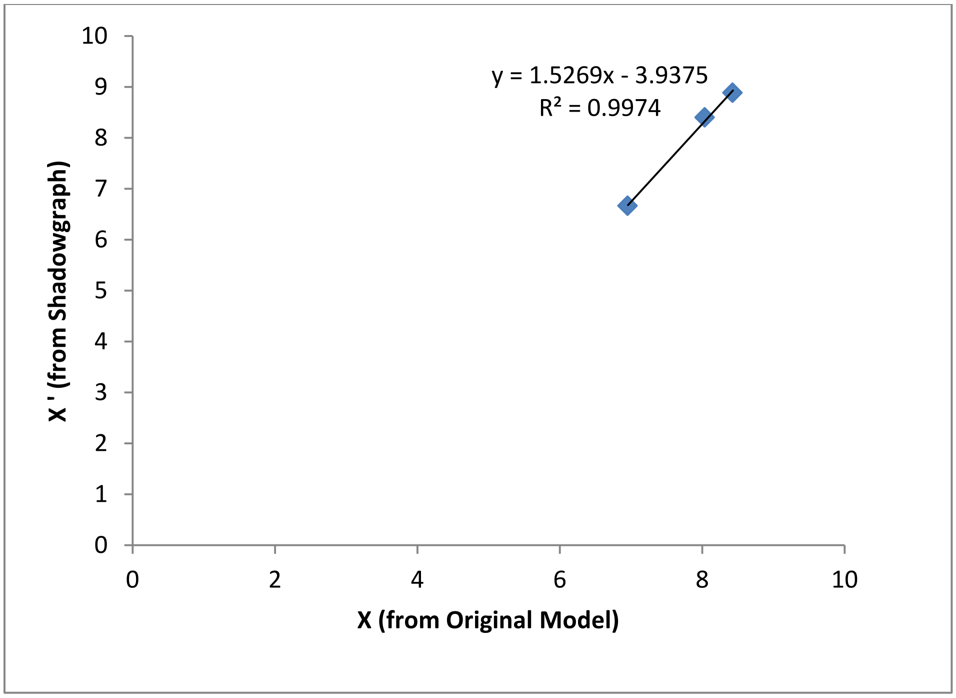

Figure 6-5: Comparison of X (from original method) and X' (from shadowgraph)

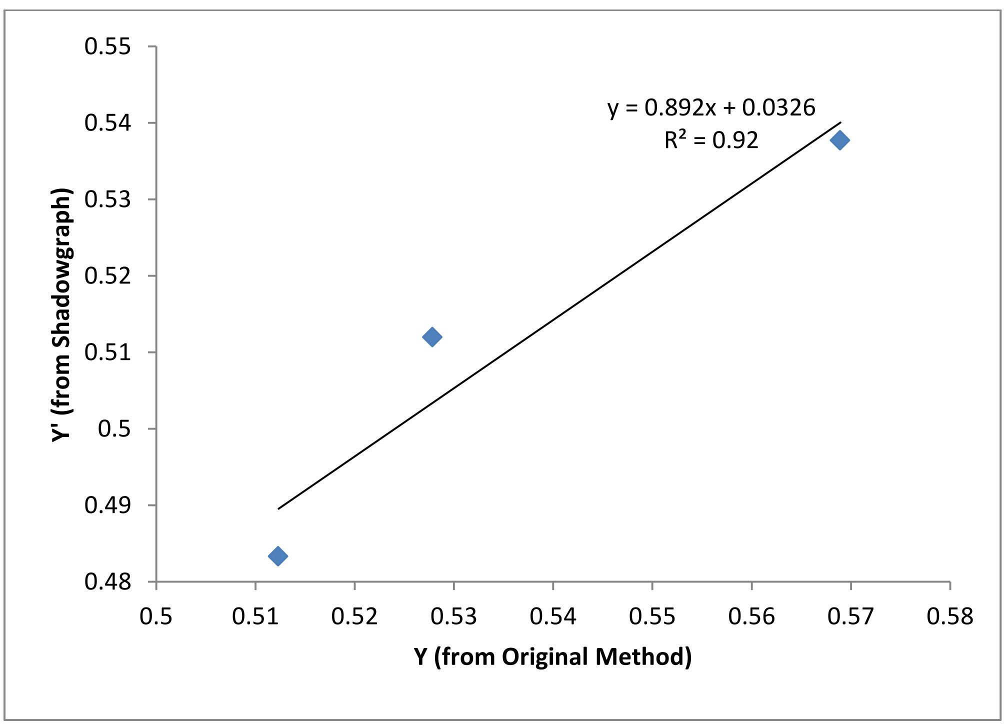

Figure 6-6: Comparison of Y (from original method) and Y' (from shadowgraph)

Table 6-5: Comparison of measured settling velocity with predicted settling velocity from Shah's model and proposed model

Flow index 'n'	Consistency Index 'K'	Diameter (mm)	Settling Velocity (Shah and Chhabra) (m/s)	Settling Velocity (proposed model) (m/s)	Measured Settling velocity (m/s)	Error (%) By Shah and Chhabra model	Error (%) By Proposed Model
0.8177	0.0277	0.71	0.027	0.029	0.030	10.9	3.4
		1.18	0.055	0.062	0.068	21.2	9.5
		1.5	0.077	0.090	0.077	0.91	16.8
		2.0	0.114	0.139	0.151	24.7	8.30
0.7407	0.0697	0.71	0.017	0.016	0.013	27.9	17.4
		1.18	0.036	0.035	0.032	11.6	7.8
		1.5	0.052	0.051	0.054	3.6	4.7
		2.0	0.079	0.080	0.070	12.7	14.
0.7142	0.1162	0.71	0.013	0.011	0.013	4.4	17.6
		1.18	0.027	0.024	0.022	20.6	9.1
		1.5	0.039	0.036	0.033	16.1	7.6
		2.0	0.060	0.057	0.049	21.9	16.0

6.6.1 Additional Comparison

The developed model for settling velocity of sphere in Power law fluid is compared with a completely new set of data measured using shadowgraph. The CMC wt% 0.1714 has been prepared and settling velocity of spheres has been measured. The results are shown in table 6-6. The average error of 9.7% is observed with the new proposed model while it is 14.5% from the original Shah and Chhabra model [16].

Table 6-6: Comparison of proposed model with measured data

Flow Index'n'	Consistency Index 'K' (Pas^n)	Predicted Settling Velocity (m/s) from Proposed model	Predicted settling velocity by Shah and Chabbra Model (m/s)	Measured Value of settling velocity by shadowgraph (m/s)	Error (%) in prediction by Proposed model	Error (%) in prediction by Shah and Chhabra Model [16]
0.7803	0.0453	0.0208	0.0211	0.0276	24.4	23.8
		0.0456	0.0436	0.0519	12.1	16.03
		0.0660	0.0615	0.0659	0.19	6.65
		0.1028	0.0929	0.1047	1.80	11.26

6.7 Conclusions

Experiments of falling spherical particles in power law fluid have been conducted successfully. The nature of the dependency of 'n' and 'K' on the settling velocity has been developed. It is observed that there exists a strong correlation of n and K with the percent error of settling velocity. It has been observed that the dependency is higher for highly non-Newtonian fluids and it decreases as n approaches the value 1 i.e. the Newtonian behavior. A new correlation has been proposed which is found to be more efficient in predicting the settling velocity of spherical particles in power law fluid. The average error from the developed model is found to be 10.4% as compared to the original value of 14.9 %.

6.8 References

1. Shah, N. Subhash., Fadili, EI. Youness., and Chhabra, R.P., 2007, "New model for single spherical particle settling velocity in power law (visco-inelastic) fluids", International Journal of Multiphase Flow, Vol. 33, pp. 51–66.
2. Dallon, D.S., 1967, "A drag coefficient correlation for spheres settling in Ellis fluids", PhD Thesis, University of Utah, Salt Lake City, UT.
3. Prakash, S., 1983, "Experimental evaluation of terminal velocity in non-newtonian fluids in the turbulent regime", Indian Chemical Engineers, Vol. 25, No. 1.
4. Reynolds, P. A., and Jones, T. E. R., 1989, "An experimental study of the settling velocities of single particles in non- Newtonian fluids", International Journal of Mineral Processing, Vol 2, pp. 47-77.
5. Peden, J.M., Luo, Y., 1987, "Settling velocity of variously shaped particles in drilling and fracturing fluids", SPE Drill. Eng., Vol. 2, pp.337–343.
6. Koziol, K., and Glowacki, P., 1988, "Determination of the free settling parameters of spherical particles in power law fluids", Chemical Engineering Process, Vol. 24, pp. 183-188.
7. Machac, L., Ulbrichova, L., Elson, T.P., Cheesman, D.J., 1995. Fall of spherical particles through non-newtonian suspensions. Chem. Eng. Sci. 50, 3323–3327.
8. Shah, S.N., 1982, "Proppant settling correlations for non-newtonian fluids under static and dynamic conditions", Trans. AIME 273 (Part 2), pp. 164–170.
9. Shah, S.N., 1986, "Proppant settling correlations for non-newtonian fluids", SPE Prod. Eng. (Nov), pp. 446–448.

10. Kelessidis, V.C., 2004, “Terminal velocity of solid spheres falling in newtonian and non-Newtonian liquids”, Tech. Chron. Sci., 24, pp.43–54.

11. Lali, A. M., Khare, A. S., Joshi, J. B., and Nigam, K. D. P., 1989, “Behavior of solid particles in viscous non- newtonian solutions: Settling velocity, wall effects and bed expansion in solid-liquid fluidized beds, Powder Technology, Vol. 5, No. 1, pp 39-50.

12. Chhabra, R.P., 1990, “Motion of spheres in power law (viscoinelastic) fluids at intermediate Reynolds numbers, a unified approach”, Chem. Eng. Process. 28, pp.89–94.

13. Chhabra, R.P., 2002, “Sedimentation of particles in non-Newtonian media”, Hydrotransport, Vol.15, pp.135-148.

14. Acharya, A., Mashelkar, R. A., and Ulbrecht, J., 1976, “Flow of inelastic and viscoelastic fluids past a sphere”, Rheological Acta, Vol. 15, pp. 454-463.

15. R. Darby, 1996, "Determining settling rates of particles”, Chemical engineering, Vol. 103, No.12, pp. 109-117.

16. Ceylan, K., Herdem, S., and Abbasov, T., 1999, “A theoretical model for estimation of drag force in the flow of non-newtonian fluids around spherical solid particles”, Powder Technology, Vol.103, pp.286–291.

17. Matijasic, G., and Glasnovic, A., 2001, “Measurement and evaluation of drag coefficient for settling of spherical particles in pseudo plastic fluids”, Chem. Biochem. Eng., Quarter 15, No. 1, pp. 21–24.

18. Graham, D.I., and Jones, T. E.R., 1994, “Settling and transport of spherical particles in power-law fluids at finite Reynolds number”, J. of non-Newtonian fluid mechanics, Vol. 54, pp.465-488.

Chapter 7

Experimental Investigation of Settling Velocity of Natural Sands in Power Law Fluid using Particle Image Shadowgraph

This chapter focusses on the detailed experimental study of the settling velocity of natural sand particles in power law fluid. Initially, review of different work carried out in the past and also the motivations for the current study are introduced. The approach for the conducted study is presented in the next section. Rheological properties of the fluid and experimental result on natural sands have been presented in detail. Empirical correlations developed for predicting the settling velocity of sand using various equivalent diameter concepts have also been presented in this chapter. Multiple linear regression technique has been applied to the experimental data and an improved correlation has been developed. Last section of the chapter summarizes important observations made during the study.

7.1 Introduction

In almost all the real applications of solids transport, non-spherical particles are encountered. [1]. There are a few correlations for Reynolds number and drag coefficient of regular non-spherical particles like cylinder, disc, and prism. However, these relations are found to be inefficient for highly irregular particles. There are relatively very few studies conducted on fluid particle systems of this kind. Moreover, very little is known about the drag [1].

The irregular shaped particle settles at lower velocity as compared to spherical particle because the decrease in sphericity, increased roughness and enlarged projected area leads to higher drag. The orientation of irregular particle is not predictable and depends on the relative position of centre of gravity and centre of force [2, 3].

There are a numerous correlations for settling velocity of spheres in non-Newtonian fluids; however, unlike the case in Newtonian fluids, there is no universally accepted correlation for drag for particles settling in non-Newtonian fluids. Moreover the error from the different correlations shows that the nature of fluid particle system for non-Newtonian fluid is far more complex as compared to Newtonian fluid.

Deosarkar et al. [4] studied the settling velocity of magnetite ore in different concentration of CMC mixture. In his study, they proposed the drag versus Reynolds number relationship which can be an important piece of information for magnetite associated fluid particle systems. Later in 1994, Chhabra and Madhav [5] studied the settling behavior of prism, cylinder, and needle in shear thinning polymer solution. Using the equivalent volume sphere diameter they proposed a simple correlation between the drag and Reynolds number for these non-spherical particles. The developed correlation is given by equation 7-1.

$$C_D = \frac{32.5}{Re}(1 + 2.5Re^{0.2}) \qquad \textbf{Eq. (7-1)}$$

The model given by Eqn. 7-1, predicts the actual values with an average error of 13% and with maximum deviation of 21%. In fact, the model accuracy had not been validated with independent experimental measurement because of the lack of literature on power law fluid. For conical shaped particle, the model was found to be giving maximum error of order 45%, which indicates that the model is not general and can only be valid for regular non-spherical shapes used during the study.

Chabbra and Agarwal [6] studied the settling velocity behavior of cubes in Newtonian and power law fluid. In their studies, they proposed a drag model given by equation 7-2, which can be used to predict the drag value for both types of fluid and for any particle. The equation looks complex and lengthy to use. Moreover, an additional parameter; the ratio of surface area and projected area normal to the direction of settling is required. Determining the orientation of irregular particle during the fall is a difficult task.

In another attempt to study drag on irregular particle, Rajitha [7] developed a correlation given by equation 7-2. The term Ac/A_p used in the correlation is given by equation 7-3.

$$C_d = C_{do} + \left(\frac{A_c}{A_p}\right) C_{d\infty} (C_{do})^{2B} k \left[\frac{6Xb}{6Xb + C_{do}}\right]^{B} + C_{d\infty} \left[\frac{6Xb}{6Xb + 128 C_{do}}\right]^{\frac{11}{12}} \qquad \textbf{Eq. (7-2)}$$

$$\frac{A_c}{A_p} = \left(\frac{4}{\varphi}\right) \left(\frac{D_s}{D_n}\right)^2 \qquad \textbf{Eq. (7-3)}$$

D_n is the diameter of the circle with equivalent projected area

Even with so many constant and parameter as an input in the model, the model (eqn.7-2) was not predicting the values very well. The mean deviation was found to be 25 % and 30% for Newtonian and power law fluid respectively. Chhabra and Agarwal [6] also found that the model (eqn. 7-2) gave a mean error of 21% when compared with the available literature data. The proposed model may give even more error in case of natural sediments which are highly irregular as compared to prism, cube or cylinder which are regular non-spherical particles.

There have been numerous studies on the settling behavior of fine particles (<30µm) in the literature [8, 9]. One of the complexities involves with these particles are that they occur and settle in floccules and not as an individual particle [10]. The authors had given a relatively simple power law model for the settling velocity of fine particles which was found to have good predicting capabilities [10].

Mohammed [11] proposed three different sets of settling velocity equations for spheres and crushed rocks in non-Newtonian fluid. The proposed model is a function of settling velocity with flow behavior index (n), concentration, and particle diameter. In his study, Mohammed [11] found that there exists a linear relationship between the crushed rock diameter and settling velocity with decreased n leading to a lower velocity. The model is based on the equivalent volumetric sphere diameter, which is very tough to measure for small sand particles. Moreover, the author failed to validate the correlation predictability with independent data and also did not present the correlation properly (only the graphical presentation of data is given).

Numerous studies have been reported in the literature on the drag coefficient of non-spherical particles but none of the authors have reported the applicability of such correlation for the case of non-Newtonian fluid. Different empirical correlations have been proposed for the regular non-spherical particle like disk, prism, needle etc. Even the correlations developed for specific shapes are not very efficient and give a lot of error in prediction. This shows the complexities involved in handling the non-Newtonian fluid. For irregular particle like sand, the condition of drag acting on the particle can be even more intricate to judge. A large section of the slurry transportation, drilling, and mining application deals with the sand transport in non-Newtonian fluids. Even though settling velocity play a vital role in designing such processes, it has not been studied in detail by many people in the past.

This work aims at studying the settling behavior of natural sand particles in a power law fluid using PIS technique. The detailed investigation of the shape and size of the sand particle and the dependency of drag acting on it with varying flow and consistency index of the fluid has been studied. Later on a drag correlation model for natural sand with the measured equivalent diameter and fluid rheological parameters has been developed. The model is found to be very accurate and is predicting the values well within the acceptable range for such complex fluid particle systems.

7.2 Experimental Procedure

The experiments are conducted using the experimental procedure described in chapter 2 of the thesis. Four different concentrations of CMC mixture have been prepared and the settling velocity of four sieve sizes has been measured using PIS technique.

7.3 Approach

It is well accepted fact that the flow behaviour index 'n' plays a significant role in determining the drag coefficient acting on the particle's surface. Normal C_d vs Re relationship has failed to capture the drag behavior in case of non-Newtonian fluid and had led to serious error in prediction. Describing the drag coefficient as $(C_d^{(2-n)}Re^2)^{0.5}$ was found to capture the behavior well as compared to C_d. The proposed drag coefficient had incorporated the effect of flow index on the drag acting on the particle. This term had been used by Shah and Chhabra [10] in their study to develop an efficient empirical correlation for drag coefficient of spherical particle in power law fluid.

It has been well accepted fact that the shape of the particle greatly influences the nature of drag acting on the particle. There have been different equivalent diameters which are used for defining the shape and size of a particle. However, there does not exist any universally accepted parameter to define it efficiently. Keeping this in mind six different diameters has been used in the study to develop a drag correlation for the natural sand particle for power law fluid. Different diameters measured for natural sands using PIS technique have been used in the study. The diameters are measured at their settling velocity stage so the orientation of the irregular particle which can change during the fall has been automatically taken care of. Different empirical correlations for predicting the value of settling of sand particles using different diameter has been developed. One of the major advantages of the study is that one can use any associated diameter to predict the settling velocity and thus providing a great flexibility. This study is solely for the natural sand settling in power law fluid and this may not be valid for other irregular particles. Multiple linear regression analysis has been performed with each fluid data and coefficients are also reported as function of n and K. The multiple linear regression tools have enhanced the efficiency in the prediction and error has been reduced by 3-5%.

7.4 Rheological Characteristics of the Fluids

Four different concentrations of Carboxy Methyl Cellulose (CMC) have been mixed in water to have solutions with varying rheological parameters. The rheological characterization of test fluids has been carried out using BOHLIN rheometer and the results are reported in Table 7-1.

Table 7-1: Fluid rheology for CMC solutions

Fluid Type	Flow Index 'n'	K (Pas^n)
CMC Wt% 0.142 (Type 1)	0.8177	0.0277
CMC Wt% 0.174 (Type 2)	0.7803	0.0453
CMC Wt% 0.214 (Type 3)	0.7407	0.0697
CMC Wt% 0.285 (Type 4)	0.7142	0.1162

7.5 Experimental Measurements

Four different sieve sizes of the natural sand have been used with four different concentrations of CMC solutions (table 7-1 and table 7-2). The settling velocity of the particles is measured using the PIS setup developed for the study. For each fluid particle system three or more sets of experiments are performed to have a better accuracy and repeatability of the experimental results. Thus total 48 sets of experiments are conducted and the measured average values are reported in table 7-2. Apart from the settling velocity of the particles, different diameters associated with each particle are also measured.

Table 7-2: Settling velocity of natural sand

Mean Sieve Diameter (mm)	Settling Velocity (m/s) In Fluid 1	Settling Velocity (m/s) In Fluid 2	Settling Velocity (m/s) In Fluid 3	Settling Velocity (m/s) In Fluid 4
0.35-0.40	0.06	0.047	0.028	0.021
0.71-0.85	0.082	0.060	0.033	0.028
0.85-1.18	0.112	0.090	0.075	0.048
1.18 -1.67	0.009	0.006	0.006	0.005

The relation between various equivalent diameters with mean sieve diameter is given by below equations (7-4 to 7-9). They have been derived in chapter 3. The correlations can be used to derive various equivalent diameters using mean sieve diameter. The measured diameters for natural sand particles are given in Table 7-3.

$$S_{DV90} = 1.4217d_s + 0.0003 \quad \textbf{Eq. (7-4)}$$

$$S_{D10} = 0.8416d_s^{1.1396} \quad \textbf{Eq. (7-5)}$$

$$S_{DV10} = 0.9058d_s - 0.0525 \quad \textbf{Eq. (7-6)}$$

$$S_{D32} = 1.0766d_s + 0.0028 \quad \textbf{Eq. (7-7)}$$

$$S_{DV50} = 1.0544d_s + 0.0088 \quad \textbf{Eq. (7-8)}$$

$$S_{D_c} = 1.2489d_s - 0.1267 \quad \textbf{Eq. (7-9)}$$

Table 7-3: Measured diameter values for natural sand

D_{sieve} (mm)	D10 (mm)	D32 (mm)	DV10 (mm)	DV50 (mm)	DV90 (mm)	Dc (mm)
0.35	0.227	0.328	0.235	0.309	0.439	0.310
0.775	0.778	0.906	0.698	0.874	1.250	0.841
1.01	0.944	1.090	0.864	1.087	1.355	1.135
1.4	1.011	1.471	1.195	1.421	1.981	1.622

7.6 Model Development

Keeping the effect of 'n' on the drag coefficient in mind , equations 7-10 and 7-11 have been used to study the variation of drag with respect to Reynolds number. The definition of Reynolds number used here is based on the average surface shear rate and is given by equation 7-11. The use of such Reynolds definition has been suggested by Shah and Chhabra [12] during their empirical study on the spherical particle in power law fluids. The definition of Reynolds number and drag coefficient (see equation 7-4) given by Shah and Chhabra [12] has been used to develop the correlation. The particle diameter definition in case of non-regular particle has been changed. Using the least square regression analysis, curve fits for different 'equivalent diameter' terms have been obtained and given by equation 7-12 to 7-18.

In addition, multiple linear regression analysis has been performed using Matlab to find a relation between these curve fit parameters with the fluid properties. The regression coefficient for all these developed relationship is found to be well within the acceptable limit and is given in table 7-4.

$$Y = \left(C_d^{2-n} Re^2\right)^{0.5} = \left(\frac{13.08^{2-n}}{2^{2(n-1)}}\left(\frac{d_p^{n+2}\rho_o^n\left(\rho_p-\rho_f\right)^{2-n}}{K^2}\right)\right)^{0.5} \qquad \textbf{Eq. (7-10)}$$

$$Re = \frac{d_p^n v_t^{2-n}\rho_o}{2^{n-1}K} \qquad \textbf{Eq. (7-11)}$$

7.6.1 Mean Sieve Diameter model

The sieve diameter which has been frequently used in the study of natural sediments is used to develop a correlation for natural sands. The sieve diameter is the easiest diameter to measure for non-spherical particles and thus a model based on sieve diameter can be more conveniently used in various applications. Though the sieve diameter is not able to incorporate the shape effect competently it has still been used frequently in the sand related study. The plot of the modified drag coefficient (Y) with respect to Reynolds number is shown in figure 7-1. The measured settling velocity given in table 7-3 and the measured mean sieve diameter has been used to calculate Y and Re. The curve fit equation is given by equation 7-12 and a regression coefficient of 0.9796 is observed.

$$Y = 6.83862Re^{0.4341} \qquad \textbf{Eq. (7-12)}$$

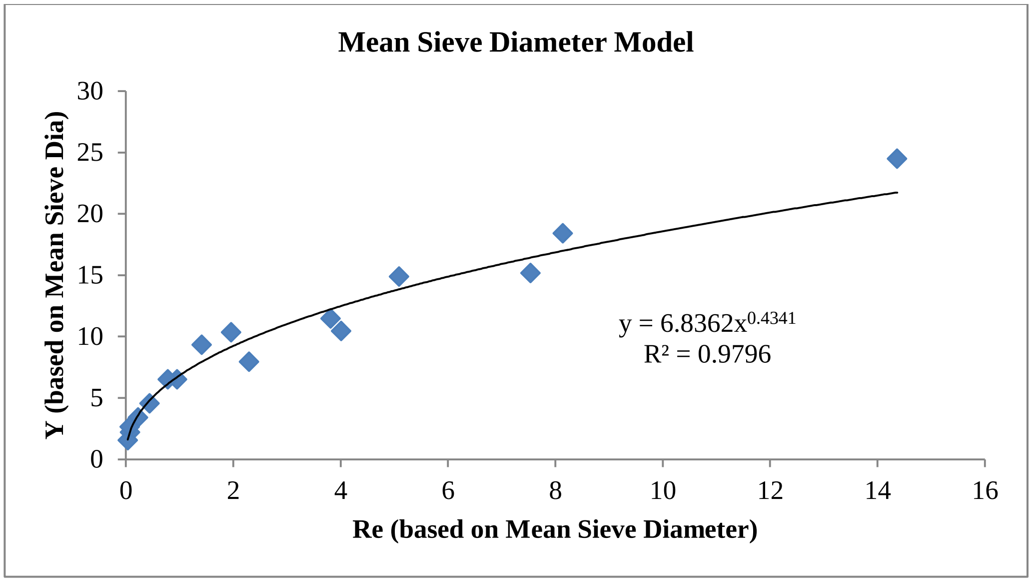

Figure 7-1: Y vs Re plot for Natural Sand using Mean Sieve Diameter

When the equation 7-12 is used for predicting the settling velocity of sand particle, its giving an average error of 18.42%. Two of the data point is giving high error and exclusion of those two points reduces the average error to 14.1%.

7.6.2 D10 Diameter Model

D10 is a one dimensional measurement. It can be defined as the number length mean or the arithmetic mean. D10 for the sand particles have been measured using PIS. The similar procedure of plotting the Y versus Re has been done as in section 7.6.1, only the mean sieve diameter has been replaced with D10 diameter. The D10 is a one dimensional measurement and is the number length mean or the arithmetic mean. It is yet one more diameter which can be measured easily and thus a model based on it will be helpful tool to predict the settling velocity readily. The plot of Y versus Re is shown in the Figure 7-2. The regression analysis tool has been used and a power law equation is proposed which is given by equation 7-7. The regression coefficient for the proposed correlation comes out to be 0.9722.

$$Y = 5.4958Re^{0.4808} \quad \textbf{Eq. (7-13)}$$

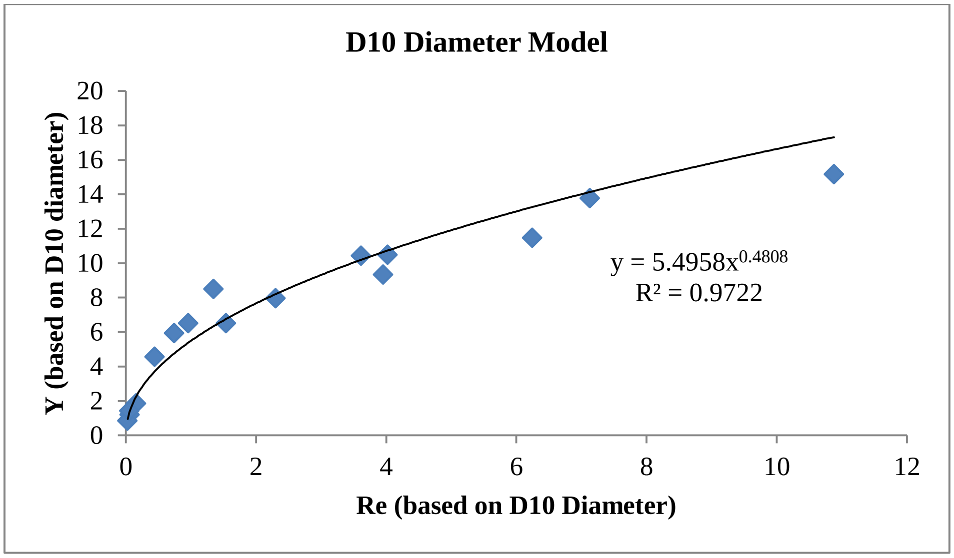

Figure 7-2: Y vs Re plot for natural sand using mean sieve diameter

The average error in the prediction of settling velocity of sand by relation 7-13 is giving a mean error of 20.48% when compared with the measured result given in table 7-3. Here one point is found to be outlier and omission of it leads to an average error of 17.4 %. In other word the developed correlation is predicting the 87.5% measured data points given in table 7-3 with an error of 17.4 %.

7.6.3 Sauter Mean diameter Model

It is defined as the diameter of a sphere with the same volume/surface area ratio as that of particle of interest. Using this diameter the modified drag coefficient (Y) and Re has been calculated using the equation 7-4 and 7-5. The plot of the calculated values is shown in Figure 7-3. The power law least square regression of the data points give correlation (equation 7-8) with regression coefficient of 0.9866. The predicted settling velocity from the model when compared with the measured data gives an average error of 14.78%.

$$Y = 7.1781Re^{0.4605} \qquad \textbf{Eq. (7-14)}$$

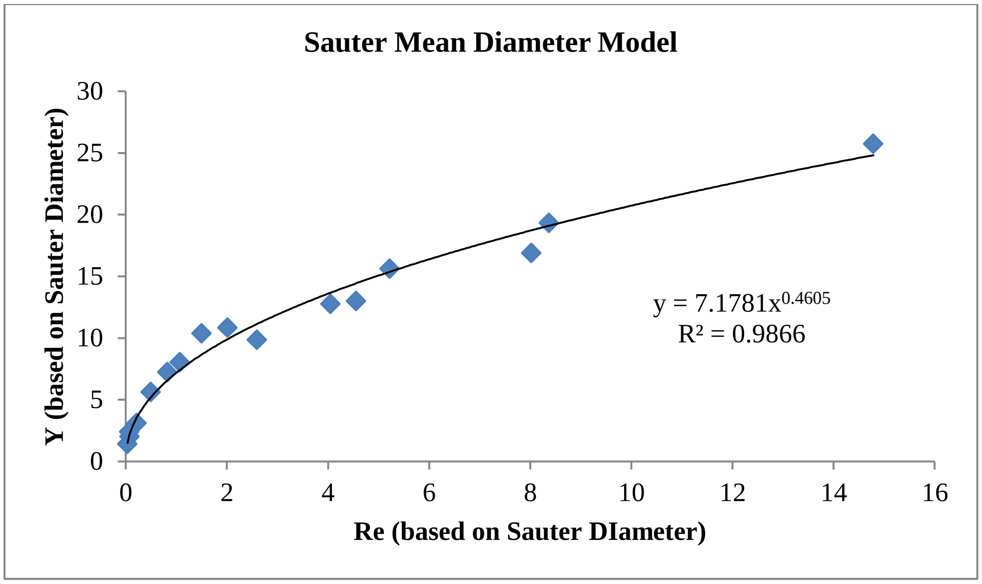

Figure 7-3: Y vs Re plot for natural sand using Sauter mean diameter

7.6.4 DV10 Diameter Model

In the volume weighted particle size distribution the maximum particle size is reported for a given volume percentage of the samples. DV10 represents the maximum particle size below which 10% of the sample volume exists. An empirical model based on it has been developed as given in equation 7-9. The regression coefficient is found to be 0.9839. The average error values in predicted values of settling velocity are found to be 17.26%. The further analysis of the error it has been observed more than 75% of the data is found to be giving an average error of 14%.

$$Y = 5.5058Re^{0.4844} \qquad \textbf{Eq. (7-15)}$$

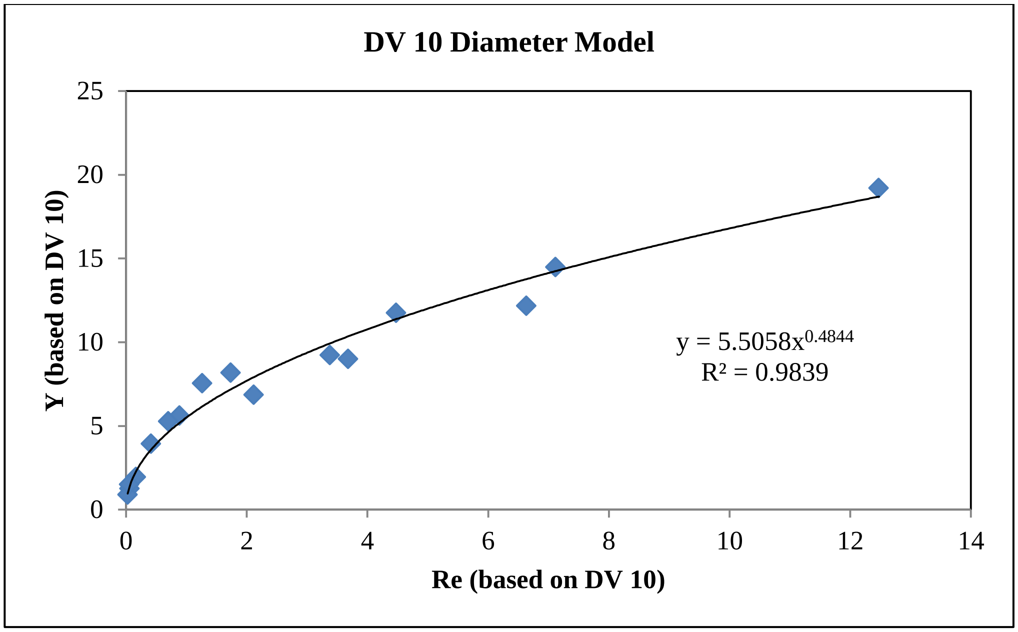

Figure 7-4: Y vs Re plot for natural sand using DV 10 diameter

7.6.5 DV50 Diameter Model

In the volume weighted particle size distribution, the maximum particle size is reported for a given volume percentage of the samples. DV50 represents the maximum particle size below which 50% of the sample volume exists. Volume of the individual particle is calculated and DV 50 represents the diameter below which 50% of the total volume of all the calculated particle exists. The correlation developed empirically is given by equation 7-10 .The average error given by the 7-16 is found to be 15.36% when compared with the measured values given in table 7-3. The developed relation 7-16 is predicting more than 75% of the measured data points with an average error of 12.13%. The regression coefficient of curve fit is 0.9854.

$$Y = 6.9336Re^{0.4676}$$ **Eq. (7-16)**

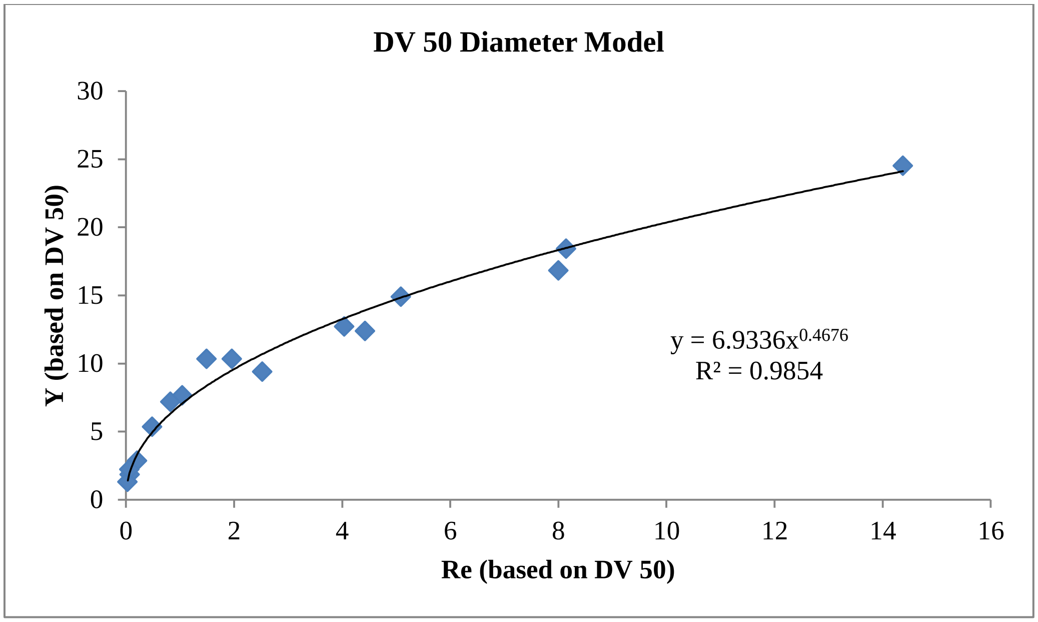

Figure 7-5: Y vs Re plot for natural sand using DV 50 diameter

7.6.6 DV90 Diameter Model

Yet one more volumetric diameter DV 90 has been measured and used in the study. DV 90 represents the maximum particle size below which 90% of the sample volume exists. The volume of the individual sand particle is measured and DV 90 represents the diameter below which the 90% of the total volume exists. The plot for modified drag coefficient (Y) vs Reynolds number is shown in figure 7-6. The functional relationship of the curve is given by equation 7-17. The relation 7-17 is predicting the measured value by shadowgraph with an average error of 16.41%. The relation is predicting more than 80% of the data points giving an average error of 13.3 %. The regression coefficient for the fit is found to be 0.9858.

$$Y = 9.6171Re^{0.4575}$$ **Eq. (7-17)**

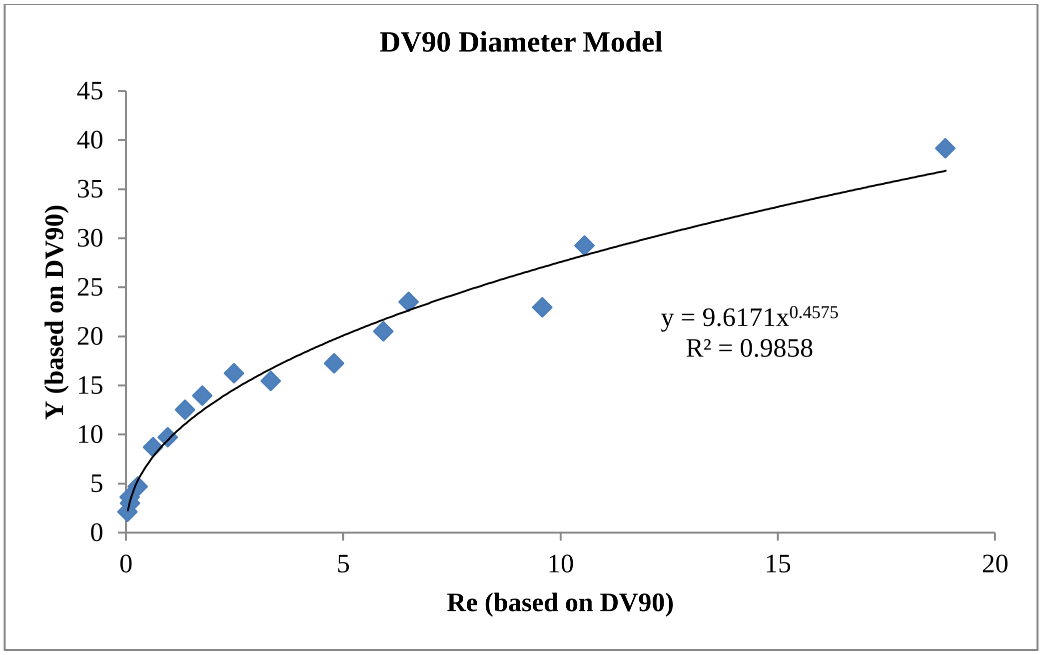

Figure 7-6: Y vs Re plot for natural sand using DV 90 diameter

7.6.7 Equivalent Circular Diameter

Equivalent circular diameter is that of a circle with the area equivalent to the actual area of the particle image. The reported correlation for predicting the settling velocity is given by equation 7-12. The regression coefficient is found to be 0.9794. The average error of 18.5% is observed in predicted values by the correlation 7-18 when compared with the measured value from shadowgraph (given in table 7-3).for predicting the settling velocity. Moreover it has also been observed that for more than 80% of the measured data points, the equation is predicting the values with an average error of 15.1 %.

$$Y = 7.1661Re^{0.4862} \qquad \textbf{Eq. (7-18)}$$

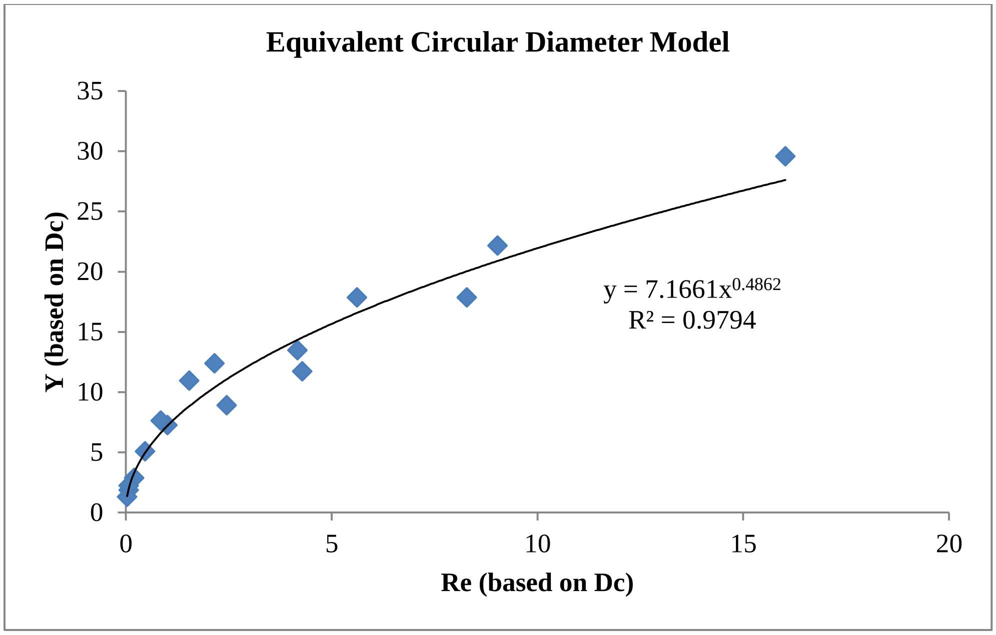

Figure 7-7: Y vs Re plot for natural sand using equivalent circular diameter

7.7 Multiple Linear Regression Approach

Multiple Linear Regression (MLR) is also a technique which is used for the estimation of the independent variable y which is dependent on many factors x. The goal is to determine a first order relationship between y and the many dependent variables x.

$$y = a_1x_1 + a_2x_2 + a_3x_3 \dots \dots \dots .. a_nx_n + e \qquad \textbf{Eq. (7-13)}$$

In equation 7-13, the terms a1, a2,… an refer to the weights of each of the influencing variables x towards the response of y,and e is the error or the residual of the regression.

$$y = (a_1x_1 \dots \dots . + a_nx_n) + e \qquad \textbf{Eq. (7-14)}$$

$$Y = XA + e \qquad \textbf{Eq. (7-15)}$$

In equation 7-15, X and A are the vectors of the dependent variable y, independent variables x_i and the weights a_i

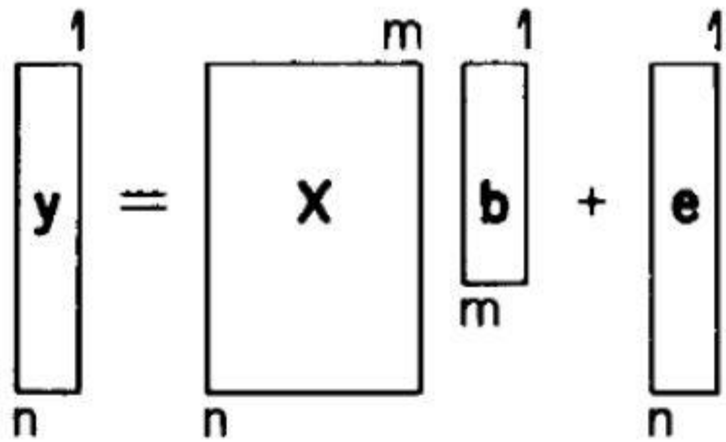

Figure 7-8: Illustration of MLR (Geladi and Kowalski [13])

Figure 7-8, illustrates the MLR regression model. Where n refers to the number of samples and the m refers to the number of independent variables.

There are naturally three cases that are possible with the number of independent variables and number of samples.

(i) m>n : In this case, there are many solutions that are possible for a good fit, and the solutions are not necessarily the best fit parameters for the new data point.

(ii) m=n: When the number of samples is equal to the number of independent variables, there exists a unique solution for which the residual reduces to 0.

(iii) m<n: This case doesn't yield an exact solution for regression parameter b. However, this can be done by minimizing the length of the residual vector. This is done through the least squares technique where,

$$a = (X'X)^{-1}X'Y \qquad \textbf{Eq. (7-16)}$$

While doing this, however, in a few cases the inverse of X'X may not exist.

It is an approach to model the functional relationship between two or more variable by least square error fitting using a linear equation. The functional relationship between the coefficient of the correlations with respect to the fluid rheological parameter ‘n’ and ‘k’ has been determined for each diameter type. The approach of calculating the settling velocity still remains the same and instead of using the curve fit coefficient as discussed above, the new coefficients are used. This has been done to enhance the predicting capability of the empirical equation. The functional relationship of A and B with rheological parameters of fluid is given in table 7-4.

$$Y=ARe^{B} \qquad \textbf{Eq. (7-17)}$$

A, B of the above relation is found as a function of n and K using the experimental data.

7.7.1 Steps to use the Model

- Decide which diameter to use based on the availability of the information.
- Once the diameter is decided or measured, Based on ‘n’ and ‘k’ calculate A and B using respective model.
- Using equation 7-4 calculate Y.
- Once Y, A. and B are calculated estimate Reynolds number using 7-17.
- Lastly use the 7-5 correlation to estimate the settling velocity of natural sand.

Table 7-4: Functional relationship of coefficient with n and K

Diameter	A	B	Error in prediction of Settling Velocity
Mean Sieve	$7.5712n + 17.2208k$	$0.4998n + 1.0159k$	15.5
D10	$5.5309n + 20.7869k$	$0.5682n + 1.0711k$	17.4
D32	$7.5536n + 22.7522k$	$0.5377n + 1.0616k$	10.83
DV10	$5.51n + 21.3382k$	$0.5691n + 1.1277k$	10.85
DV50	$7.1895n + 23.3244k$	$0.5475n + 1.0764k$	10.64
DV90	$10.2285n + 28.63k$	$0.5322n + 1.0588k$	12.67
Dc	$7.1631n + 27.801k$	$0.573n + 1.1534k$	13.1

7.8 Discussion

The settling velocity of natural sands in power law fluid has been evaluated using PIS technique. Reynolds number of $0.01<Re<17$ is encountered during the course of the study. The natural sand of mean sieve diameters 0.35-1.4 mm has been used. Different geometrical diameter of the sand particle has been measured using the optical measuring technique (shadowgraph). Based on the experimental data empirical correlation for different equivalent diameters of natural sand with mean sieve diameter has been proposed.

It has been observed that all the developed correlation is predicting the settling velocity of natural sand particle with an average error of less than 20%. While the Sauter mean diameter model is found to give the least average error of 14.7%, the linear diameter or D10 diameter model is giving the maximum average error of 20%. Comparing the average error in the prediction, the Sauter mean diameter is found to be the best followed by DV 50, DV 90, Dc, mean sieve diameter, DV 10, and D10. The error in prediction also indicates that the capability of a diameter to incorporate the shape effect of sand particle. The multiple linear regressions have been successfully used to develop the relation between the coefficient and fluid rheological parameters. It has been observed that the operation has enhanced the predicting capability by 3-5% and the average error in the prediction of settling velocity has been reduced to less than 15%.

7.9 Conclusion

Different correlations to predict the settling velocity values for natural sands in power law fluids have been developed. Different correlations have been developed with the aim of providing the user greater flexibility to predict the settling velocity with diameter at hand for the sand particle. The use of multiple linear regression mathematical tools has enhanced the predicting capability of the developed correlations. The study is solely for the natural sands particle in power law fluid and may not be valid for other irregular particle.

7.9 References

1. Chhabra, R.P., 2002, “Sedimentation of particles in non-Newtonian media”, Hydrotransport, Vol. 15, pp. 135-148.
2. Harris, K Courtney, 2003, “Sediment transport processes in coastal environments”, a part of online class lecture, Virginia Institute of Marine Science.
3. Malaika, Jamil., 1949, “Effect of shape of particles on their settling velocity”, PhD thesis, the University of Iowa.
4. Deosarkar, P Manik, Sathe, S Vivek, and Chandra Ghamta, Kartik., 2010, “C_D-N_{Rep} relationship for solid-liquid suspensions”, Int. J. of chemical engineering and applications, Vol. 1, No.1, pp.10-14.
5. Chhabra, R P., and Madhav, Venu G., 1994, “Settling velocities of non-spherical particles in non-newtonian polymer solutions”, Powder Technology, Vol. 78, pp. 77-83.
6. Chhabra, R P., and Agarwal, Neha., 2007, “Settling velocity of cubes in Newtonian and power law liquids”, Powder Technology, Vol. 178, pp. 17-21.
7. Rajitha,P., Chhabra, R P., Sabiri, N E., and Comiti, J., 2006, “Drag on non-spherical particles in power law non-Newtonian media”, Int. Journal of Mineral Processing, Vol. 78, pp. 110-121.
8. Han, N.B., and Lu, Z.Y., 1983, “Settling properties of the sediments of the Changjiang Estuary in salt water”, Proceedings of International symposium on sedimentation on the continental shelf, China ocean press, pp. 483-493.
9. Li, Y., Wang, Y. Q., and Lin, Y. A., 1995, “Investigation on settling characteristic of flocs in the Changjiang estuary”, China ocean engineering, Vol. 9, No. 3, pp. 325-334.

10. Shi, Zhong., Zhou, Jun Hua., Eittreim, L Stephen., and Winterwerp, Johan C., 2003, “Settling velocities of fine suspended particles in the Changjiang Estuary, China”, Journal of Asian Earth Sciences, Vol. 22, pp. 245–251.

11. Mohammed, A R Muhammed., 2013, “Studying the factors affecting the settling velocity of solid particle in non-Newtonian fluids”, Nahrain University college of engineering journal, Vol.16, No.1, pp. 41-50.

12. Shah, N Subhash, Fadili, EI Youness, and Chhabra, R.P., 2007, “New model for single spherical particle settling velocity in power law (visco-inelastic) fluids”, Int. J. of multiphase flow, Vol.33, pp. 51-66.

13. Geladi, P., and Kowalski, B. R., 1986, “Partial least-squares regression: a tutorial”, Analytica Chimica Acta, Vol.186, pp.l-17.

Chapter 08

Experimental Study on the Rheology of Carbopol

This chapter is focussed on the rheological study of Carbopol mixture. The chapter starts with the discussion of various related studies conducted on the yield power law fluids prepared by using Carbopol. The next section is focussed on the study of the behavior of the Carbopol mixture with concentration and the effect of sodium hydroxide titration on the mixture. The last section consists of the different constraints due to which the study of settling velocity of particles was not possible using current shadowgraph setup within the stipulated time.

8.1 Introduction

The rheological characteristics (i.e. the relationship between shear stress and shear rate) of the yield power law (YL) fluid as described by Herschel-Bulkley model is given by eqn. 8-1.

$$\tau = \tau_y + K\,(\Upsilon)^n \qquad \textbf{Eq. (8-1)}$$

Particles will not settle in the yield power law fluid if the yield stress value balances the particle's weight and the failure of surrounding fluid doesn't occur. This criterion has been derived from the plastic theory and is valid for static plastic material. According to the plasticity theory particle will settle only if the criteria by equation 8-2 is satisfied:

$$\tau_y \leq a_{cr}\left(\rho_p - \rho_o\right) g d \qquad \textbf{Eq. (8-2)}$$

Where a_{cr} is coefficient calculated from the fluid and particles physical properties

According to the study done on various data available in the literature by Chhabra [1], he empirically determined the values of a_{cr} to be in the range of 0.048-0.20. Based on the plasticity theory the critical value for the coefficient is found to be 0.065 (ref?). Ashley and Smith [2] reported the coefficient value to be 0.048 using the fluid mechanical approach.

A viscoplastic fluid has capability of holding particles in suspension and thus can be used for various industrial applications like long distance coarse particle transport, suspension of solids in drilling etc. Chhabra [3] reviewed the available literature on the yield fluid and concluded that most of the previous work has been concentrated on defining a criterion for a particle to settle in fluid, flow visualization around the particles settling in the fluid, and development of a standard drag curve for viscoplastic fluid. He mentioned that various authors in past have used the criterion for particle settling in term of gravity yield parameter (Y), which is defined as:

$$Y = \frac{\tau_o}{gd(\rho_p - \rho_o)} \qquad \textbf{Eq. (8-3)}$$

Some researchers studied the settling condition numerically and reported the values of Y between 0.04 to 0.08. Contrarily experimental investigations have reported the values of Y to be close to 0.2 (refs). There exist discrepancies amongst previous studies and no fixed criterion has been developed for the settling of particle in terms of gravity yield parameter till date. One of the important reasons that lead to variant Y values can be the measurement of yield strength of fluid which may be different for different measuring techniques.

Another group of authors have experimentally and numerically studied the sheared zone envelope surrounding the falling sphere and have reported different shapes and diameter for it (refs). Numerous attempts have been made in the past to develop a drag-Reynolds number correlation for the viscoplastic fluid (refs). However, this resulted in a family of curves unlike a single curve in case of Newtonian fluid.

Anshley and Smith [2] conducted experiments on tomato sauce, the rheological properties of which can be defined by the Bingham fluid model. They reported a 10% deviation in the settling velocity values for different sets of experiments. They proposed that the falling sphere creates a fluidic envelope of 1.41D around itself which is steady and moves along with the sphere and creates a localized transformation between fluidic and plastic states. The dynamic state of the fluid was explained as $\rho u^2/((\eta u/d)+K\tau_y)$ and termed as as dynamic parameter. Later on different authors estimated different values for K. Dedegil [3] proposed K=1, Du Plessis and Anshley [2] took it as 0 and $7\pi/24$, while Mitra [4] assumed it to be 1/6 in his study. There exists different explanation for these values for 'K' and also there does not exist an universally accepted parameter for defining the rheological behavior of such fluid making them even more complex to handle such fluid particle systems.

Anshley and Smith [2] plotted the drag coefficient verses dynamic parameter values and stated that the relation can be used to predict the settling velocity of the particle. This has not been validated with an independent experimental data set. Moreover the model is based on various theoretical assumptions like defining the stress envelope of 1.41 D and many others.

Atapattu [6] proposed a new model for drag coefficient in Bingham fluid based on the available literature and his experimental measurements. The model converged to Newtonian curve for n=1 and with zero yield. However, the average and maximum error reported were 30% and 48% respectively.

Pazwash and Robertson [13] proposed a relation between the difference of drag coefficients for Bingham fluid and Newtonian fluid, as a function of Hedstrom number as:

$$C_{DB} - C_{DN} = 36\left(\frac{He}{Re_B^2}\right) \qquad \textbf{Eq. (8-4)}$$

The relation is valid for $60<Re_B<2000$ and $920<He<3600$

The authors stated that for higher Re_B values, the drag coefficient for Bingham fluid becomes equal to drag coefficient of Newtonian fluid.

Saha and Mitra [4] attempted to develop a C_d-Re_p model similar to Newtonian fluid for Bingham plastic fluid. They used the following relation (Eq. 8-5) for Reynolds number in Bingham fluid for dynamic condition:

$$Re_B = \frac{\rho_o v^2}{\frac{\eta v}{d} + K\tau_o} \qquad \textbf{Eq. (8-5)}$$

Different authors have proposed different values for K values. In this case authors used K=1/6,. They proposed a correlation between $C_D Re_m^2$ and Re_m (Eqs. 8-6 and 8-7). The model is same for Bingham fluid except that in this case it also depends on settling velocity (v).

$$C_D Re_m^2 = \left(\frac{4}{3}\right) g d^3 \rho_o (\rho_s - \rho_o) / \left(\left(\frac{\eta v}{d}\right) + \frac{\tau_o}{6}\right)^2 \qquad \textbf{Eq. (8-6)}$$

$$Re_m = \frac{d v \rho_o}{\eta + \left(\frac{\tau_o d}{6v}\right)} \qquad \textbf{Eq. (8-7)}$$

Experimental results from different studies have been collected and plotted for the above relations (Eqs. 8-6 and 8-7) and it was found that the values were lying on the curve. In their study, Saha and Mitra [4] used the value of $d_{critical}$ as proposed by Dedegil [3] (Eq. 8-8). According to this relation, the particles having a diameter lower than $d_{critical}$ will not settle in the fluid.

$$D_{critical} = \left(\frac{3\pi}{2}\right)\left(\frac{\tau_o}{(\rho_s - \rho_o) g}\right) \qquad \textbf{Eq. (8-8)}$$

For $Re_m > 1$, the drag curve for Bingham fluid is found to be matching with the Newtonian drag curve. For the intermediate regime the authors proposed the following correlation for drag coefficient:

$$C_D = 18.5 / Re_m^{0.75} \qquad \textbf{Eq. (8-9)}$$

Authors claimed that the correlation is predicting the value within 1% error. However, the validity of the developed correlation has been tested with very limited experimental data from the literature.

A detailed experimental study of the variation of steady state settling velocity of spheres in Carbopol 941 solution has been reported [5]. It is a general observation by different authors like Chhabra [1] and Attapatu et al. [6] that there exists a very poor reproducibility of the settling velocity experimental data in viscoplastic fluid. One of the important characteristic of Carbopol polymer is that it doesn't get dissolved in water rather gets dispersed. It has been noticed that Carbopol 941 solution when neutralised with Sodium hydroxide solution creates a three dimensional dense and structured molecular structure which provides a yield in the fluid. Authors of this study mentioned that the settling velocity of spheres attain a constant value after 3-4 spheres are made to fall in the same path. This can lead to the conclusion that the fluid network gets broken completely and thus provides unequal resistance to the subsequent spheres falling through the fluid.

The authors also studied the extent of network recovery with respect to time. Different time intervals were selected and the velocity of first sphere in each set of experiments was used to make the judgement. For a fully recovered structure, the settling velocity for all the spheres subsequent to the first one should be same as of the first sphere.. Interestingly, the authors observed that the settling velocity of first sphere (within each set of experiments) decreased with the increased time interval. Another independent study has reported similar observations [7]. It was observed that time duration of approximately 2 hours are required for the mending process of disintegrated molecular structure for a 0.3% Carbopol solution. Using the general diffusivity concept for polymer molecule given by Kroschwitz [8], the coefficient of diffusivity varies from 10^{-4}-10^{-13} mm^2 s^{-1}. Based on the diffusivity constant and the assumption that the shear zone can be up to the diameter of the falling sphere the time for reunion of the polymer structures were estimated.

Carbopol molecules consist of some linear chain polymer impurities which are responsible for formation of network like structure for the polymer when dissolved in a solvent [7]. The average molecular size of the Carbopol particle is 0.2μm and after absorbing water it becomes around 3.9 μm. Using the above mentioned diffusivity constant (10^{-4}-10^{-13} mm^2 s^{-1}) and the sphere size equivalent to the swollen polymer molecular size, the solution takes about 2 hours to reintegrate its distorted shape. It has been clearly mentioned that the time proposed is just a speculative duration based on different assumptions and a more detailed study of the polymer molecular structure is required to give a better approximation. The authors have used only one concentration of polymer solution, thus it could be safely argued that the network structure and the strength of intermolecular bond could be very different for different concentrations of the same polymer or for a different polymer. Therefore, the results and learnings from this study cannot be generalised.

Chao et al. [7] varied the time interval between two spheres falling in viscoplastic fluid and reported that the settling velocity of second sphere increases with decreased time interval. Such behavior of settling velocity is due to its dependence on the local disturbance in the polymer solution. It is stated that with the fall of sphere, a zone of sheared and less dense structured molecular network is created in the viscoplastic plastic which takes time to get back to its original state. This phenomenon results in dependence of the settling velocity of spheres on the time interval between them. The sheared fluid because of the settling sphere creates a less resistive fluid for the following sphere. It has been postulated that depleted fluid behind the falling sphere allows the neighbouring polymer molecule to diffuse into the region and occur gradually with time.

In 2007, Chhabra [9] reviewed the literature available on visco-plastic fluid and reported existence of lot of uncertainties in estimation of the settling behavior of particle in this type of fluid. The flow of sphere in visco-plastic fluid is more complicated because of the thixotropic and time dependent behavior of viscosity and elasticity. Moreover the settling velocity of sphere is dependent on the fluid state; the values are lower for the undisturbed fluid as compare to disturbed fluid state. .

Martinez et al. [10] studied the behavior of settling spheres in visco-plastic fluid for Re<1, using particle image velocimetry. The effect of molecular structure of polymer solution on settling velocity of particle was discussed. The equation of motion of particle in Bingham fluid is generally defined with the use of Reynolds number, Re_p (ratio of inertial and viscous forces), Bingham number, B_n (ratio of yield stresses and viscous stresses, Richardson number, R_i (ratio of kinetic and potential energies) and ρ_q (density ratio of solid to liquid). Authors attempted to study the equation of state numerically and also estimated the yield stresses surfaces experimentally. The carbopol 940 mixture and glass spheres of different diameter were used for the experiments. They observed that after the fall of sphere in the fluid, the disturbed Carbopol solution takes around 48 hours to regain its original state. A detailed study of flow field around a freely falling sphere in viscoplastic fluid has been presented with the help of PIV measurements. The stress field generated in front and back of the sphere has been explained and is correlated with the Carbopol rheology behavior properly.

Rheological properties of the Carbopol mixture exhibit a drastic change in yield value with change in pH [11]. It is reported that with increasing pH, the yield strength of the Carbopol solution first increases till a certain pH value (termed as critical pH), beyond which a decrease in yield values was observed. . Other rheological properties such as elastic modulus also attain a maximum value for an intermediate pH value of the solution. This behavior of Carbopol solution with change in pH has been explained in the study. The authors suggested that the small addition of NaOH developed an osmotic pressure which makes the particle swell. This swelling of particle with the addition of NaOH gradually reaches a point where the volume fraction of particle reaches its maximum close packing. Beyond this point, because of limited space the swollen particle starts to get compressed and form network structure with surrounding molecules. This leads to an increase in the values of yield stress and elasticity values. Further addition of NaOH results in the dissociation of the carboxyl group of the acrylic acid. The dissociation of the carboxylic group together with the presence of excessive sodium ions in solution generates a net inward osmotic pressure which makes the particle to de-swell slightly. This inward osmotic pressure and de-swelling of particles leads to a decreased value of yield stress and elastic modulus of the Carbopol solution at pH values beyond the critical pH.

More recently, Gumulyaa [12] examined the settling behavior of sphere falling behind the other sphere. The author tried to correlate the settling velocity with the dynamic and static rheological properties of the fluid. The experiments were conducted in a time gap of 15 min assuming that the disturbed network of polymer retains 95% of its shape in the given duration. The general equation for yield fluid (Eq. 8-1) is valid for fluid in static condition and is not applicable for the study of settling of particle. Therefore, for sedimentation studies a transient rheological model which can capture the behavior of fluid's rheology with changing shear rate needs to be developed.

The author examined the change in structure of fluid and proposed a correlation with time and change in shear rate. In his observation he found that the sphere falling behind the other sphere seems to have higher settling velocity. The reason for the phenomenon is given by the fact that there occur local changes in the connectivity of intermolecular structure within the fluid. Using the experimental results the author proposed a general correlation based on the fluid structure parameters. The proposed model has not been validated using other independent data sources and hence the reliability of the model could be questioned. Moreover the proposed model requires quite a few fluids’ structural parameters which require a lot of effort and assumption. The model is very complicated and requires rigorous calculations.

8.2 Important Observation from the Literature

- There occur local changes in the connectivity of intermolecular structure within the fluid when a particle falls through it, thus offering a different resistivity to the subsequent falling particles after it. It is a general observation that the sphere falling after another sphere will have a higher settling velocity compared to sphere it is following.
- It has been found that after the fall of sphere in the fluid, the disturbed Carbopol mixture takes around 48 hours to regain its original state after the fall of the sphere.
- Rheology of the Carbopol solution changes drastically with change in solution pH. Both yield strength and bulk modulus first increase with an increase in solution pH reaching a maximum value at the critical pH, beyond which they decrease. This phenomenon can be explained through generation of osmotic pressure due to dissociation of carboxylic groups of the polymer and presence of Na ions in excess.
- There exists a wide variation in the yield strength measurement done by the authors and that’s why several of them have estimated different values for same parameter for critical conditions.

8.3 Mixing procedure for Carbopol 940

One of the important characteristic of Carbopol polymer is it doesn’t get dissolved in water rather gets dispersed in water. It is rather a tough task to mix Carbopol in water as compared to other polymer.

Carbopol powder has a very low density and thus exists in a very fluffy powder form. It is highly recommended to segregate the polymer particle with minor crushing using spoon or stick so that its lump free. When introduced in the water it is advisable not to put in even small lumped molecule because of its cross linked structure it attains a chewing gum like strong structure which will not dissolve ever in water.

The rpm of the agitation should be within the range of 850-1150 rpm. Going beyond this rpm would lead to an improper mixing of the polymer. It is strictly advisable to introduce the polymer at the centre of the vortex generated due to agitation, pouring of the polymer some other position in the water would lead to bad mixing. Introduce the polymer as slow as you can, for addition of 1gm of polymer in 350 ml of water had taken around 45 minute of time duration. After complete introduction of polymer in water allow the mixture to agitate at the given range of rpm for 15-20 minutes. The physical property of the mixture is that it is not as clear as water.

8.4 Rheological Measurement of Carbopol

Different weight concentration of Carbopol has been prepared and tested using different controlled mode of Bohlin Rheometer. The Carbopol wt% of 0.571 without NaOH has been measured and reported in the figure 8-1 and 8-2. It can be observed that the fluid is not giving any yield strength. This is on the line with the observation made in the literature that for the wt% < 1 the fluid does not exhibit enough yield strength. Following the Gutowski [11] study in the prepared solution NaOH has been added and mixed properly. Due to the addition of the sodium hydroxide the physical structure of the fluid changed considerably and appearance converted from fluid to gel like structure.

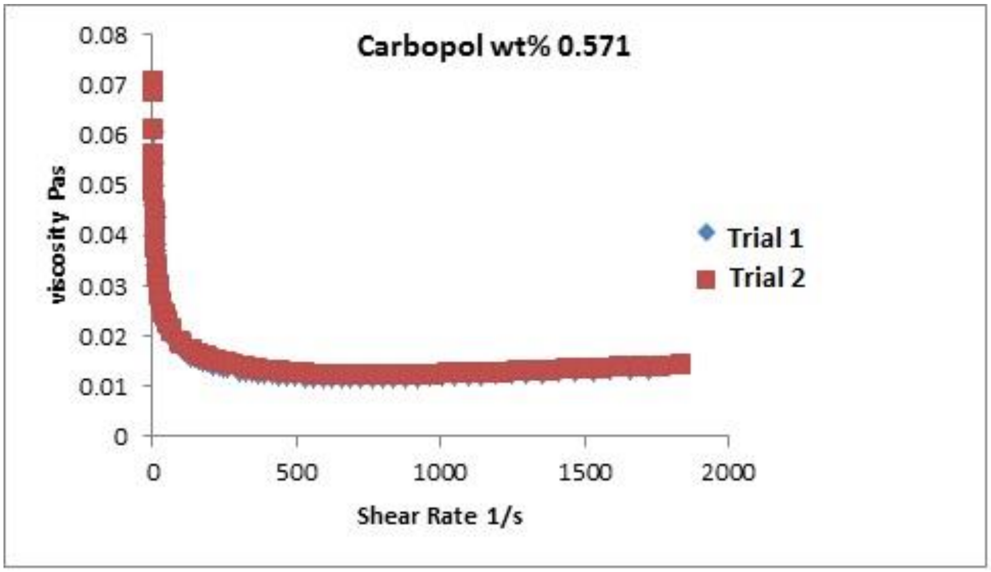

Figure 8-1: Viscosity versus shear rate for Carbopol solution (wt% 0.571)

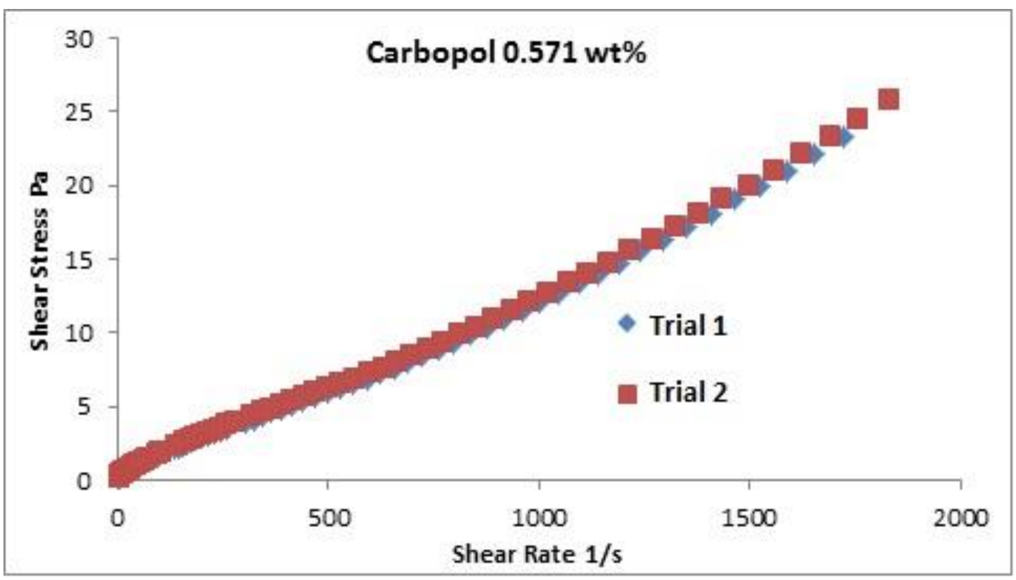

Figure 8-2: Shear stress versus shear rate for Carbopol solution (wt% 0.571)

It is observed that with the addition of NaOH the fluid viscosity has changed to a very high extent (see figure 8-3). It happens due to the generation of osmosis pressure and swelling of the particle which pushes the molecules close to each other forming a highly dense gel like structure. Due to the presence of network structure in the fluid the viscosity has been changed considerably. On analysing the yield stress plot it can be seen that with the addition of sodium hydroxide the fluid gives a considerable amount of yield strength (See figure 8-4).

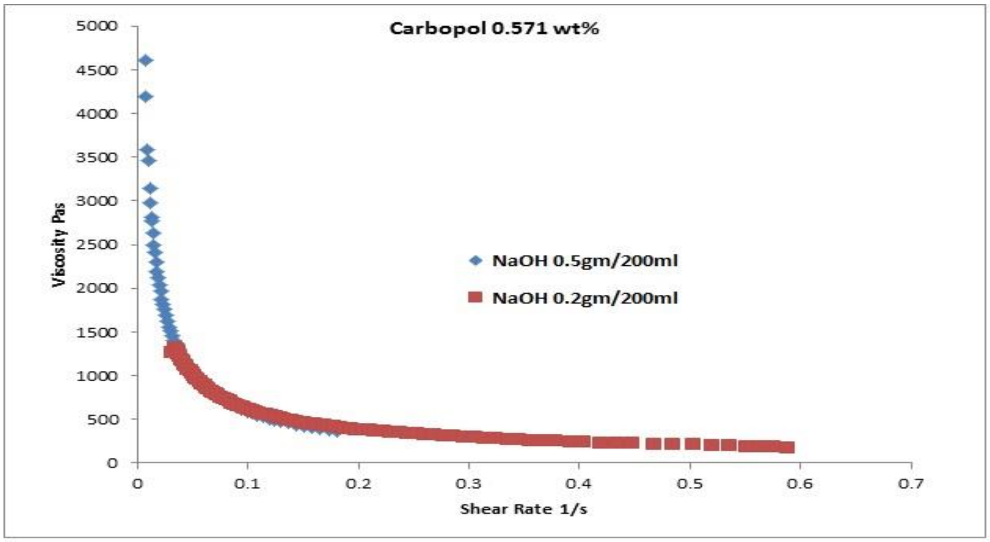

Figure 8-3: Viscosity versus shear rate for Carbopol solution (wt% 0.571) after NaOH titration

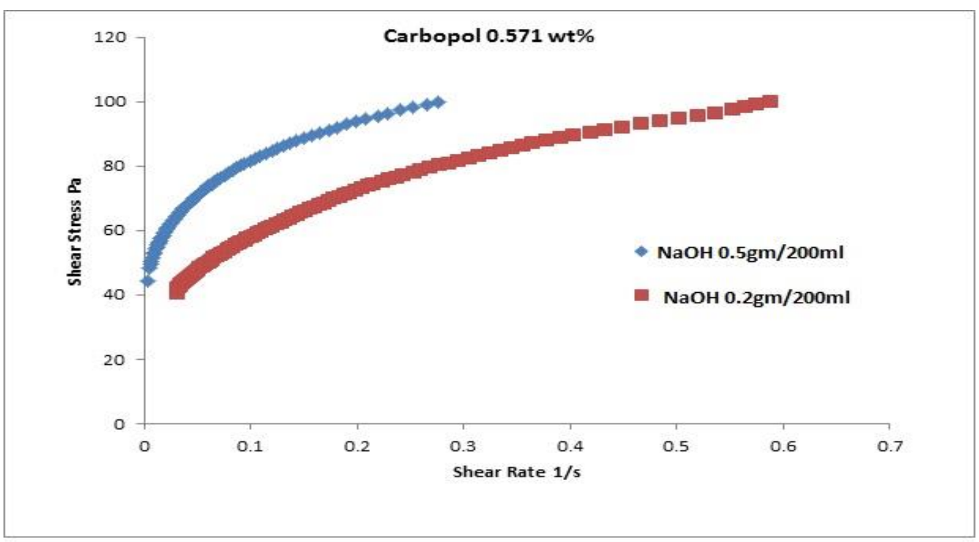

Figure 8-4: Shear stress versus shear rate for Carbopol solution (wt% 0.571) after NaOH titration

In yet another observation it has been noticed that the proper ratio of Carbopol and NaOH is required to have an increased yield or viscosity value. The same amount of NaOH has been added to the carbopol solution of wt% 0.2857 and it has been noticed that yield strength has been reduced to 2-3 Pa which was earlier 35-45 Pa for Carbopol wt% 0.571. It is observed that decrease in 50% in the Carbopol concentration lead to twelve fold decrease in the yield strength of the fluid. Similar observation has been noticed for the viscosity change of the fluid with decreasing the concentration by 50% leads to decrease of viscosity by several thousand centipoises. This shows the severity of network structure formed in the fluid. Even a slightly high concentration of Carbopol leads to more packed network structure which affects the viscosity and yield strength significantly.

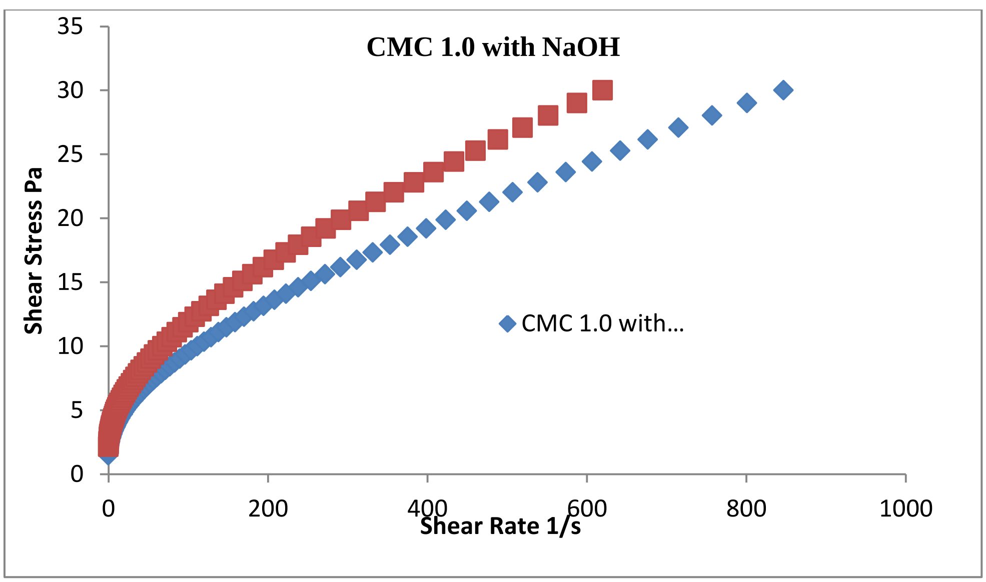

Figure 8-5: Shear stress versus shear rate for Carbopol solution (wt% 0.285) after NaOH titration

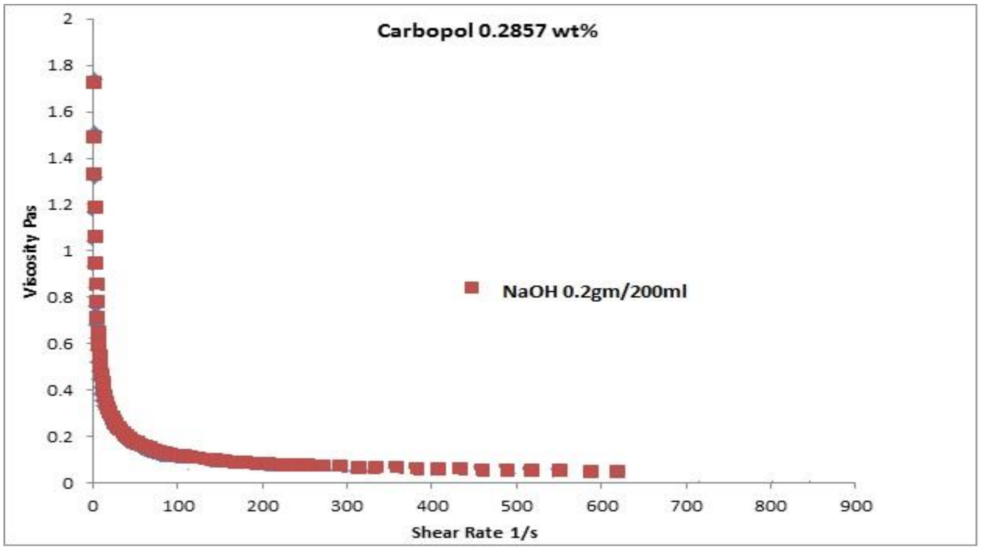

Figure 8-6: Viscosity versus shear rate for Carbopol solution (wt% 0.285) after NaOH titration

Yet one more study on the rheology of the Carbopol has been conducted. The effect of addition of NaOH in the Carbopol solution has been studied. It has been found that once the critical concentration of sodium hydroxide has been reached it starts reversing the effect on the rheology. It has been found that the Carbopol 0.71 wt% solution when titrated till 0.1gm/400 ml of NaOH shows an increase in the viscosity and yield strength. It has been observed that for low concentrations of Carbopol solution there does not exist significant yield strength no matter how much the quantity of base titration we add. It thus further conveys information that in the solution there should exist certain concentration of carbopol molecule which after titration and swelling comes in contact with other molecule forming a network structure. Since the carbopol molecules are in the dispersed state in the water the lower concentration of carbopol does not allow one molecule to interact with other molecule.

The plot 8-7 and 8-8 shows that adding NaOH beyond the acceptable limit leads to lose of rheological properties of the Carbopol solution. A proper ratio of Carbopol and NaOH is thus required to build a fluid with significant yield and viscosity values.

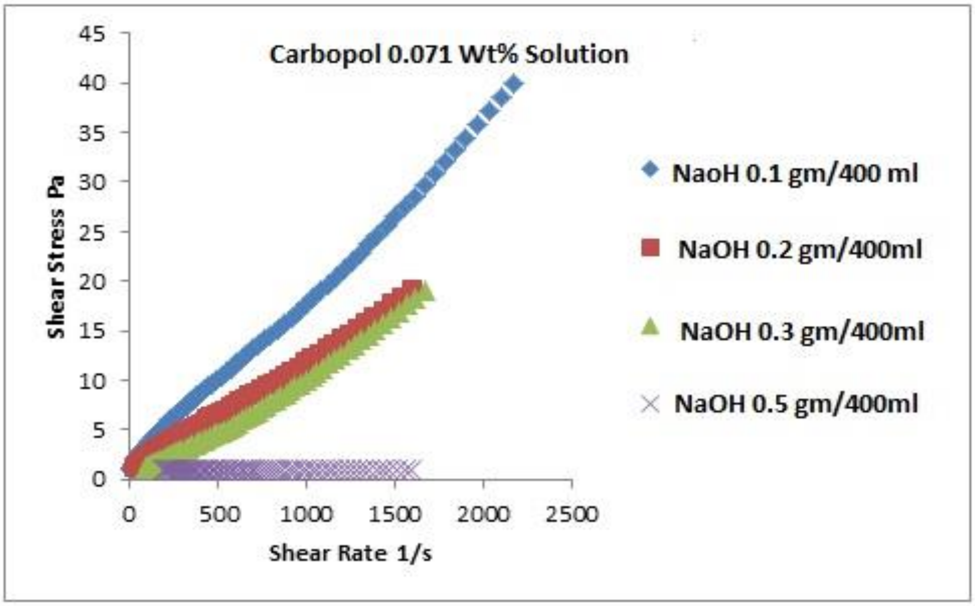

Figure 8-7: Shear stress versus shear rate for Carbopol solution (wt% 0.071) after NaOH titrations

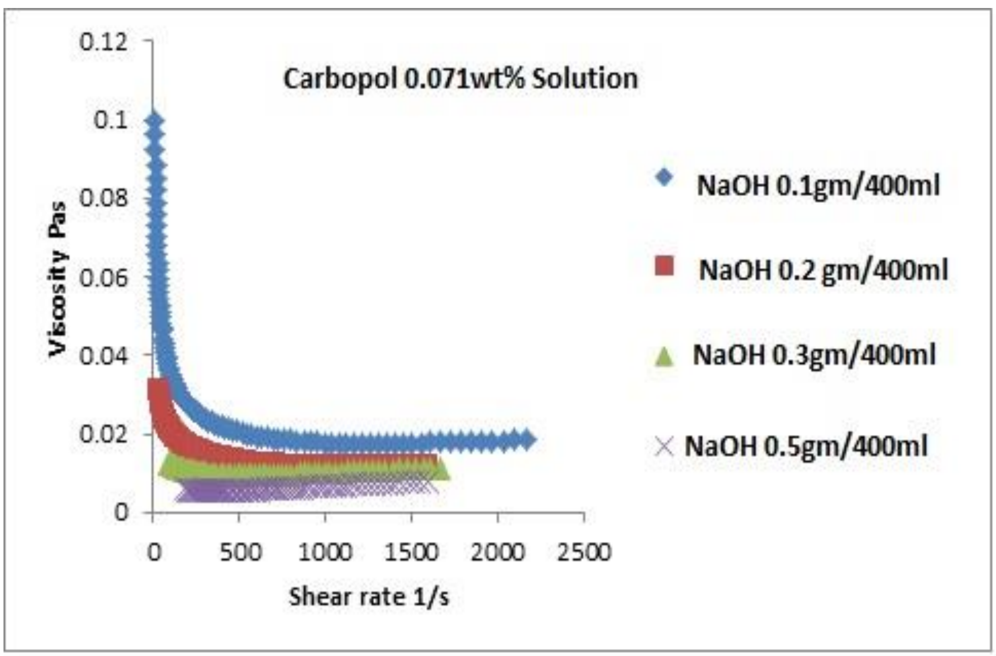

Figure 8-8: Viscosity versus shear rate for Carbopol solution (wt% 0.071) after NaOH titrations

8.5 Constraints

There exist few major constraints which are not allowing the shadowgraph experiments to be performed. It is a very pertinent complexities involved with the yield fluid is that there does not exists a repeatability in the experiments until and unless the polymer is allowed to regain its original state. The time taken requires may take up to two days. This is the case with one-eight spheres fall which has been reported in the literature. The damage may be more complex in case of our experiment because to make the particle fall exactly in the focal plane of the camera we are dropping more than 20 particles at a time and in that only one or two fall in the plane which can be captured by the shadowgraph. Chhabra [9], Chhabra [1], Gumulya [12], Anshley and Smith [2], Martinez [10], Dedegil [3], Mitra [4], and Saha [4] and have found similar phenomenon of disintegration of polymer structure during the fall of spheres in the yield power fluid.

One the most relevant work is conducted by Martinez [10] in which he studied the behavior of one sphere falling behind the other. He observed that the sphere falling behind seems to have higher settling velocity because of the disintegrated fluid structure which was caused by the first sphere. He analyzed the scenario for the two spheres. We can't perform such study because of the constraint of the shadowgraph as mentioned earlier that we require more than 10 particles to make at least one fall in the plane. One more important observation made by these authors is that the settling particle when falling in the yield fluid creates a yield shear zone around them which found to be moving with the sphere. In this zone the fluid seems to have fluidic behavior and within this zone the plastic behavior of the fluid doesn't occur. Different authors have given different opinions for the fluidic zone, some of them have given the effect to be kidney shape and with diameter 1.41 D, while some of they have reported it to be 5-8 times as that of the diameter. In our case the complexities are even caused by this fluidic zone because for higher number of particles the one may influence each other zone and affect the settling behavior.

Moreover the study of fluid rheology and to look into the breaking and uniting of gel structure need a better microscopic study plus a lot of hit and trial. In our case even this may be even more complicated as the number of particles is more and the damage in the gel structure will be more complicated. In addition we can’t increase the Carbopol concentration to have a significant yield value because this will decrease the transparency of the fluid and shadowgraph may not be applicable for such studies.

8.6 References

1. Chhabra, R.P., 1993, “Bubbles, drops, particles in non- Newtonian fluids”, CRC Press, Inc., Boca Raton, FL.
2. Ansley, W Ralph., and Smith, N Terence, 1967, “Motion of spherical particles in a Bingham plastic”, AIChE Journal, Vol. 13, No. 6, pp. 1193-96.
3. Dedegil, M V., 1987, “Drag coefficient and settling velocity of particles in non-Newtonian suspension”, J. of Fluids Engineering, Vol. 109, pp. 319-325.
4. Saha, G., Purohit,N K.,and Mitra, A K., 1992, “Spherical particle terminal settling velocity and drag in Bingham liquids”, International Journal of Mineral Processing, Vol. 36, pp. 273-281.
5. Hariharaputhiran, Mariappan., Subramanian, Shankar R., Campbell,Gregory A., and Chhabra, Raj P., 1998, “The settling of spheres in a viscoplastic fluid”, J. of Non-Newtonian fluid mechanics, Vol. 79, pp. 87-97.
6. Atapattu, D. D., R. P. Chhabra, and P. H. T. Uhlherr., 1990, “Wall effect for spheres falling at small Reynolds number in a viscoplastic medium,” J. of Non-Newtonian Fluid Mech., Vol. 38, pp. 31-42.
7. Y.I. Cho, J.P. Hartnett, and W.Y. Lee, 1984, “Non-Newtonian viscosity measurements in the Intermediate shear rate range with the Falling Ball Viscometer", Journal of Non-Newtonian Fluid Mechanics, Vol.l5, pp.61-74.
8. J.I. Kroschwitz. (Ed.), 1986, “Encyclopedia of polymer science and engineering”, vol. 5, Wiley-Interscience, New York.
9. Chhabra, R.P., 2007, “Bubbles, Drops, Particles in Non-Newtonian Fluids”, CRC Press, Inc., Boca Raton, FL.

10. Martinez, D M., Frigaard, I A., Burghelea, T I., and Putz, A M V., 2008, “Settling of an isolated spherical particle in a yield stress shear thinning fluid”, Physics of Fluid, Vol. 20.

11. Iris, Gutowski., 2010, “The effects of pH and concentration on the rheology of Carbopol gels”, MSc thesis, department of physics, Simon Fraser university.

12. Gumulyaa, M M.,Horsleya, R R., Wilson, K C., and Pareeka, V., 2011, “A new fluid model for particles settling in a viscoplastic fluid”, Chemical Engineering Science, Vol. 66, pp. 729-39.

13. Pazwash, H., and Robertson, J. M., 1975, “Forces on bodies in Bingham fluids”, J. of Hydraulic Research, Vol. 13, pp. 35-55.

Chapter 9

Conclusions and Recommendations

Based on the experimental study the following conclusions can be offered:

9.1 Conclusions

- A new experimental technique for measuring the settling velocity, size, and shape of the particle has been developed. The experimental technique used in this work also describes a new application of shadowgraph technique in fluid particle systems.
- The measurement technique is based on the double frame image processing and is found to be very accurate in terms of size, shape, and velocity measurements.
- Davis 8.0 software used in the study is found to be highly reliable and proficient tool for image processing, giving different information about the fluid particle systems behavior.
- In a quest for more accurate predicting model to for sphere in Newtonian fluid, a new empirical model has been developed using dimensionless diameter and settling velocity.
- It was noted from the experimental results that for a particular sieve diameter, there exists a range of sizes, centricity, and settling velocity values.
- Ellipse is found to be the best shape to define the shape of natural sands.
- Two empirical correlations for predicting the settling velocity of natural sand in water have been proposed which are found to be most accurate model till date.
- Flow behaviour index ‘n’ and consistency index ‘K’ of the fluid are found to have significant effect on settling velocity of particle in power law fluid. Use of Newtonian drag curve for power law fluid (as suggested in different literature) is found to be highly erroneous.
- A new correlation for predicting the settling velocity of spherical particles in power law fluid has been proposed. The new model gives more accurate

prediction of sand settling velocity in power law type fluids than the models previously published in the literature.

- Different correlations based on seven equivalent diameters for sand particles have been developed with the aim of providing the user greater flexibility to predict the settling velocity with diameter at hand for the sand particle. The study is solely for the natural sands particle in power law fluid and may not be valid for other irregular particles.
- Relationship between sieve diameter and different equivalent diameter for natural sand particles has been developed. New correlations were found to be very efficient in predicting more accurate values of sand settling velocities in power law type fluids..
- Effect of Sodium hydroxide on the yield strength of Carbopol solution has been verified experimentally.

9.2 Future Work

- The use of different correlations can be even more generalized by conducting experiments with different size of particles and fluids, so that the range of Reynolds number for the correlations can be increased.
- Development of parameter and correlations for gel structure breakage and their recovery with time in case of yield fluid (Carbopol) is recommended to have a better understanding of settling velocity in yield fluid.
- The setup can be used to develop correlations for other commonly occurring particles like bitumen, coal, rock, limestone etc. to enhance the efficiency of various related operations with these particles.
- The current setup can be upgraded to use on the moving fluid in different pipe geometry to give a better insight of the fluid particle system in such conditions.

- The setup can be even improvised to calculate the lift velocity and lift force acting on the particle in the pipeline transport which can determine the critical velocity required to transport different particles at a time.